(12)

DNA-TR-82-145

AD-A144 486

THEORETICAL INVESTIGATION FOR IMPROVEMENT OF BALLISTIC ARMOR BLANKETS

Y. Marvin Ito
Richard B. Nelson
A. Anton Frederickson III

California Research & Technology, Inc
20943 Devonshire Street
Chatsworth, California 91311

1 May 1983

Technical Report

CONTRACT No. DNA 001-82-C-0093

APPROVED FOR PUBLIC RELEASE;
DISTRIBUTION UNLIMITED.

THIS WORK WAS SPONSORED BY THE DEFENSE NUCLEAR AGENCY
UNDER RDT&E RMSS CODE S400082466 A99QAXFB00039 H2590D.

Prepared for
Director
DEFENSE NUCLEAR AGENCY
Washington, DC 20305

Destroy this report when it is no longer needed. Do not return to sender.

PLEASE NOTIFY THE DEFENSE NUCLEAR AGENCY, ATTN: STTI, WASHINGTON, D.C. 20305, IF YOUR ADDRESS IS INCORRECT, IF YOU WISH TO BE DELETED FROM THE DISTRIBUTION LIST, OR IF THE ADDRESSEE IS NO LONGER EMPLOYED BY YOUR ORGANIZATION.

UNCLASSIFIED

SECURITY CLASSIFICATION OF THIS PAGE (When Data Entered)

REPORT DOCUMENTATION PAGE		READ INSTRUCTIONS BEFORE COMPLETING FORM
1. REPORT NUMBER DNA-TR-82-145	2. GOVT ACCESSION NO AD-A144486	3. RECIPIENT'S CATALOG NUMBER
4. TITLE (and Subtitle) THEORETICAL INVESTIGATION FOR IMPROVEMENT OF BALLISTIC ARMOR BLANKETS		5. TYPE OF REPORT & PERIOD COVERED Technical Report 6. PERFORMING ORG. REPORT NUMBER CRT 3520F
7. AUTHOR(s) Y. Marvin Ito Richard B. Nelson A. Anton Frederickson III		8. CONTRACT OR GRANT NUMBER(s) DNA 001-82-C-0093
9. PERFORMING ORGANIZATION NAME AND ADDRESS California Research & Technology, Inc. 20943 Devonshire Street Chatsworth, California 91311		10. PROGRAM ELEMENT, PROJECT, TASK AREA & WORK UNIT NUMBERS Task A99QAXFB-00039
11. CONTROLLING OFFICE NAME AND ADDRESS Director Defense Nuclear Agency Washington, DC 20305		12. REPORT DATE 1 May 1983 13. NUMBER OF PAGES 160
14. MONITORING AGENCY NAME & ADDRESS(if different from Controlling Office)		15. SECURITY CLASS. (of this report) UNCLASSIFIED 15a. DECLASSIFICATION/DOWNGRADING SCHEDULE N/A since UNCLASSIFIED

16. DISTRIBUTION STATEMENT (of this Report)

Approved for public release, distribution unlimited.

17. DISTRIBUTION STATEMENT (of the abstract entered in Block 20, if different from Report)

18. SUPPLEMENTARY NOTES

This work was sponsored by the Defense Nuclear Agency under RDT&E RMSS Code S400082466 A99QAXFB00039 H2590D.

19. KEY WORDS (Continue on reverse side if necessary and identify by block number)

Armor Blankets	Armor Designs	Numerical Modeling
Ballistic Armors	Penetration Mechanics	Ceramic
Lightweight Armors	Deformation Mechanisms	Kevlar
Composite Armors	Numerical Code Analysis	

20. ABSTRACT (Continue on reverse side if necessary and identify by block number)

This report describes a theoretical effort using numerical code simulations and supporting test data for the evaluation of potential design concepts to advance the state-of-the-art in lightweight armor technology. The overall program emphasized the investigation of the physical mechanisms and influential material and structural parameters which affect the penetration of lightweight armor. The increased knowledge and understanding gained thereby could then be used to rationally develop improved armor designs.

DD FORM 1 JAN 73 1473 EDITION OF 1 NOV 65 IS OBSOLETE

UNCLASSIFIED

SECURITY CLASSIFICATION OF THIS PAGE (When Data Entered)

20. ABSTRACT (Continued)

The requirements of a very lightweight armor system capable of providing multi-hit ballistic protection against small arms ammunition exceed the capabilities of any single state-of-the-art material. In order to effectively utilize the positive attributes of available materials, a multi-phase armor system with a hard front phase to break-up the projectile and a tough rear phase to arrest residual momentum is necessary. The front phase should incorporate high strength lightweight ceramics, notably Boron Carbide. The preferred primary back phase material is Kevlar fabric.

Disc type ceramic platelets were investigated as a possible front face element which would effectively engage as much mass as possible with the projectile during impact while at the same time providing low areal density and multi-hit capability. These results suggest that if the ceramic material could be made more resistive to tension failure the platelet might hold together long enough to transfer significant amounts of projectile momentum.

The use of biaxial prestressing was considered as a method to enhance the strength of a ceramic front phase. The impact environment was found to be sufficiently harsh to overcome the available prestress. Early failure mechanisms were delayed but major failures eventually developed in the unprestressed orientation and led to ceramic plugging. Thus, additional strength enhancement in the third direction is necessary.

The use of a buffer layer between the front phase and the back phase was also investigated, as there appears to be some potential in using such a buffer to cushion impact of the ejecta from the front phase to the back phase and coat the sharp front face/projectile fragments with a buffer material.

By virtue of the very low amount of front face mass which can be made to interact effectively with the projectile the attainment of a very lightweight armor is a formidable task. It appears that significant improvements relative to current lightweight armors are limited by the low tensile strength and ductility of state-of-the-art front face materials. Therefore, it is recommended that promising avenues for improving these characteristics be actively pursued.

PREFACE

This final report describes a theoretical investigation for potential improvement of ballistic armor blankets performed for the Defense Nuclear Agency (DNA) under Contract DNA001-82-C-0093. An exploratory screening investigation was performed under Contract DNA001-81-C-0268. The U.S. Army Ballistic Research Laboratory (BRL) provided ballistic range test data for correlation and evaluation. The DNA contract technical monitor was Capt. David J. Rehbein.

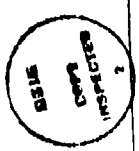

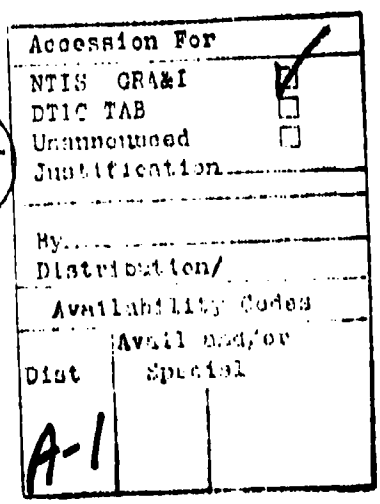

CONVERSION FACTORS

To Convert From	To Metric (SI) Units	Multiply By
feet/second (fps)	meters/second (m/s)	0.3048
inch (in.)	meter (m)	0.0254
kip (1000 lbf)	newton (N)	4448.222
kip/inch^2 (ksi)	mega pascal (MPa)	6.894757
pound-force (lbf)	newton (N)	4.448222
pound-force/inch^2 (psi)	kilo pascal (kPa)	6.894757
pound-mass (lbm)	kilogram (kg)	0.4535924
pound-mass/foot^2 (psf)	kilogram/meter^2 (kg/m^2)	4.882428
pound-mass/foot^3 (pcf)	kilogram/meter^3 (kg/m^3)	16.01846

TABLE OF CONTENTS

LIST OF ILLUSTRATIONS

List of Illustrations (Continued)

List of Illustrations (Continued)

List of Illustrations (Continued)

List of Illustrations (Continued)

List of Illustrations (Continued)

List of Illustrations (Continued)

SECTION I

INTRODUCTION

1.1 BACKGROUND

Protection of critical nuclear and non-nuclear battlefield systems components under circumstances where they could be subjected to impact by small arms ammunition or by high velocity fragments is of the utmost importance to assure their security and survivability. At the same time quick removal of ballistic protection is a key requirement, together with the need for rapid access to systems components protected. Recent research and testing have identified the use of lightweight armor as a potential option to provide this protection. Prototypes of "flexible armor blankets" have been developed, lab tested and subjected to limited feasibility evaluation.

The state-of-the-art in lightweight armor materials technology and possible applications to selected elements of the Theater Nuclear Force (TNF) have been identified in DNA 5631. (Summaries in this report are primarily based on extensive terminal ballistic test data contained in AMMRC-TR-79-10.) It was concluded that the methodology exists for a quantitative evaluation of the protection afforded by lightweight armor and that flexible fabric and ceramic composites show promising potential for improved ballistic effectiveness, if further reduction in weight can be achieved for practical TNF application.

The present program is intended to investigate the mechanisms by which such armor potential could be exploited.

Understanding the deformation mechanisms involved in the penetration of targets by projectiles is important in effectively designing an armor system with minimum areal density to defeat a projectile. It will be necessary to identify the essential material and structural properties and their relation to the mechanics of penetration in order to achieve this design goal.

The general objective of the program is to advance the state-of-the-art of lightweight armor technology for application to the protection of TNF systems components. The program emphasizes the theoretical investigation of the physical mechanisms and influential material and structural parameters involved in the penetration of lightweight armor. The increased knowledge and understanding gained thereby could then be used to develop improved armor designs.

1.2 STATE-OF-THE-ART

Extensive ballistic testing during the past few decades has provided terminal ballistic data (e.g., AMMRC-TR-79-10) for various homogeneous and composite armor materials. Each material has certain attributes and limitations. The following are identified as desirable attributes of candidate lightweight armor materials:

- Ballistic Protection: from hard-steel kinetic energy ammunition and fragments up to caliber .30 in size

- Weight Efficiency: threat protection with minimum weight less than 5 psf

- Multi-Hit Capability: maintain penetration resistance performance to within 3 calibers of previous impact

- No Rear Surface Spallation: threat protection without rear surface spallation or scabbing

Lightweight protection against hard-steel cored armor-piercing (AP) ammunition requires the combination of hardness and toughness. The hardness of the armor degrades the AP projectile penetration effectiveness by initiating projectile break-up. Once the AP projectile is shattered, the residual projectile and fragments must be constrained by the armor material toughness.

Metallic-metallic composites (e.g., dual-hardness steel) can be designed to produce the necessary combination of hardness and toughness, but offer little hope of meeting strict armor weight requirements without compromising multi-hit capability or rear surface spallation. Even metallic-fabric or metallic-plastic composites (e.g., hardened steel backed up by Kevlar laminate) require areal densities of more than ten pounds per square foot (10 psf).

Weight-critical armor systems look to ceramic composites to achieve maximum protection at lowest total weight (less than 10 psf). These composites present to the steel cored AP projectile an extremely hard surface (e.g., Boron Carbide, B_4C) which causes projectile break-up and a momentum trap of resin-bonded Kevlar backup material which restrains the residual fragments. However, an unconfined ceramic front plate has limited multi-hit capability, especially at low areal density.

1.3 APPROACH

As armor requirements become more severe, candidate designs become more complex, and now include woven fabrics as well as composite materials incorporating various proportions and geometric arrangements of different constituents. The design of such materials involves a large number of parameters. In this situation, there is a need for a greater understanding of the key mechanisms and interactions involved and the influence of the material and geometric parameters in defeating projectiles and fragments.

Such understanding can come from interpretation of ballistic test data trends as the parameters are varied, but this approach is often limited because of the costs of fabricating prototype materials and the difficulty in independently varying parameters. Ballistic range data need to be supplemented by dynamic observations of the phenomena occurring (e.g., using flash radiography and ultra high speed photography) and by physical theory.

Theoretical analyses utilizing finite difference and finite element models supported by test data will be the primary investigative procedure for providing insight and information which will be needed to judge the potential effectiveness of blanket armors, and to select materials and composite constructions for use in such armors.

The numerical code techniques to be used have been validated by extensive experimental comparisons in a number of directly related applications, and have been specifically adapted for efficient treatment of penetration problems:

- They treat realistic, non-ideal, non-linear conditions and properties.

- They provide detailed information which gives direct insight into the dynamic processes involved, including the evolution of these processes and determination of the armor material properties and penetrator parameters which affect these processes. Such information is very difficult to obtain from terminal ballistic experiments.

- They can be used to evaluate the effects of making changes in material properties and composite material constructions, before expensive fabrication of such materials is undertaken.

It should be noted that the accuracy of numerical solutions of penetration problems is limited by the imperfect knowledge and modeling of material properties in stress-distortion-time regimes where property measurements are difficult or impractical to make, particularly with respect to failure and post-failure characteristics. Because of this limitation, one should be cautious about depending on quantitative results of penetration solutions. The codes are much more useful, and reliable in exposing phenomena and mechanisms, and in predicting trends when parameters are varied. For these applications, exact knowledge of the material properties is less important.

The overall approach consists of a coordinated effort of analytical modeling, numerical simulations and concept evaluation. This approach would use first principle analysis to understand physical processes and geometric factors which control these processes and ballistic range tests from the U. S. Army Ballistic Research Laboratory (BRL) to provide dynamic observations for correlation and evaluation.

SECTION II

POTENTIAL DESIGN CONCEPTS

The design of a very lightweight (less than 5 psf) armor system capable of defeating a hard-steel cored caliber .30 armor piercing projectile is a formidable task. The design requires the innovative use of materials (metals, ceramics, fabrics), construction and material formation processes (quenching, thermal stress, microcomposites and prestress) and geometry (sandwich systems, buffers, air gaps, inclusions). The basic materials and their relatively straightforward applications to lightweight armor have been identified, tested and analyzed [1-5]. Ideally, for a lightweight armor design to be effective, the armor materials should have several different mechanical properties in addition to low density:

1. High bulk and shear moduli. (A very stiff lightweight material resists deformation and radiates impact stresses very quickly.)

2. High yield stress in compression. (A very high compressive yield material directly at the impact site will cause the threat to yield first and flow or shatter without damaging the armor.)

3. High stress in tension. (Compressive stress waves are always reflected off of free surfaces as tensile waves. Thus, a high tensile strength is required to maintain armor integrity in areas where reflections occur.)

4. Excellent ductility and resistance to fracture. (Once inelastic material behavior occurs it is important that the damage be stable and confined to the impact area, if multi-hit armor resistance is to be maintained.)

Many materials possess one or more of these characteristics; none possesses all of them. A number of metals possess relatively high mechanical properties, but suffer from high density. Steel and aluminum weigh 40.5 psfi and 14.5 psfi, respectively (psfi denotes pounds per square foot per inch of plate thickness). Beryllium and magnesium are exceptions, with weights of ∿9.5 psfi but beryllium is rather brittle, magnesium has marginal strength properties, and both have safety problems.

Ceramics are generally lightweight (10-20 psfi) with excellent compressive stiffness and strength properties, especially when subjected to confining pressures. Unfortunately, ceramics tend to be brittle and to have low strength and ductility in tension. A notable exception is tungsten carbide (WC) which has very good tensile properties but at the cost of a very high density (∿70 psfi).

Fabrics, especially those woven from Kevlar [5], appear to possess very good momentum resistance provided the projectile or fragment is blunt enough so perforation is not a problem and the fabric is allowed to deflect significantly during impact. Kevlar is very lightweight (7.5 psfi) and has a very high tensile strength (410×10^3 psi).

Since no material possesses all of the characteristics required to develop a lightweight armor, the only alternative is to use several materials in order that the positive characteristics

of each material may be combined to produce an effective armor system. The composite armor concept has been widely used to combine materials.

Two-layer plate armor design concepts have been previously explored [5] in which a ceramic front plate and an aluminum or fabric back plate are bonded together. This design, which is successful against a single caliber .30 AP threat, weighs less than 10 psf, but more than the 5 psf level.

Based on this work it is clear that ceramic plate armors on the order of 5 psf cannot survive the impact, even with very good back support and further, that multi-hit resistance is limited. Thus, in order for a 5 psf armor to be designed capable of defeating multi-hit threats, a more complex armor concept must be developed.

In general, a multi-phase composite system should be designed so that the specific mechanisms required to defeat the projectile are assigned to each phase. Thus, for a two-phase system, see Table 2.1 and Figure 2.1, the basic concepts, by phase, are: (1) a hard front composite phase to blunt the nosetip and initiate breakup of the projectile, and (2) a tough back composite phase which is capable of arresting the residual fragments.

This two-phase system is intended to serve primarily as a framework for discussion of lightweight armor concepts. For example, it may be preferrable to design a front phase as an assembly of platelets, each of which could have special strength properties developed by prestress or manufacturing process control. The platelets would be individually damaged by

Table 2.1. Two-Phase Composite Armor Design.

Armor Phase	Primary Purpose	Key Properties	Candidate Materials
Front	Projectile Breakup	Hardness, Stiffness	B_4C Encased in Kevlar
Back	Momentum Trap	Toughness, Flexibility	Al. Honeycomb over Kevlar

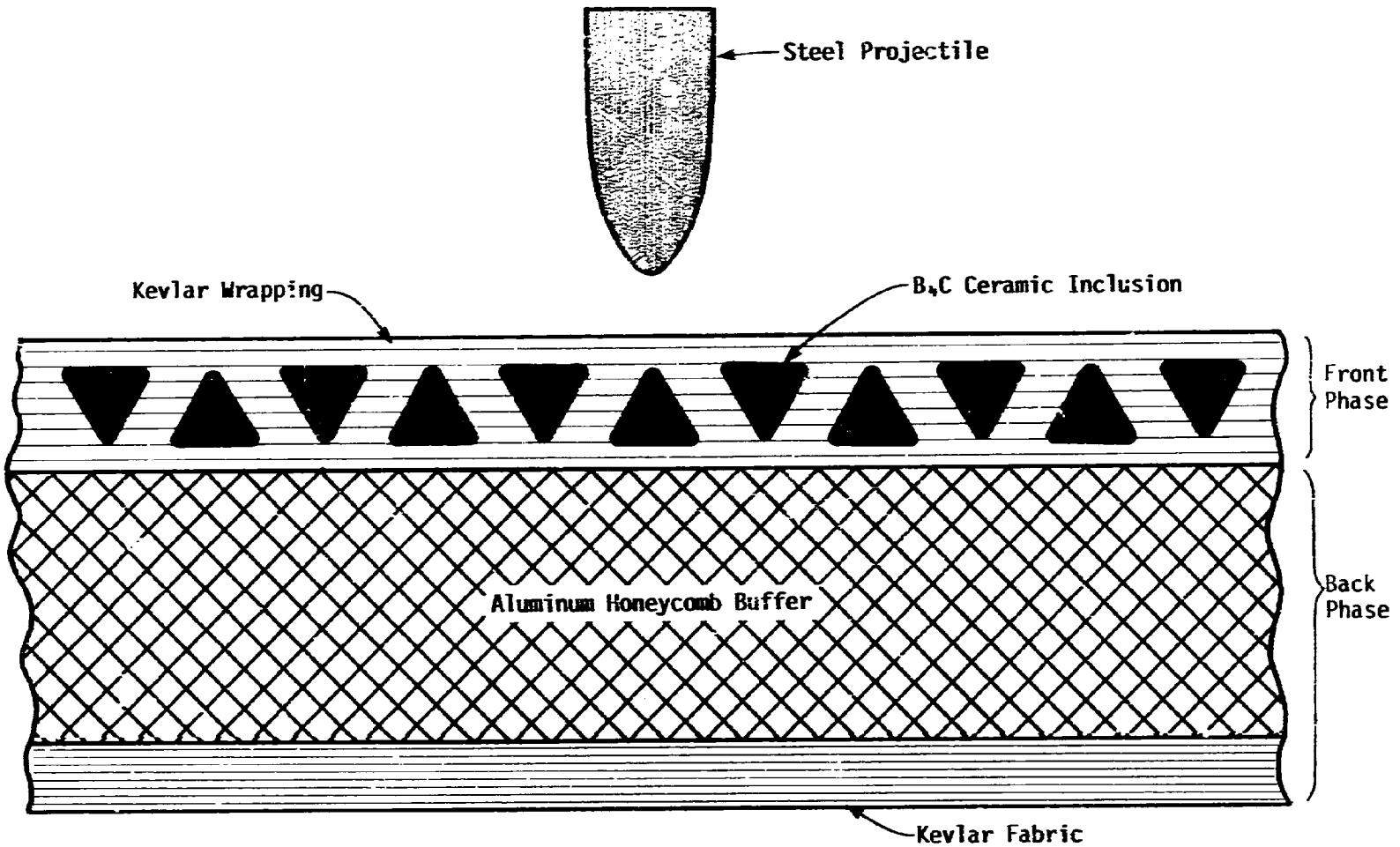

Figure 2.1. Schematic of Two-Phase Composite Armor Design Concept.

projectile impact, but the damaged region would be confined to individual platelets. Another possibility could be a composite plate made of very hard inclusions imbedded in a ductile matrix material. The consideration of a buffer region with honeycomb or felt materials may be useful in providing some control or conditioning of ejecta from the front phase. The final back layer could be developed from several different design philosophies, such as plate flexibility or rigidity, and could involve a number of different materials, including Kevlar, metals and composites.

Generally, the use of metals imposes high weight penalties when designing very lightweight armor (unless used as a honeycomb or interfacing material) so that ceramic and fabrics emerge as the primary materials for consideration. The basic response and failure mechanisms of these material is presented in Section III.

From past experience [1] it is clear that if a thin ceramic plate is to perform satisfactorily, it must be strengthened or reinforced in some manner. The use of prestress to enhance the strength of ceramics would appear to have some promise. The prestress can be thermally induced (by assembling a metal/ceramic armor at high temperature and then cooling the composite) or mechanically induced (by wrapping ceramic with high strength fibers such as glass or Kevlar). In either case, a biaxial compressive initial stress is induced in the ceramic, with attendant improvements in material strength against impact stresses. The use of prestress as a strengthening mechanism is analyzed in detail in Section IV.

Other front phase concepts involve the use of hard inclusions imbedded in a lightweight matrix or an assembly of

platelets. Research on other armor-related programs has shown that mass (in addition to hardness) is an important parameter in defeating a projectile by forcing material failure or deflecting the projectile and reducing its penetration effectiveness. With careful design, it may be possible to exploit mechanisms unique to discrete systems (such as projectile riccochet or deflection) in the 5 psf range. These concepts are analyzed in Section IV.

Recognizing that the very low density front phase will not be capable of totally defeating the threat, a backup system must be developed capable of arresting the ejecta from the front phase. As noted in Figure 2.1, the use of a buffer material can provide some benefit. First, the buffer material absorbs impact stresses and the damaged buffer material cushions the ejecta. Also, the buffer transmits impact stresses into the back plate and thus provides a precognition of the incoming fragments. Ordinary metallic honeycombs appear to be good choices for this layer.

The actual backup layer should be as soft and ductile as possible in order that the ejecta from the front phase be decelerated and defeated without penetrating the back layer. Kevlar 29 fabric is regarded as most preferable based, in part, on its extensive use and acceptance as a lightweight body armor. This material possesses exceptionally high tensile strength and is able to respond to impulsive loadings very rapidly due to high wave speed in the material. Kevlar fabric is flexible and able to undergo very substantial deformation without perforation or tearing provided the actual fibers are not sheared by sharp fragments. The response of a combined buffer/back layer system consisting of honeycomb buffer and Kevlar back layer is investigated numerically in Section V.

SECTION III

MODELING OF CANDIDATE MATERIALS

As indicated in Section II, the general two-phase design concept involves a hard front phase to blunt and shatter the projectile and a tough back phase to arrest the residual fragments. The basic state-of-the-art lightweight material for the front phase is ceramic (Boron Carbide) and for the back phase is fabric (Kevlar).

In this section a general modeling procedure of numerical analysis is used to demonstrate established response and failure mechanisms in Boron Carbide (B_4C) and Kevlar. This analysis will provide a baseline for the evaluation of design concepts in subsequent sections.

3.1 NUMERICAL MODELING

The basic numerical modeling procedure involves an explicit Lagrangian finite difference computer program, WAVE-L. This computer program has been extensively employed [6,7] to investigate nonlinear impact and penetration physics. As such, it is an excellent tool for defining major mechanisms governing lightweight armor behavior in the impact environment.

For many problems of this type, the most important and difficult aspect of conducting the numerical analysis is defining mathematical material models capable of effectively (and efficiently) capturing dominant physical processes. The most completely developed models are for metals which (assuming some ductility) fall within the realm of conventional elastic-plastic

material behavior. Physical properties for ceramic and fabric based materials are more difficult to establish due to variations in manufacturing procedures, assembly and quality control. For the purpose of the present analysis, rather general material models capable of capturing the dominant aspects of material behavior are appropriate.

Ceramic

In a ceramic material, the dependence of the yield strength on mean pressure, high strength in compression and rather low strength in tension results from yield/failure of the type shown in Figure 3.1. The surfaces, based on B_4C data [2], are typical of several high strength ceramics. In Figure 3.1, failure is reached only after surface cracks occur on three orthogonal faces. The material is assigned elastic constants $E = 51 \times 10^6$ psi and $\nu = .2$ and a density $\rho = 156$ pcf.

In addition to shear plastic flow, the ceramic is assumed to be susceptible to tensile fracture, defined to be when a maximum principal stress reaches 50 ksi after a small amount of plastic flow based on a critical strain energy release rate. This model is reasonably simple and yet retains the dominant mechanisms governing inelastic behavior and material failure.

Kevlar

Kevlar [8,9] is a lightweight material, $\rho = 90$ pcf, with a very high tensile yield (and failure) stress of 410 ksi. The shear stress/strength characteristics are defined by the manner in which the fibers are woven or wound and bonded together. For a typical biaxial Kevlar composite material the shear stiffness

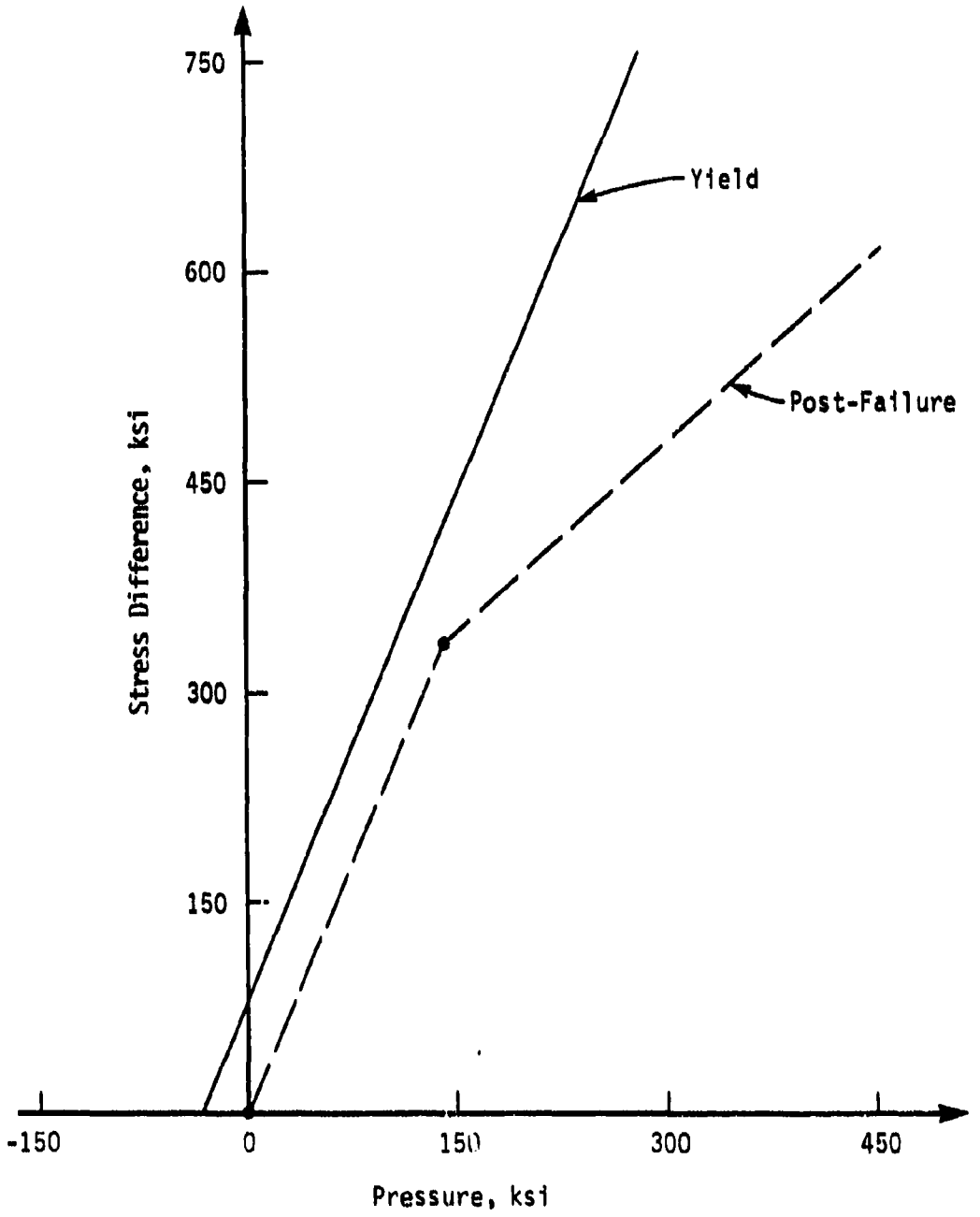

Figure 3.1. Yield and Failure Surfaces for Typical Ceramic.

is strongly influenced by the bonding agent or matrix material. As this shear stiffness is much less than that for Kevlar an orthotropic material model was developed. This gives low shear and compressive stiffness and yet maintains a high tensile modulus in the fiber directions.

Steel

A high strength steel is used with elastic properties $E = 30 \times 10^6$ psi and $\nu = .3$ and a density $\rho = 480$ pcf. The material has a yield of 250 ksi and an ultimate strength of 285 ksi. The material is represented as an elastic, isotropic work hardening plastic material.

3.2 CERAMIC PLATE RESPONSE

To demonstrate the dominant mechanism in thin ceramic target response and validate the ceramic material model, a 5 psf ceramic target is impacted by a .0132 lbm caliber .25 steel-core projectile with a 2500 fps impact velocity. The response of the target is shown in Figures 3.2 - 3.8 to 16 μsec. At these early times the mechanisms required to defeat the ceramic are all present, namely

1. The development of damage directly below the projectile, Figure 3.2 at 1.5 μsec.

2. The generation of circumferentially failed region on the rear surface, Figure 3.3 at 3.5 μsec.

3. The propagation of a conical fracture region, Figure 3.4 at 6 μsec.

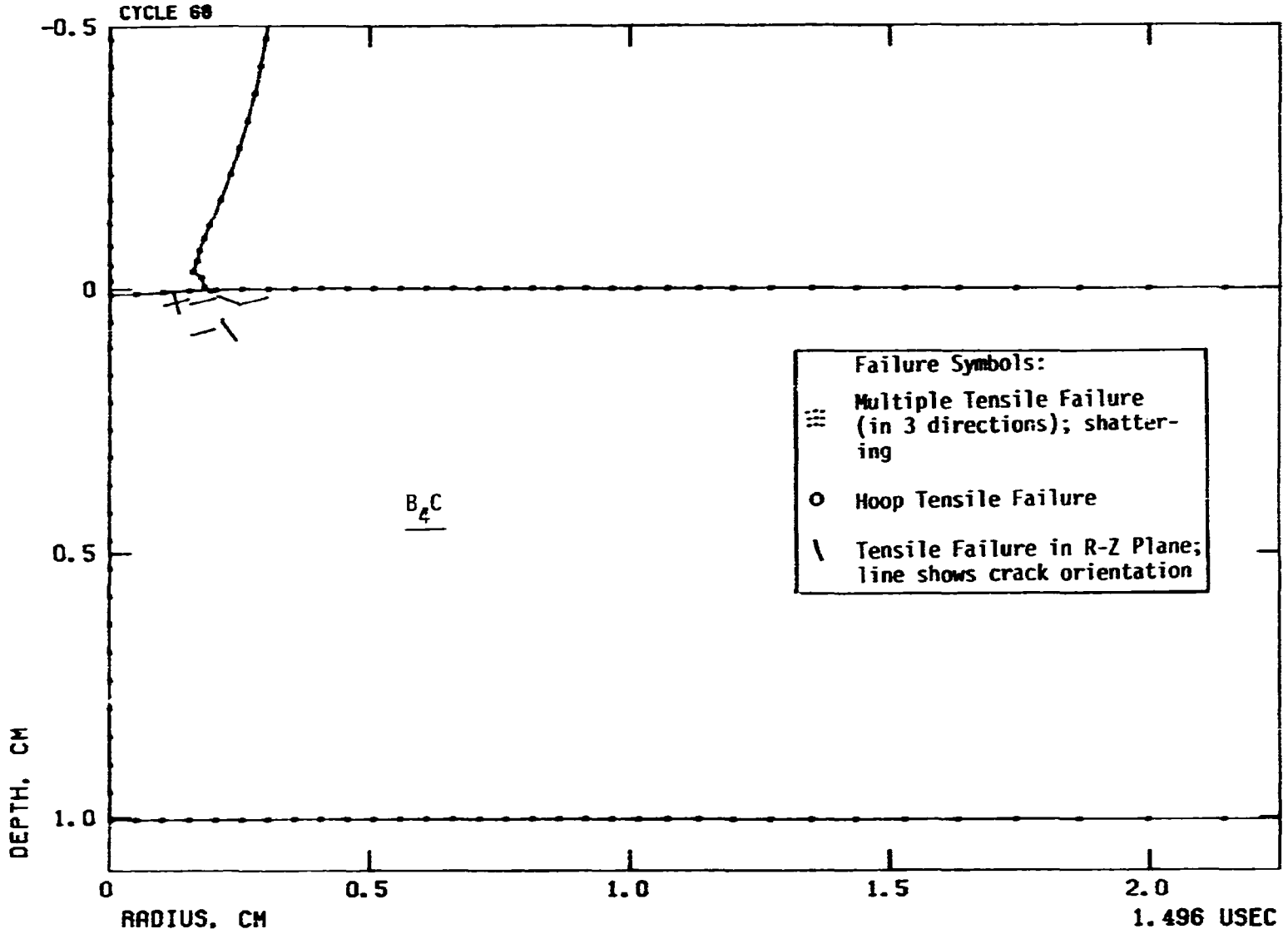

Figure 3.2. Damage in Ceramic Plate at t = 1.5 μsec.

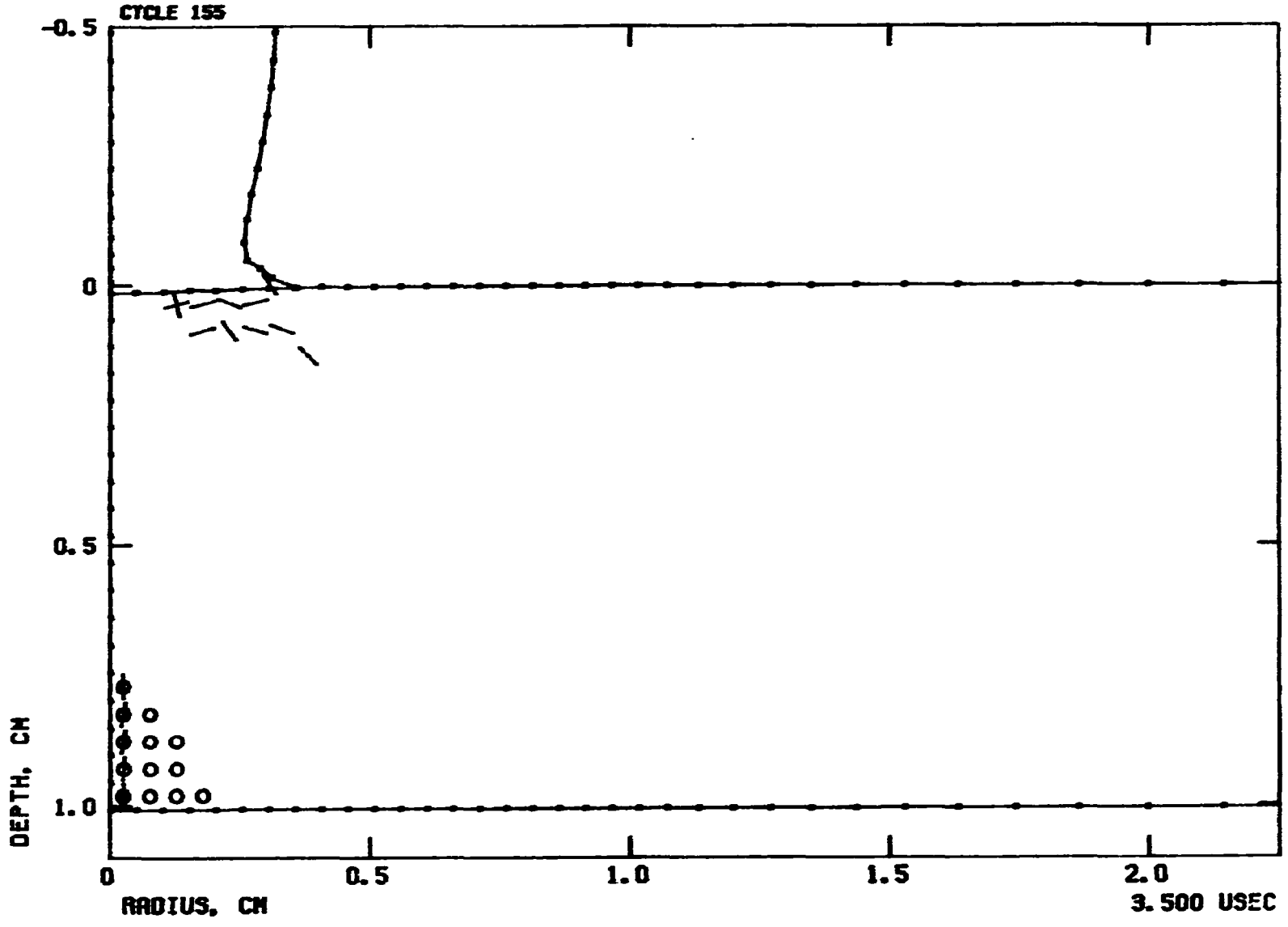

Figure 3.3. Damage in Ceramic Plate at t = 3.5 μsec.

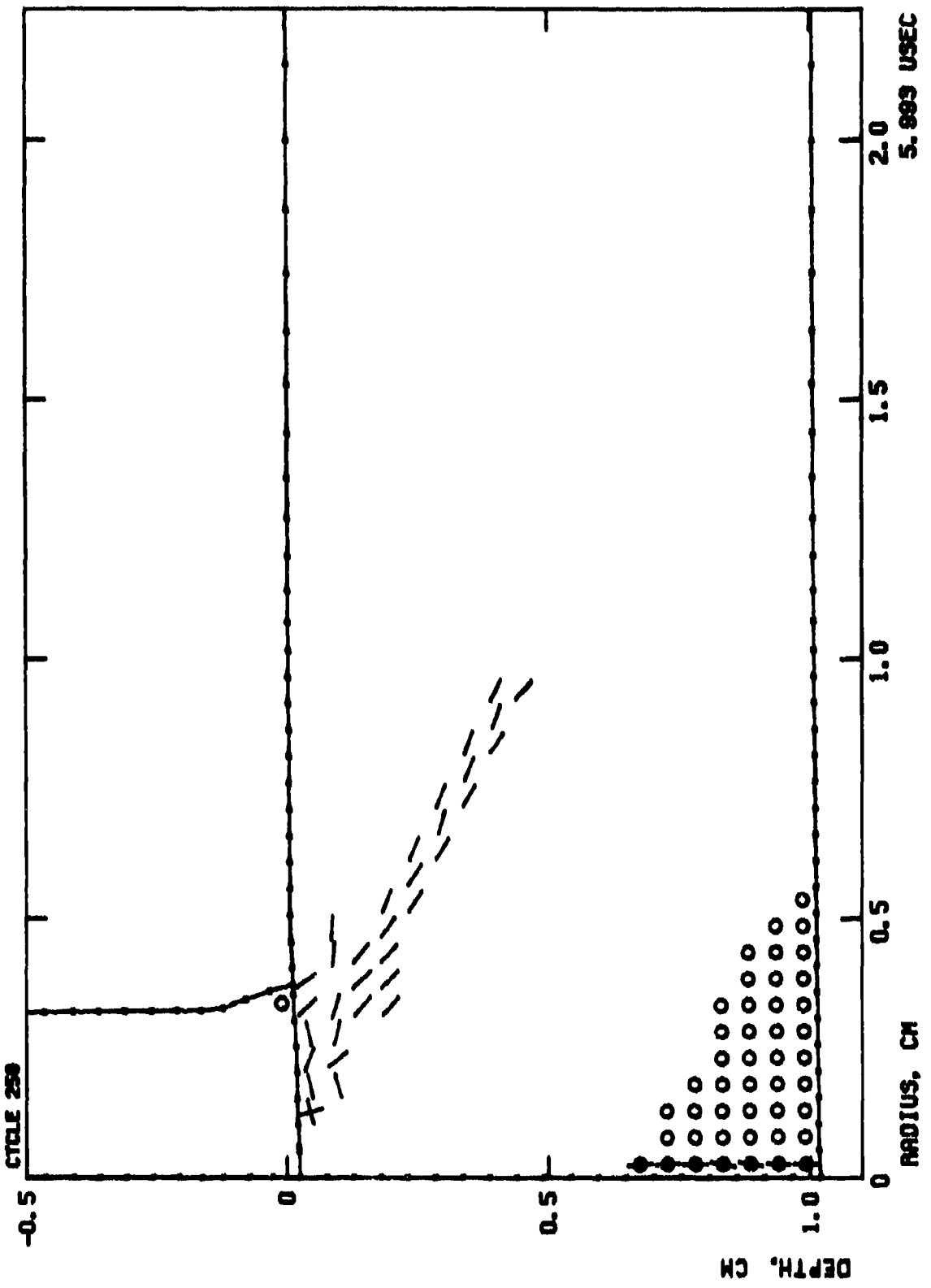

Figure 3.4. Damage in Ceramic Plate at t = 6.0 μsec.

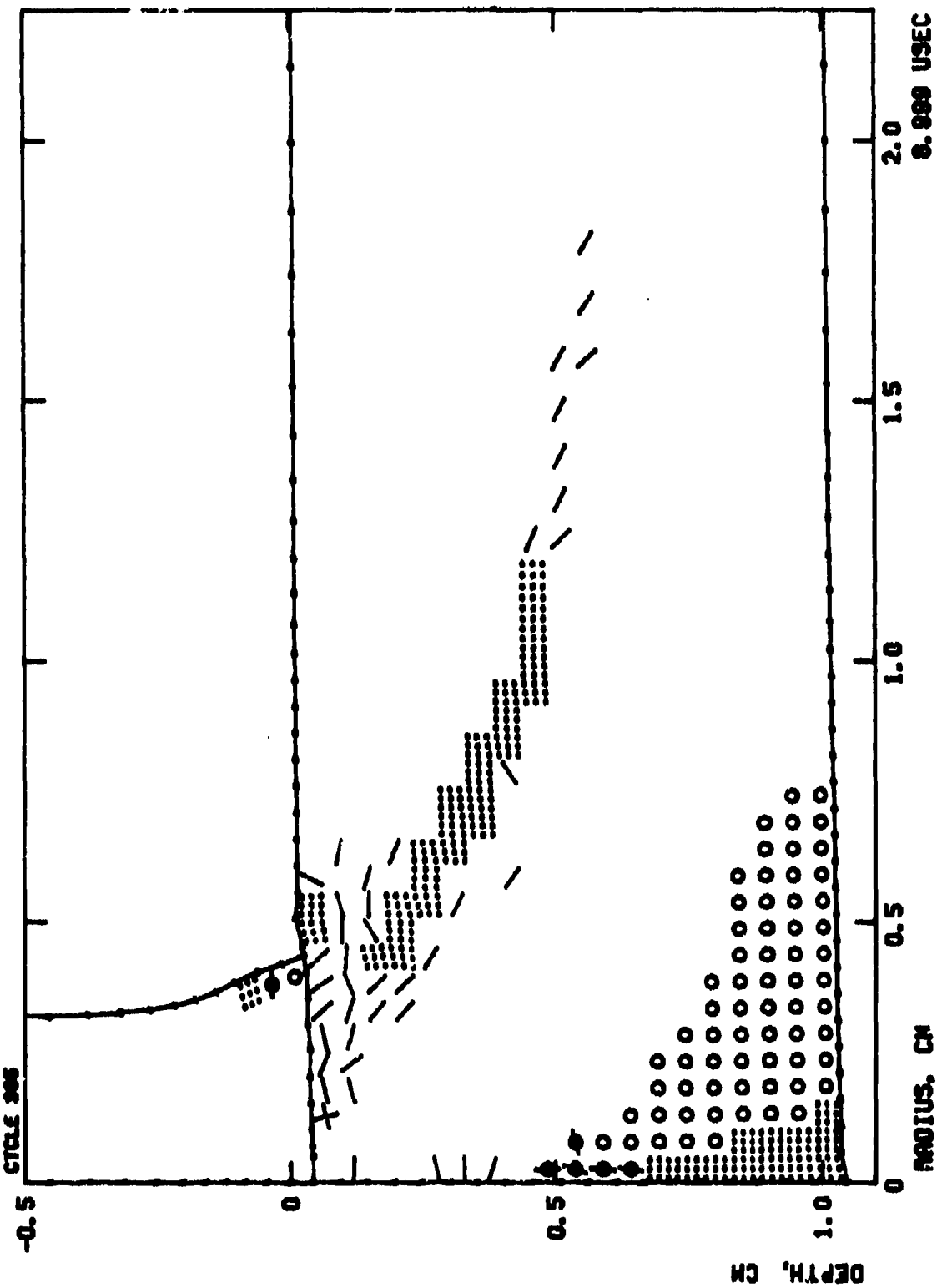

Figure 3.5. Damage in Ceramic Plate at t = 9.0 μsec.

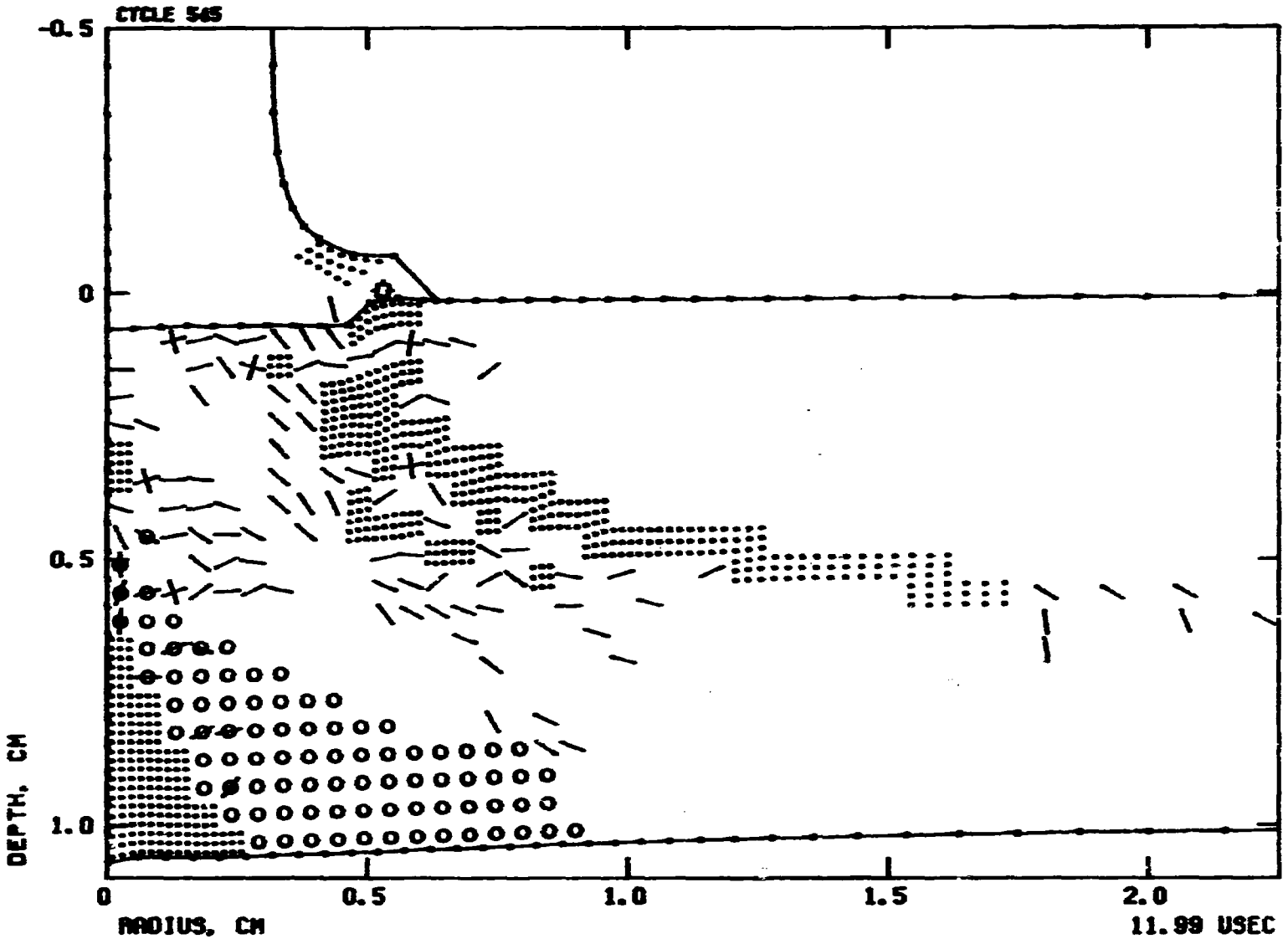

Figure 3.6. Damage in Ceramic Plate at t = 12.0 μsec.

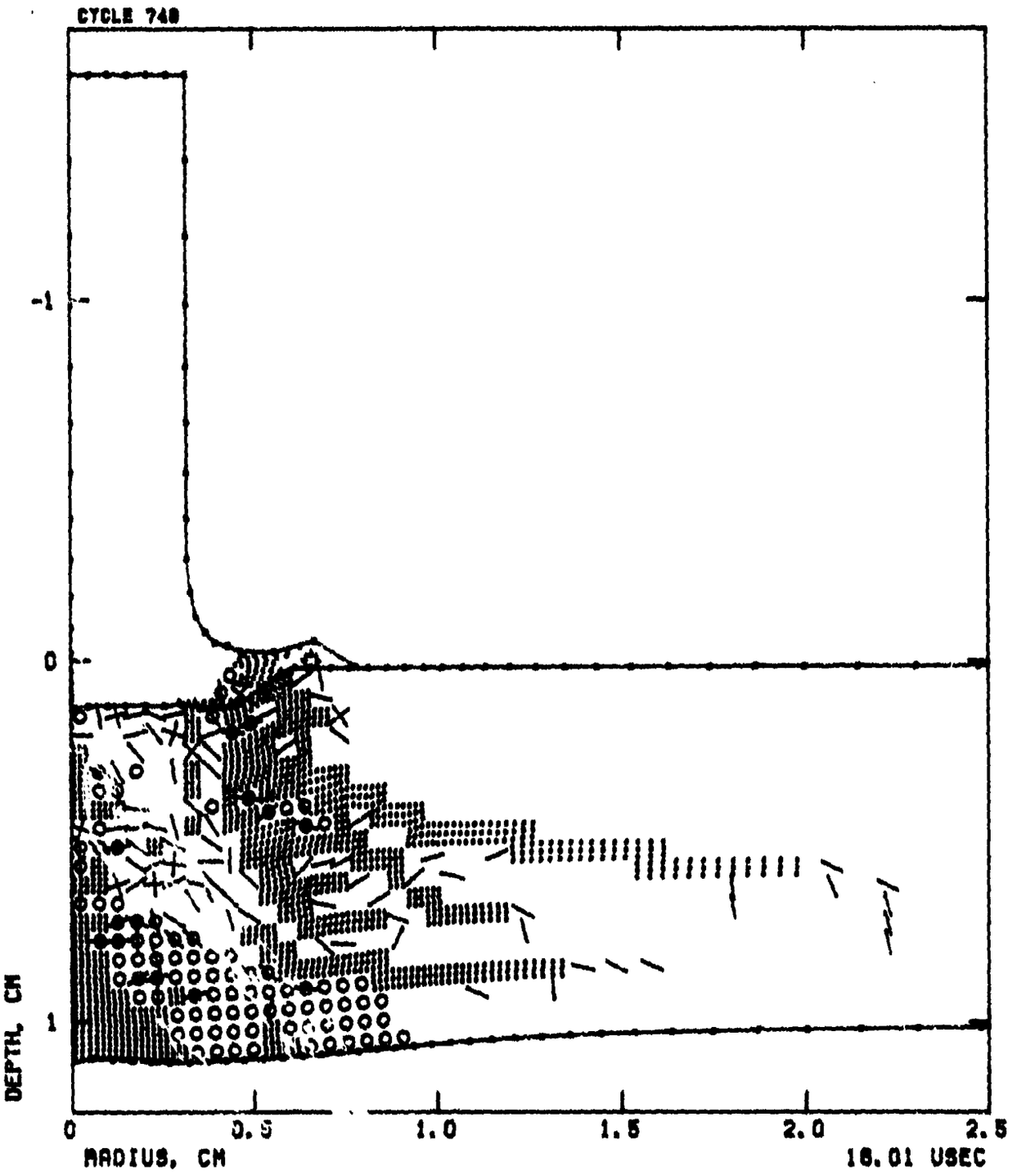

Figure 3.7. Damage in Ceramic Plate at t = 16.0 μsec.

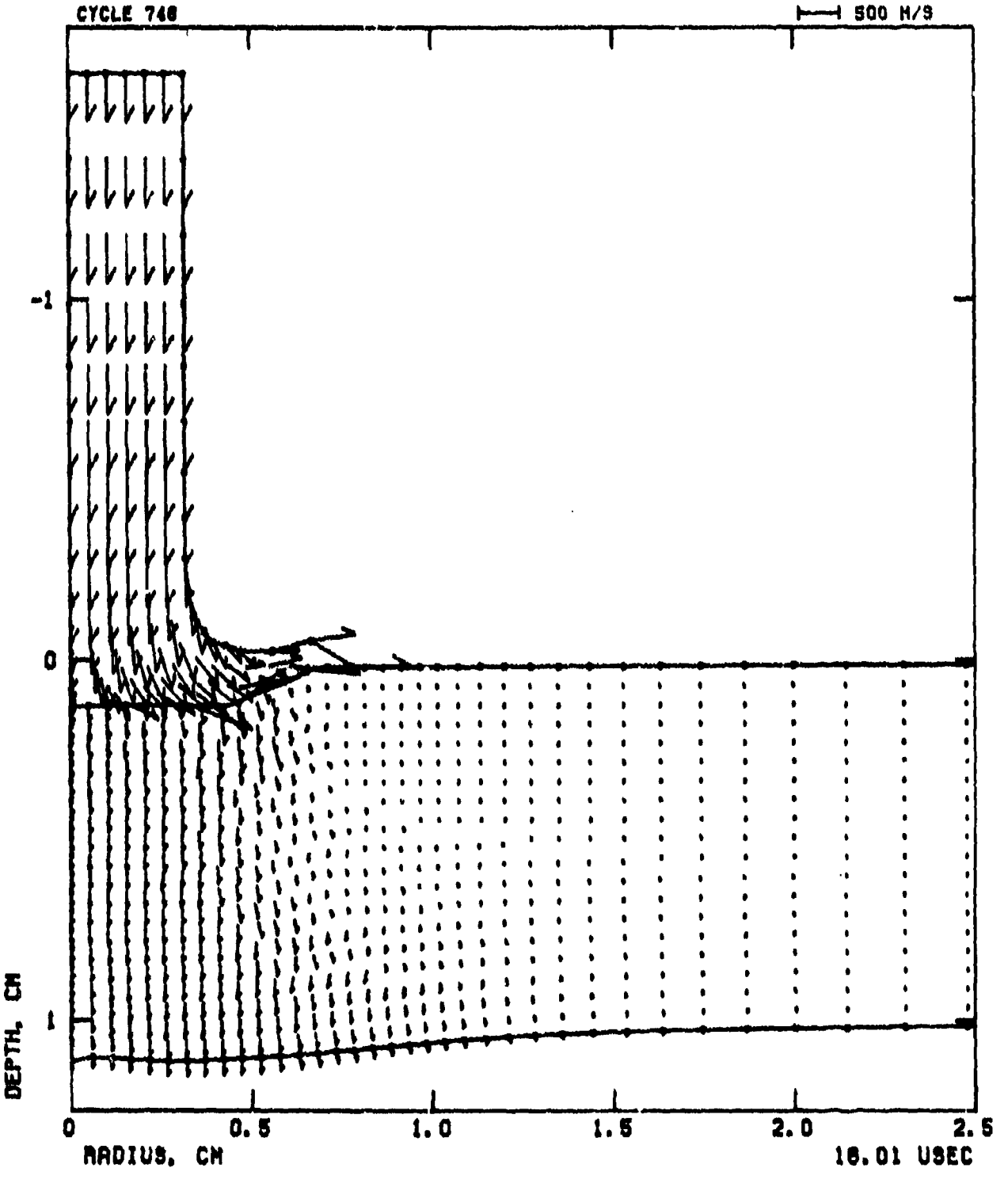

Figure 3.8. Velocity Field in Ceramic Plate at t = 16.0 μsec.

4. The general breaking up of the conical region, Figure 3.5 at 9 μsec, and coalescence with cracks from the rear surface, Figure 3.6 at 12 μsec.

5. The formation of a shear plug, Figures 3.7 and 3.8 at 16 μsec, with roughly the diameter of the blunted projectile.

These classical failure mechanisms are well known and have been confirmed experimentally [4].

It is evident that to increase damage to the projectile the ceramic failure mechanisms must either be delayed or eliminated. If the primary damage does not lead to a reduction in compressive strength, the projectile would continue to encounter a high compressive stress field. For example, if the fracture conoid could be delayed by increasing the tensile strength of the material, the ceramic would more effectively maintain its support at the impact point.

Failure directly under the projectile would be delayed if the material in this region were highly confined, as would be the other mechanisms. This is evident by reviewing the ceramic yield surface of the ceramic. Clearly, if the reference state were at high pressure, the change in stress required to achieve yield would be much larger. Alternatively, if a material were to be developed with a yield surface which extended well into the tensile range ($p < 0$), the same effect would be realized.

The presence of fracture surfaces makes unprotected, damaged ceramic front plates very sensitive to multi-hit threats.

Clearly, if at all possible ceramic front plates must be protected by more fracture resistant confining materials.

3.3 CERAMIC/KEVLAR PLATE RESPONSE

Consider the impact process of the caliber .25 steel-core on a scaled-down state-of-the-art armor system. This target consists of a .25-in. thick ceramic plate backed by .25-in. of Kevlar fabric, which results in an areal density of 5 psf.

The progression of the calculated impact response is pictured in Figures 3.9 to 3.18. Very early in the solution, Figures 3.9 to 3.11, the shock front can be seen expanding outward from the point of impact, initially with spherical symmetry. Upon encountering the Kevlar backing, this symmetry is lost as the bottom of the wave front slows due to the low transverse wave speed in that material. The area of the wave front increases with the square of the distance through which it expands. For this reason the intensity of the compressional stress wave decays at this rate. Additionally, yielding in the ceramic reduces the stress environment further through plastic dissipation. The decay in stress with distance from the point of impact can be seen clearly in Figure 3.10.

As the wave front expands, the ceramic it encounters begins expanding radially outward from the impact point. Thus, material on the impact axis moves straight down while material off the axis has a component of velocity in the radial direction away from the impact axis. The resulting motion causes radial and hoop tensile stresses to develop on the axis, expecially at the back surface. By 1.5 μsec the ceramic tensile strength is exceeded and back surface cracking initiates, Figure 3.12. The

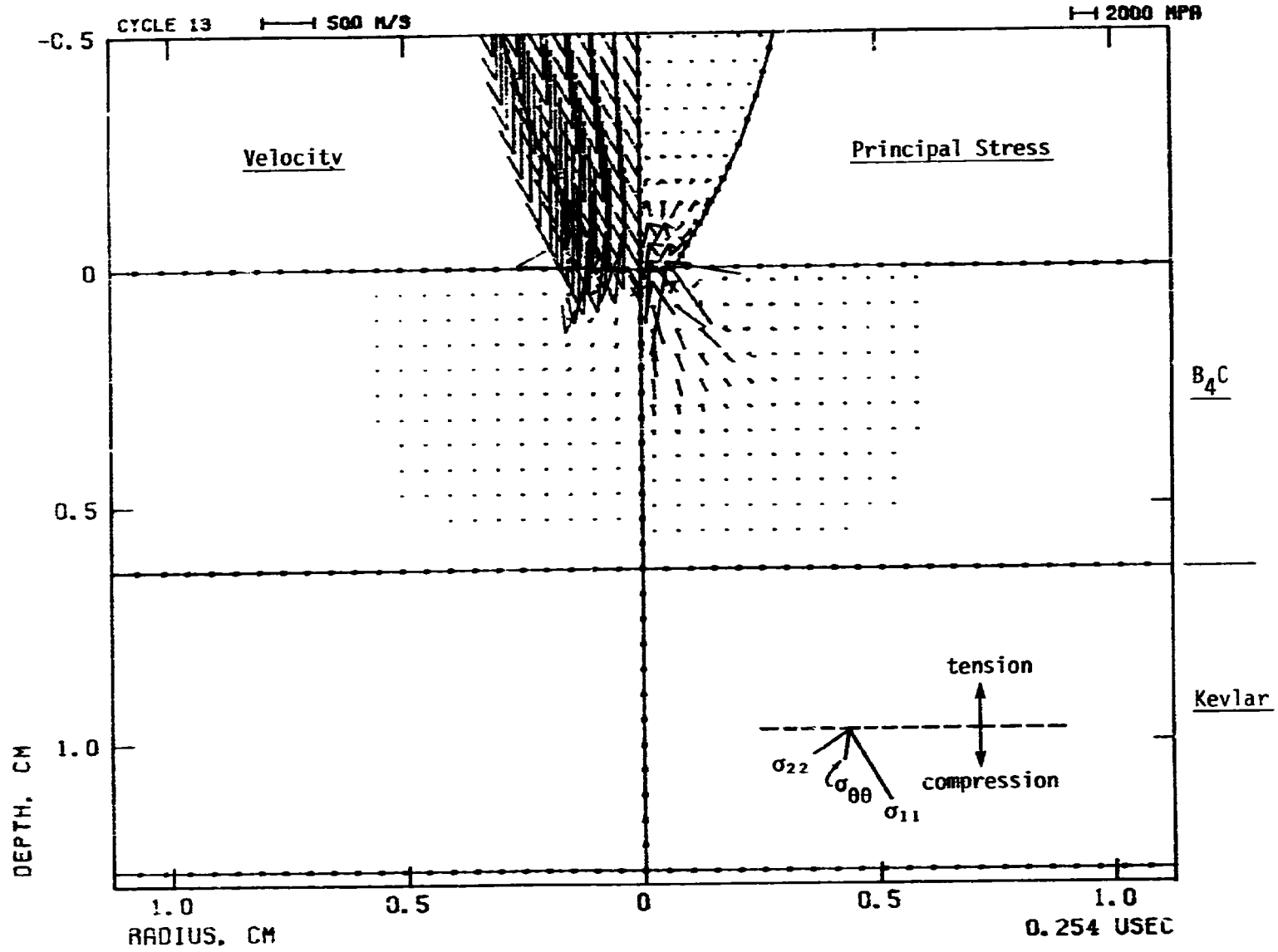

Figure 3.9. Velocity and Stress Fields in Ceramic/Kevlar Target at t = .25 μsec.

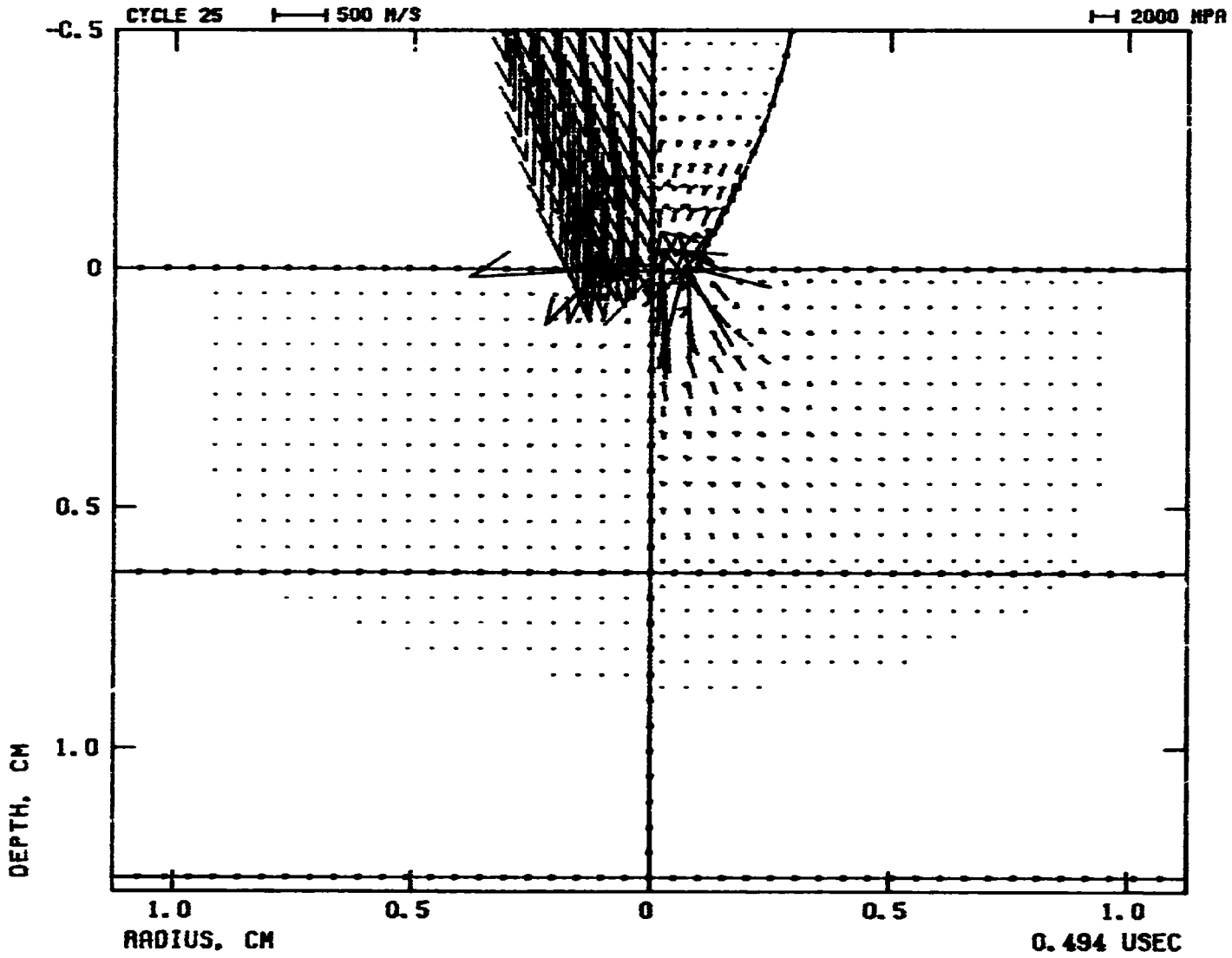

Figure 3.10. Velocity and Stress Fields in Ceramic/Kevlar Target at t = .5 μsec.

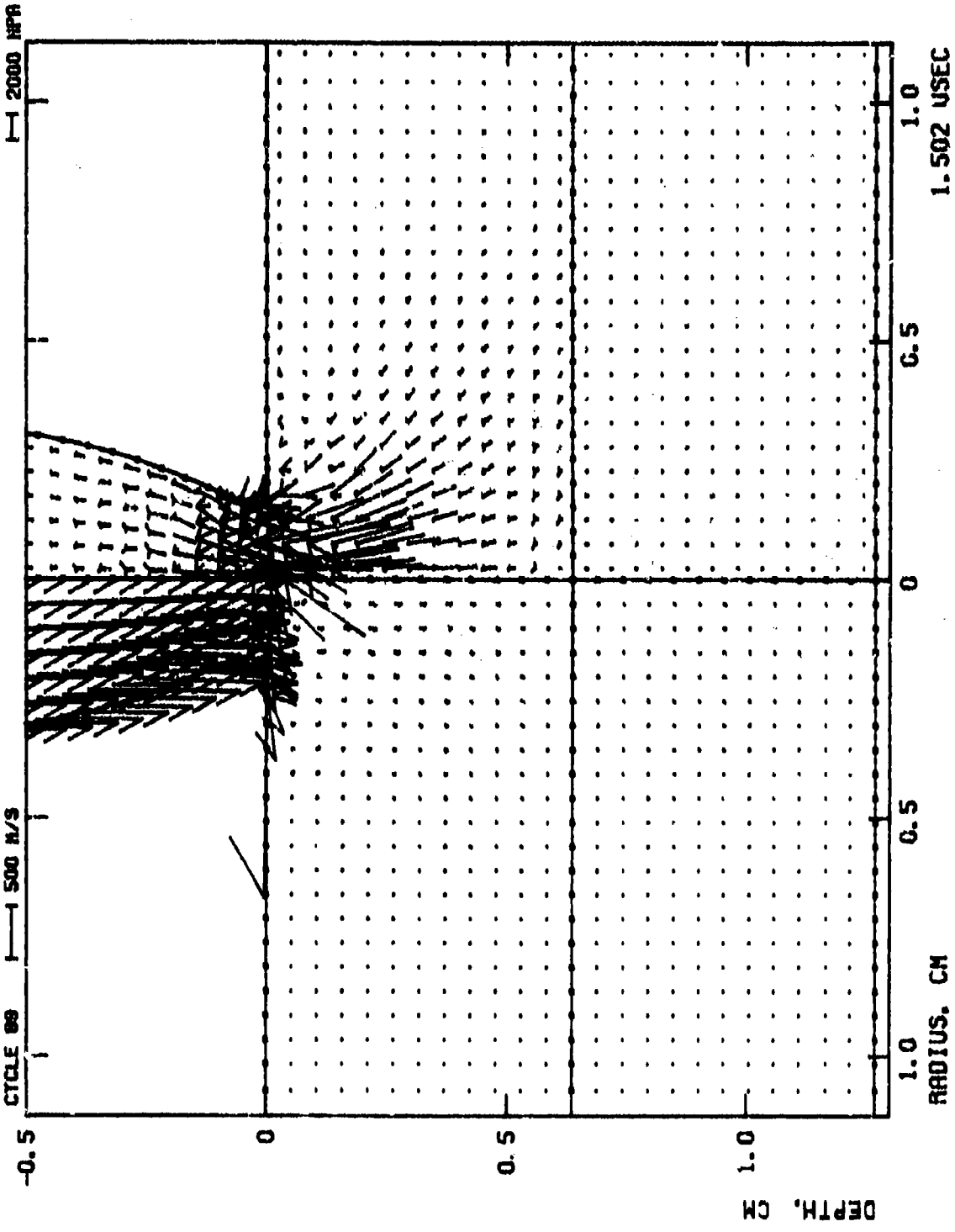

Figure 3.11. Velocity and Stress Fields in Ceramic/Kevlar Target at t = 1.5 μsec.

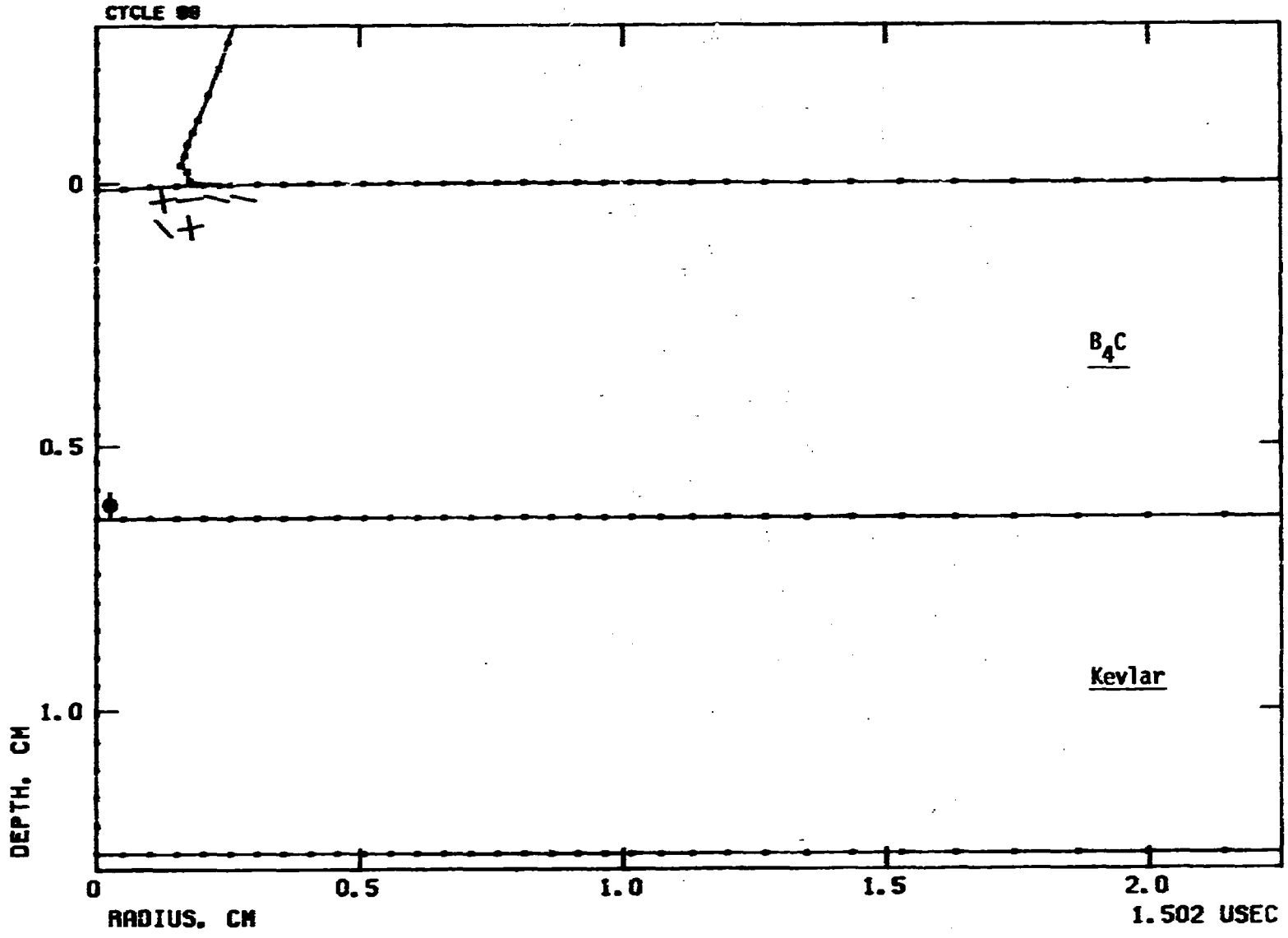

Figure 3.12. Damage in Ceramic/Kevlar target at t = 1.5 μsec.

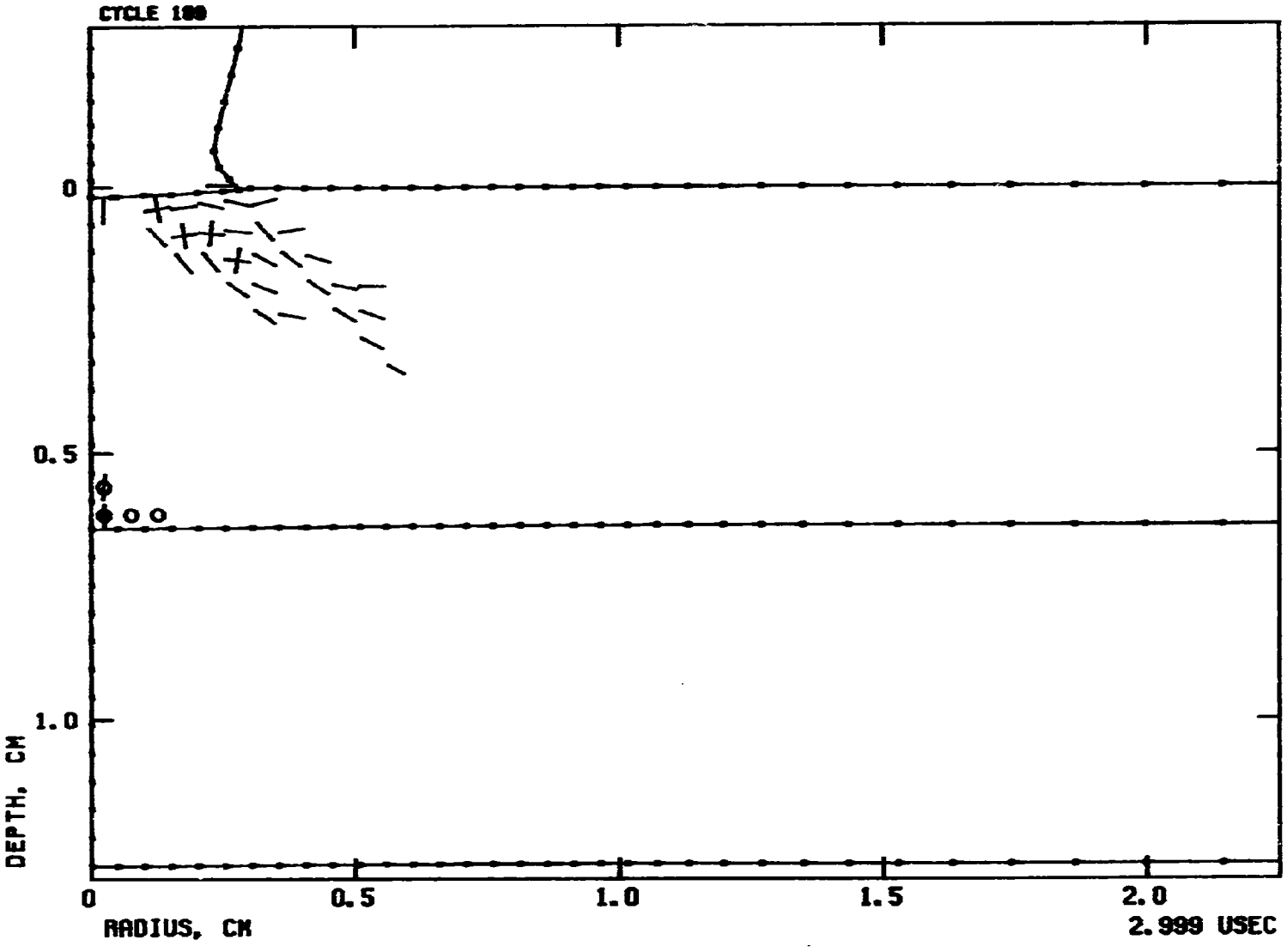

Figure 3.13. Damage in Ceramic/Kevlar Target at t = 3.0 μsec.

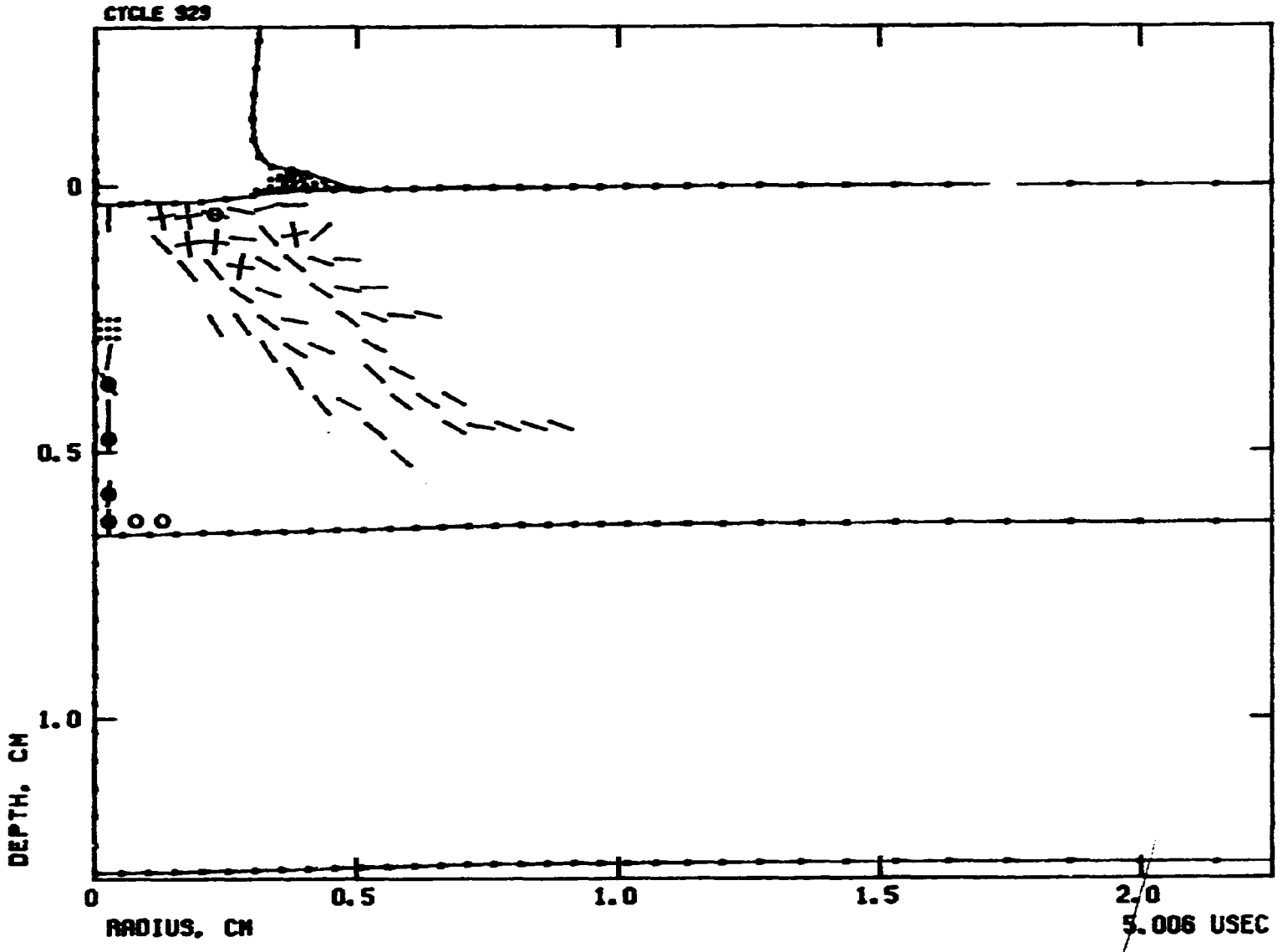

Figure 3.14. Damage in Ceramic/Kevlar Target at t = 5.0 μsec.

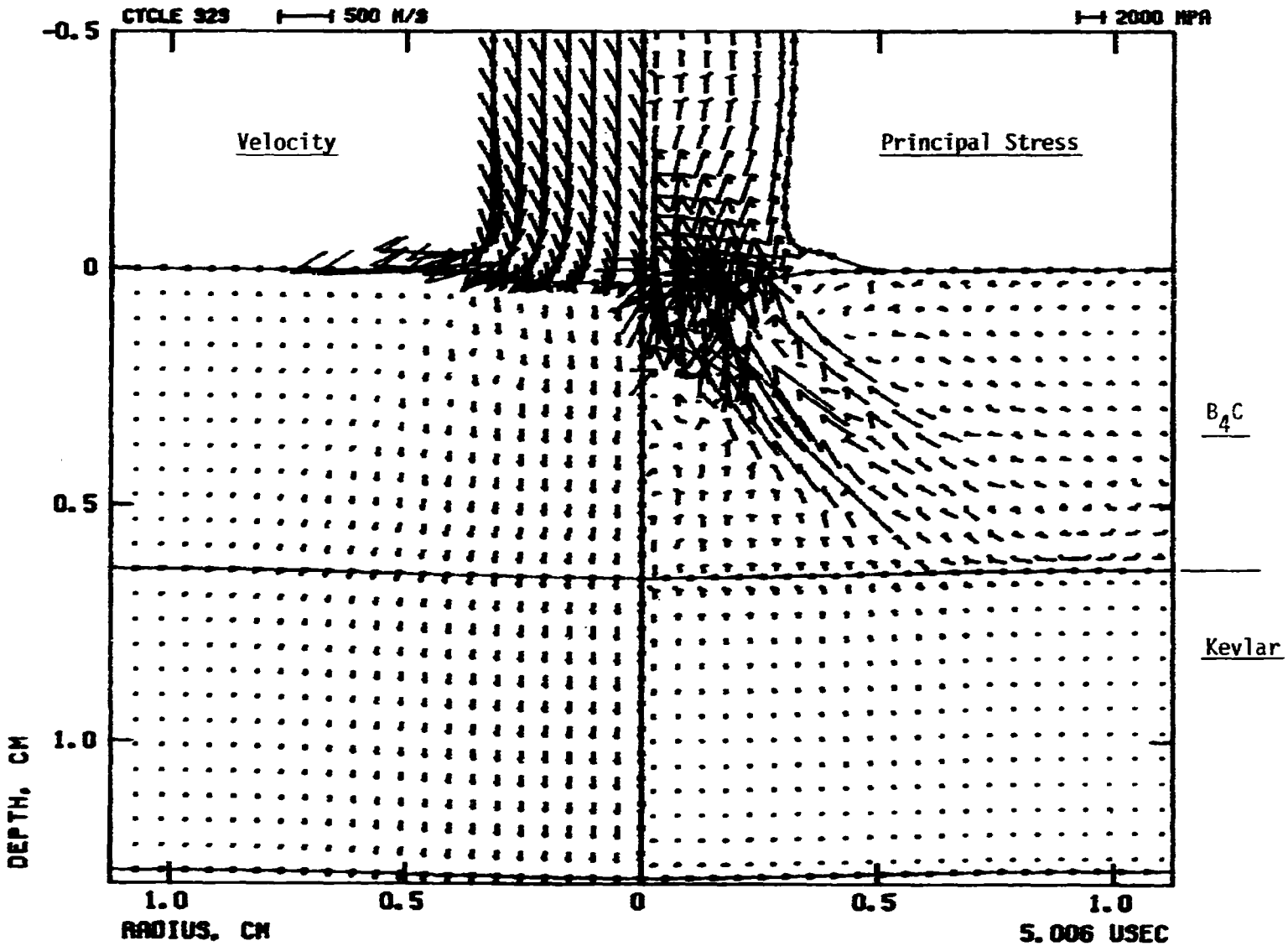

Figure 3.15. Velocity and Stress Fields in Ceramic/Kevlar Target at t = 5.0 μsec.

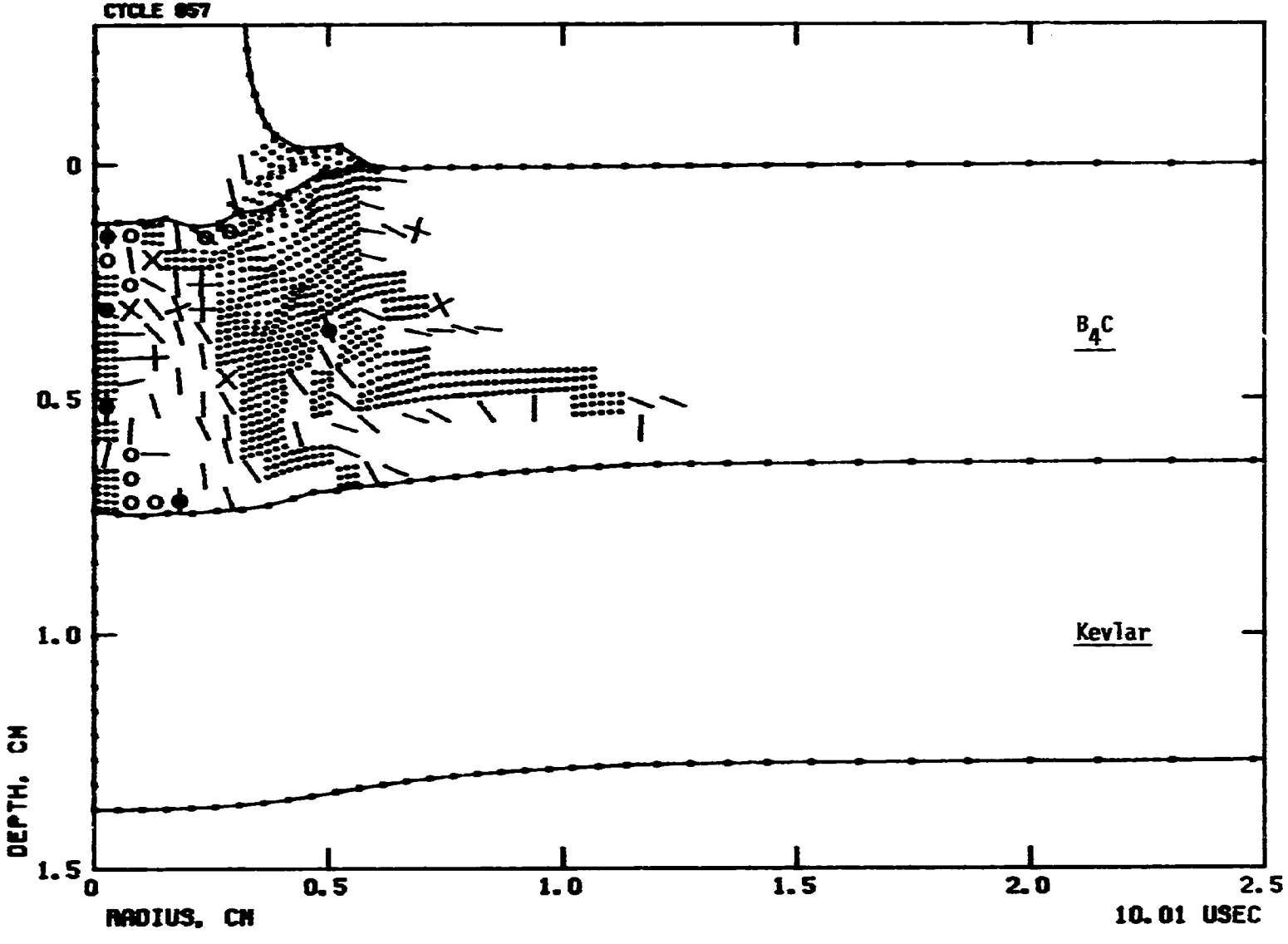

Figure 3.16. Damage in Ceramic/Kevlar Target at t = 10.0 μsec.

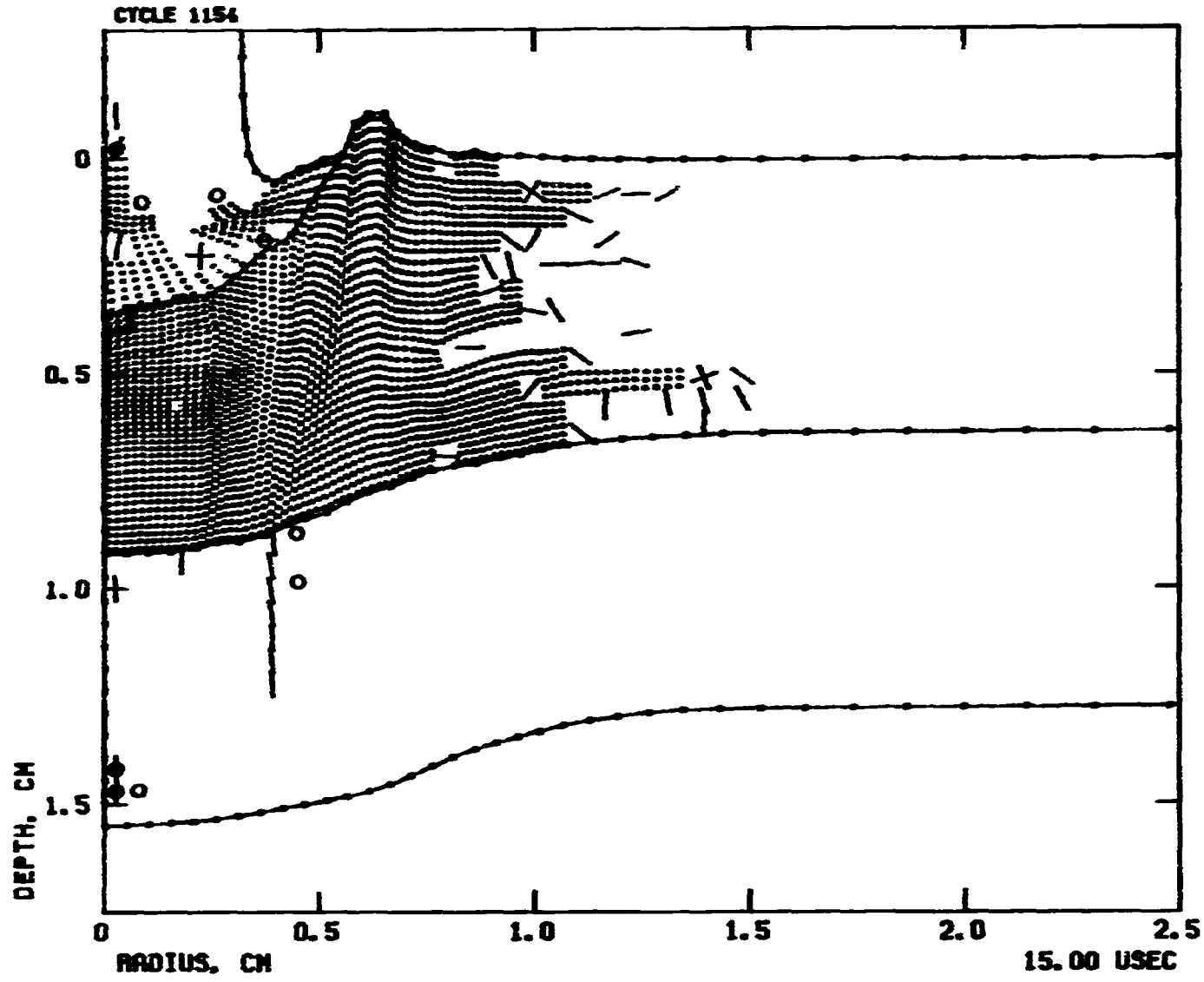

Figure 3.17. Damage in Ceramic/Kevlar Target at t = 15.0 μsec.

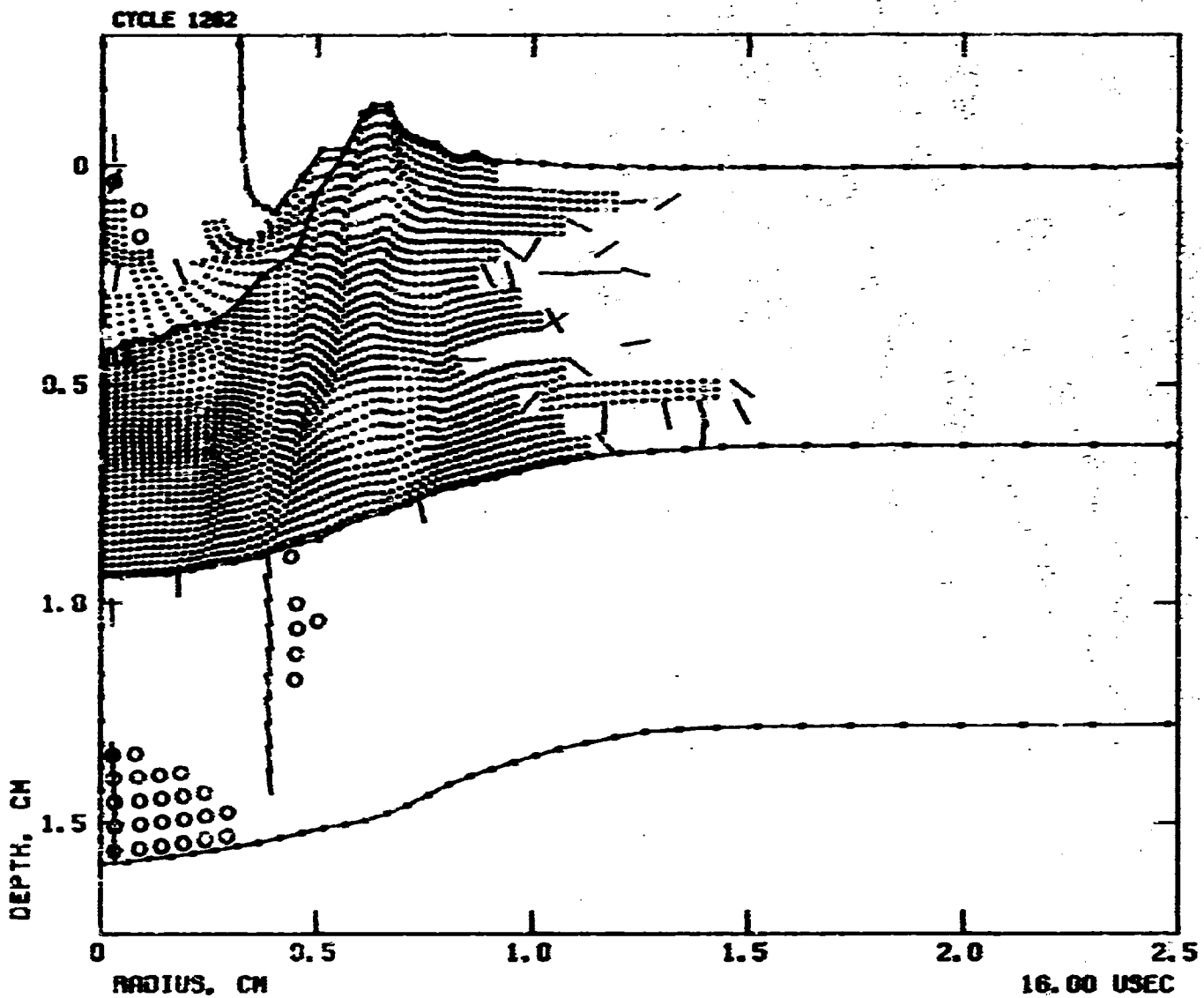

Figure 3.18. Damage in Ceramic/Kevlar Target at t = 16.0 μsec.

early time front surface cracking is caused by the interaction of tensile reflections from the ceramic surfaces

By 3 μsec, Figure 3.13, a distinct band of cracks has formed a fracture conoid emanating from the impact point at about a 45° angle. The surface cracks propagate into the ceramic at this orientation due to the dominant stress field which is characterized by compression along lines emanating from the impact point. In addition, a component of the shearing action imposed by the motion of the projectile results in tension normal to the conoid orientation. Simply stated, this tension is developed as the ceramic material in the conoid region attempts to transfer enough tensile force to accelerate material outside the conoid to keep up with the material inside the conoid. Because the ceramic thickness is on the order of the projectile diameter the material inside the conoid is accelerated at a high enough rate to cause the tensile strength in the conoid region to be exceeded. By 5 μsec, Figure 3.14, the conoid extends almost to the back ceramic surface.

The conoid formation, which causes the detachment of a relatively small mass of ceramic, severely limits the momentum transfer capability of ceramic armor. Once detachment is complete, reduction in projectile velocity is governed by conservation of momentum between the blunted projectile and the conoid area force application to the back Kevlar layer. The effects of the conoid detachment can be seen in the velocity and stress field at 8 μsec, Figure 3.15.

At later times, ceramic failures spread and merge (Figure 3.16 at 10 μsec). Because of this total shattering, the amount of ceramic involved with the projectile is reduced further to a

cylindrical shear plug ahead of the projectile. This concentrated imprint leads to tearing of Kevlar fibers beneath the ceramic plug, Figure 3.17.

As the Kevlar backing fails the last restraint to projectile motion is removed. By 16 μsec, Figure 3.19, back surface failure is nearly complete. At this point the residual velocity of projectile/target plug can be extrapolated through momentum conservation to be 1700 fps or 70% of initial impact velocity. This corresponds well with an associated test conducted by BRL.

Although the final Kevlar failure did not occur until 16 μsec, the eventual target penetration was determined as early as 5 μsec when the conoid detachment became complete. Although the Kevlar backing is capable of stopping the momentum of this impact, it could not withstand the high velocity of the residual material and the concentrated area of contact.

Thus, delaying or eliminating the fracture conoid and subsequent shear plug is of prime importance in the development of a lightweight armor front phase.

Section IV

EVALUATION OF FRONT PHASE CONCEPTS

The role of the front phase in a multi-phase, lightweight, ballistic armor is to transfer projectile momentum and to spread the effective contact area on the back surface as much as possible. Ceramics are currently regarded as the state-of-the-art materials in this application. As seen in the previous section, the accumulation of tensile failures leads to the penetration of these materials, and in the context of lighter armor systems, is the principal weakness which limits ceramic front phase capabilities in the two key areas noted above.

Based on the analyses in Section III it is evident that to improve front phase capabilities, the basic strength properties of the material (notably tensile strength) must be enhanced in some way, or the environment to which it is exposed must be alleviated. In this section concepts for improving lightweight front phase performance are examined using results of computer simulations and ballistic testing. First, mechanical prestressing will be explored as a means for improving the strength of a ceramic plate. Next, the idea of concentrating front phase ceramic into spherical inclusions or platelets will be evaluated as a means for diminishing the intensity of the tensile environment. Finally, estimates will be made of material enhancements necessary to provide adequate front phase performance.

4.1 PRESTRESSED CERAMIC

A well-known approach to strengthing brittle materials which exhibit, as do ceramics, increased strength with confining pressure is to compressively prestress. This not only increases the shear strength of a ceramic, but also the tensile strength by shifting the reference stress level. Two types of prestress mechanisms, thermal stress and mechanical stress have been considered. Thermal prestress is achieved by assembling dissimilar materials, for example ceramic rods in steel packets, at high temperatures and then cooling. This "shrink fit" approach can produce very significant biaxial stress fields if the coefficients of thermal expansion and elastic moduli differ significantly between the two materials and the assembly temperature is high. Unfortunately, examination of various ceramic and metal combinations showed that only a relatively small shift could be attained in this manner for reasonably lightweight designs.

A more promising avenue to prestressing is to use Kevlar as a wrapping material and to tightly wrap ceramic materials at or near the maximum fiber stress (410 ksi) of Kevlar. Recognizing that as wrappings are applied to a specimen, earlier wrappings are compressed by new wrapping (which lowers the stress in the earlier wrappings), the maximum achievable fiber stress attainable using Kevlar will in all likelihood be less than 300 ksi. Still this mechanism provides for more prestress at a given weight than obtainable by thermal stressing or another known method (see Figure 4.1). This prestress concept generates biaxial compression rather than triaxial compression and leaves available a low stress failure mechanism, namely tensile cracking in the unprestressed direction.

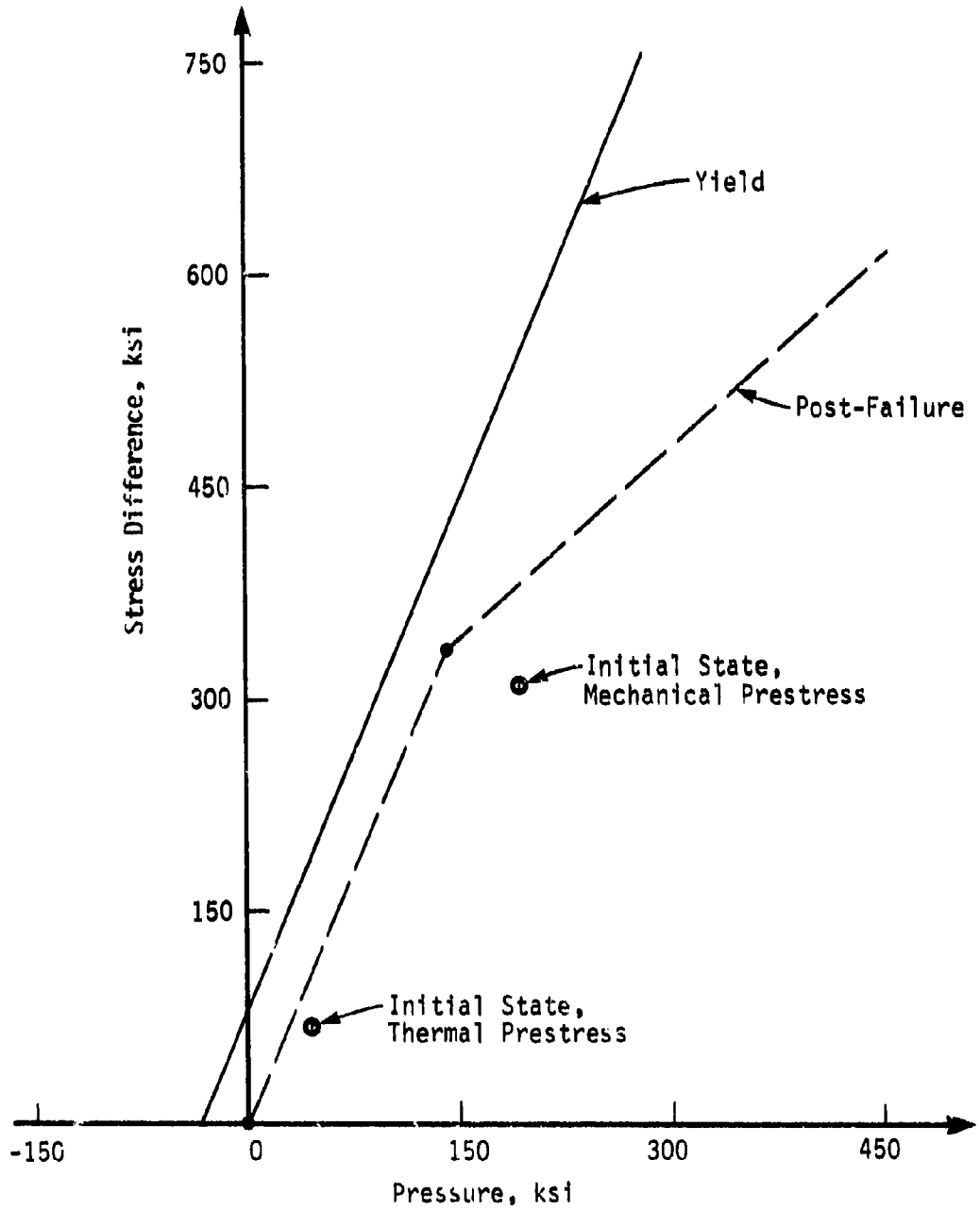

Figure 4.1. Initial Prestress State for Typical Ceramic.

Analysis of High Prestress

The analysis of a 5 psf, highly prestressed ceramic plate system is considered. The basic layout of the prestressed plate is shown in Figure 4.2 in which Kevlar fibers on the top and bottom are in a state of biaxial, in-plane, tension at 300 ksi. This results in a net shift in reference pressure of 200 ksi in the sandwiched ceramic plate, see Figure 4.1. The solution is initiated at the ceramic surface when the projectile has penetrated the front layer of Kevlar. Fibers which have been sheared in this process are not modeled in this analysis. This initial condition is based on results from an earlier calculation. Since the primary effect is the high initial in-plane compression in the ceramic these simplifications are inconsequential in terms of their effect on early time impact and penetration physics.

The progression of failures obtained by the numerical analysis are shown in Figures 4.3 to 4.6 compared to the case of non-prestressed ceramic plate backed by Kevlar presented in Section III. At 1.5 μsec, Figure 4.3, there are actually more surface ceramic failures in the prestress case. This is due to the higher magnitude shock wave transmitted through the ceramic, which in turn produces larger reflected tensile stresses. The shock wave is stronger in the prestressed target due to the correspondingly higher yield strength of the prestressed ceramic. Also, biaxial prestressing does not inhibit cracks from forming in the horizontal plane.

Cracking in the prestress directions is greatly retarded at 3.0 μsec as seen in Figure 4.4. While horizontal surface

0.25" Biaxial Kevlar Wrap:

- Kevlar wrapped at 300 ksi with 110 ksi residual tensile strength

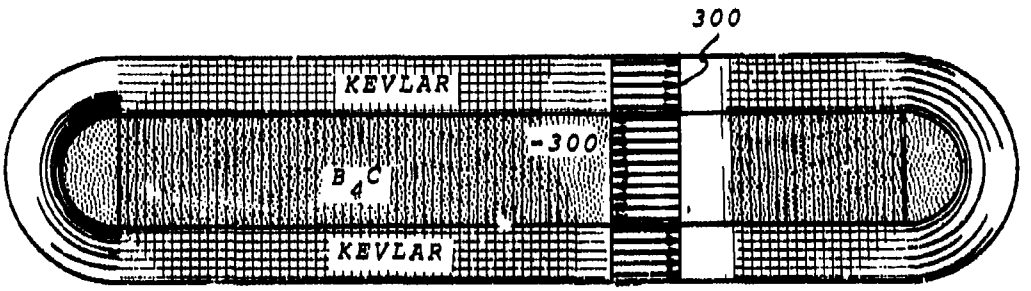

0.25" B_4C Ceramic Plate:

- Biaxial compression

  $\sigma_1 = \sigma_2 = -300$ ksi

Figure 4.2. Prestressed Ceramic Front Plate Concept.

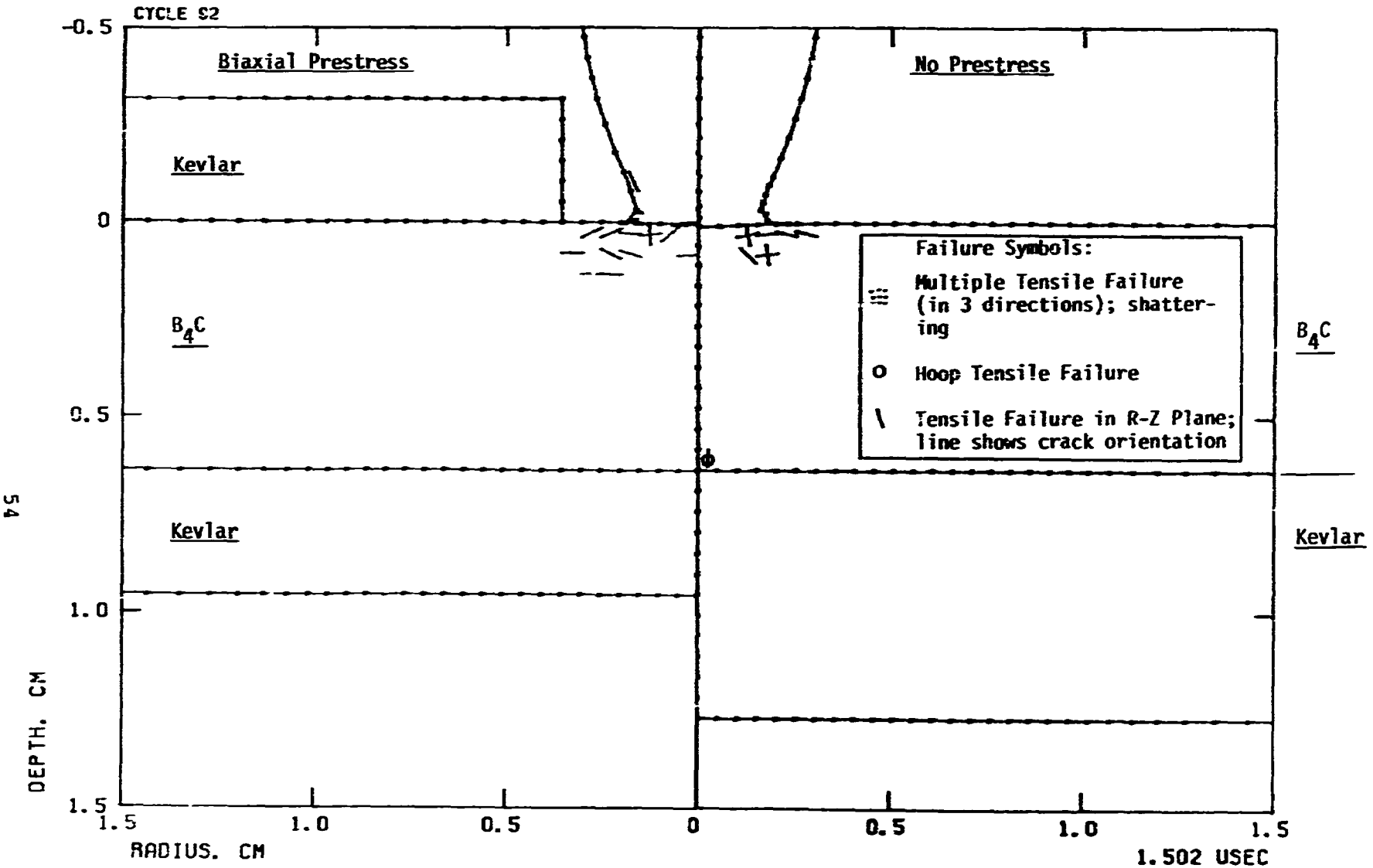

Figure 4.3. Damage in Prestressed Kevlar/Ceramic/Kevlar Concept Compared to Ceramic/Kevlar Plate at t = 1.5 μsec.

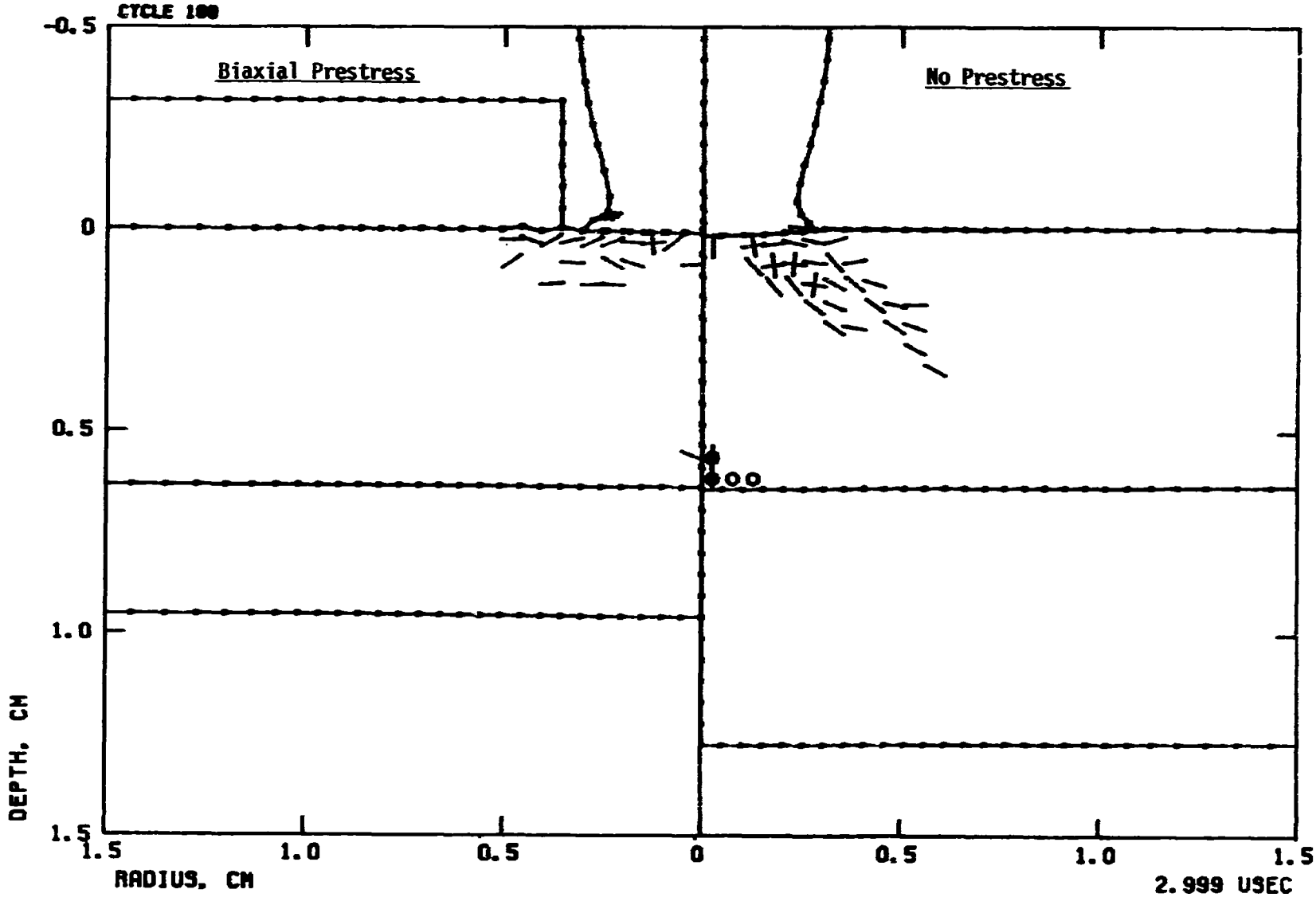

Figure 4.4. Damage in Prestressed Kevlar/Ceramic/Kevlar Concept Compared to Ceramic/Kevlar Plate at t = 3.0 μsec.

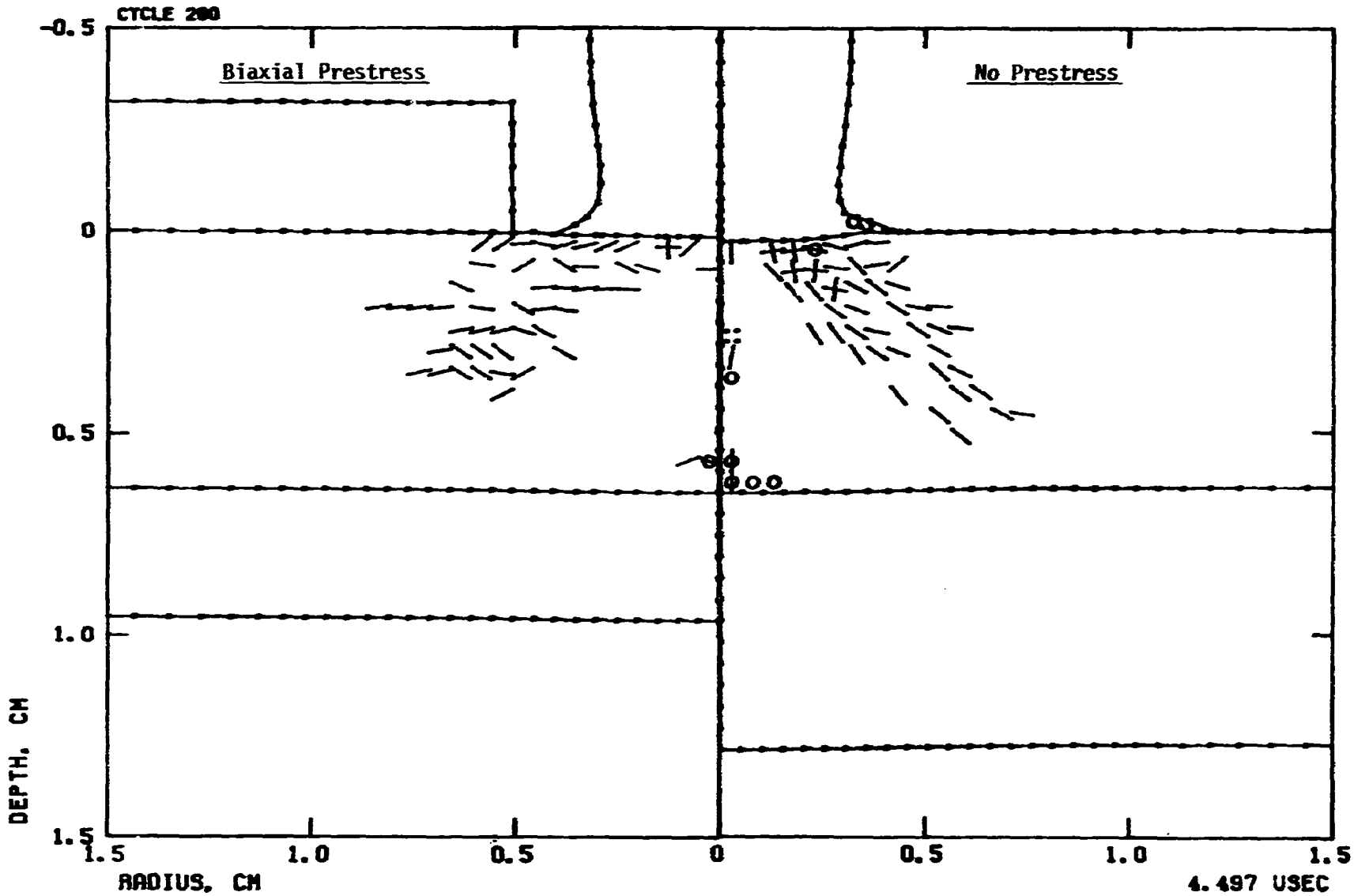

Figure 4.5. Damage in Prestressed Kevlar/Ceramic/Kevlar Concept Compared to Ceramic/Kevlar Plate at t = 4.5 μsec.

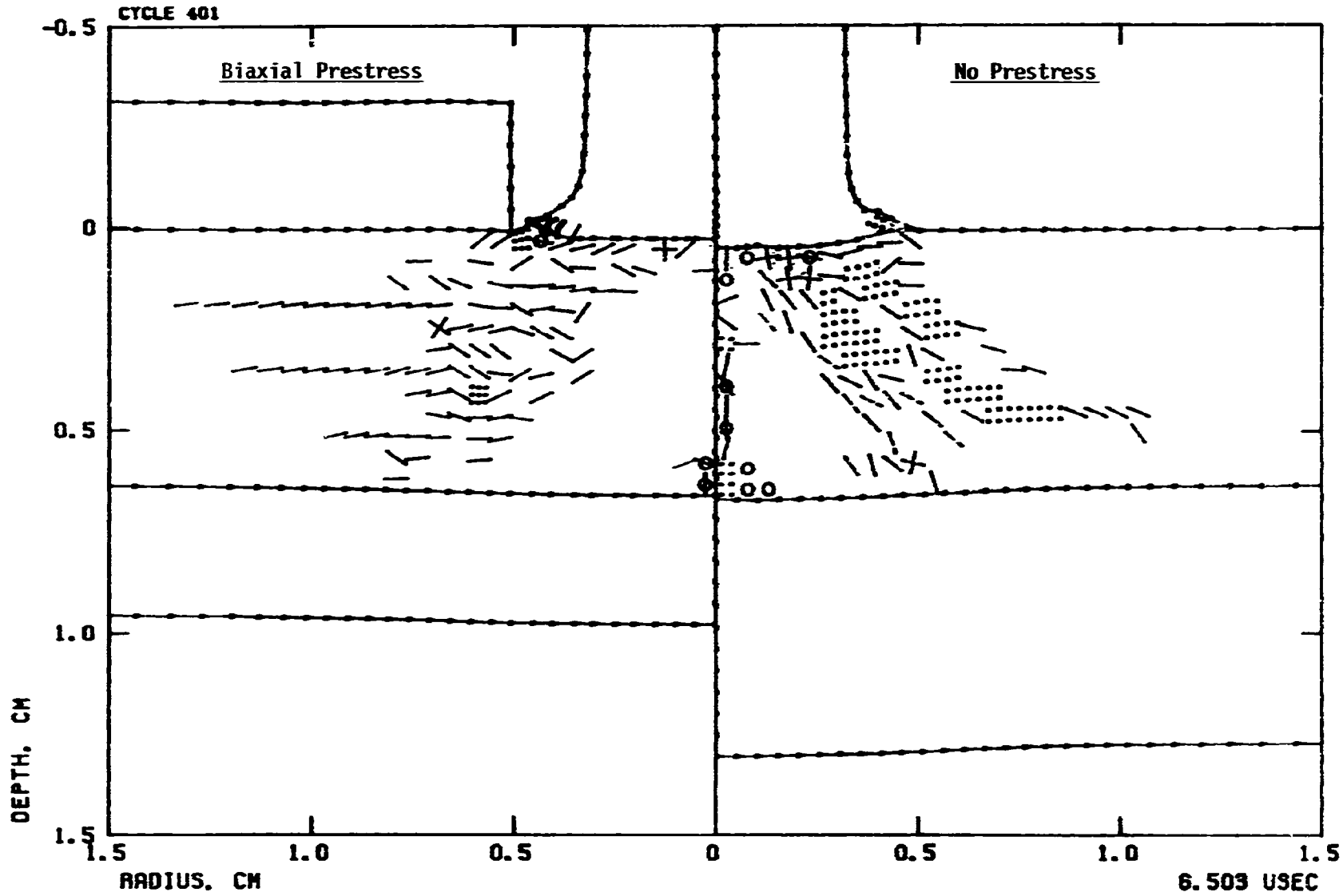

Figure 4.6. Damage in Prestressed Kevlar/Ceramic/Kevlar Concept Compared to Ceramic/Kevlar Plate at t = 6.5 μsec.

cracking has continued, conoid fracture and back surface failures are surpressed. By 4.5 μsec, however, horizontal cracks have spread into the interior of the target (Figure 4.5) and progressed through the thickness of the ceramic by 6.5 μsec (Figure 4.6). These failures, while not allowing direct separation of material as would a fracture conoid, do degrade the target strength.

Ceramic plug motion in front of the blunted projectile is evident in the velocity field plot at 6.5 μsec, Figure 4.7. Although the target is still capable of providing some additional resistance, eventual penetration is clearly indicated by the extent of failures and the velocity field. The rear surface Kevlar wrapping is also close to tensile failure due to the initial high fiber tension prestress.

Analysis of Low Prestress

Testing of Kevlar wrapped prestressed ceramic targets was conducted by BRL. Because it was believed that 300 ksi fiber prestressing would be difficult to fabricate, particularly without development of new wrapping technique, a 95 ksi fiber prestress level was selected as a more reasonable level to correlate with the test.

The calculated progression of failures for this low level of prestress is compared to high prestress in Figures 4.8 to 4.11 The early time surface cracking is not as pronounced as in the high prestress case. However, the low prestress is rapidly overcome and greater failures initiate at the ceramic back surface.

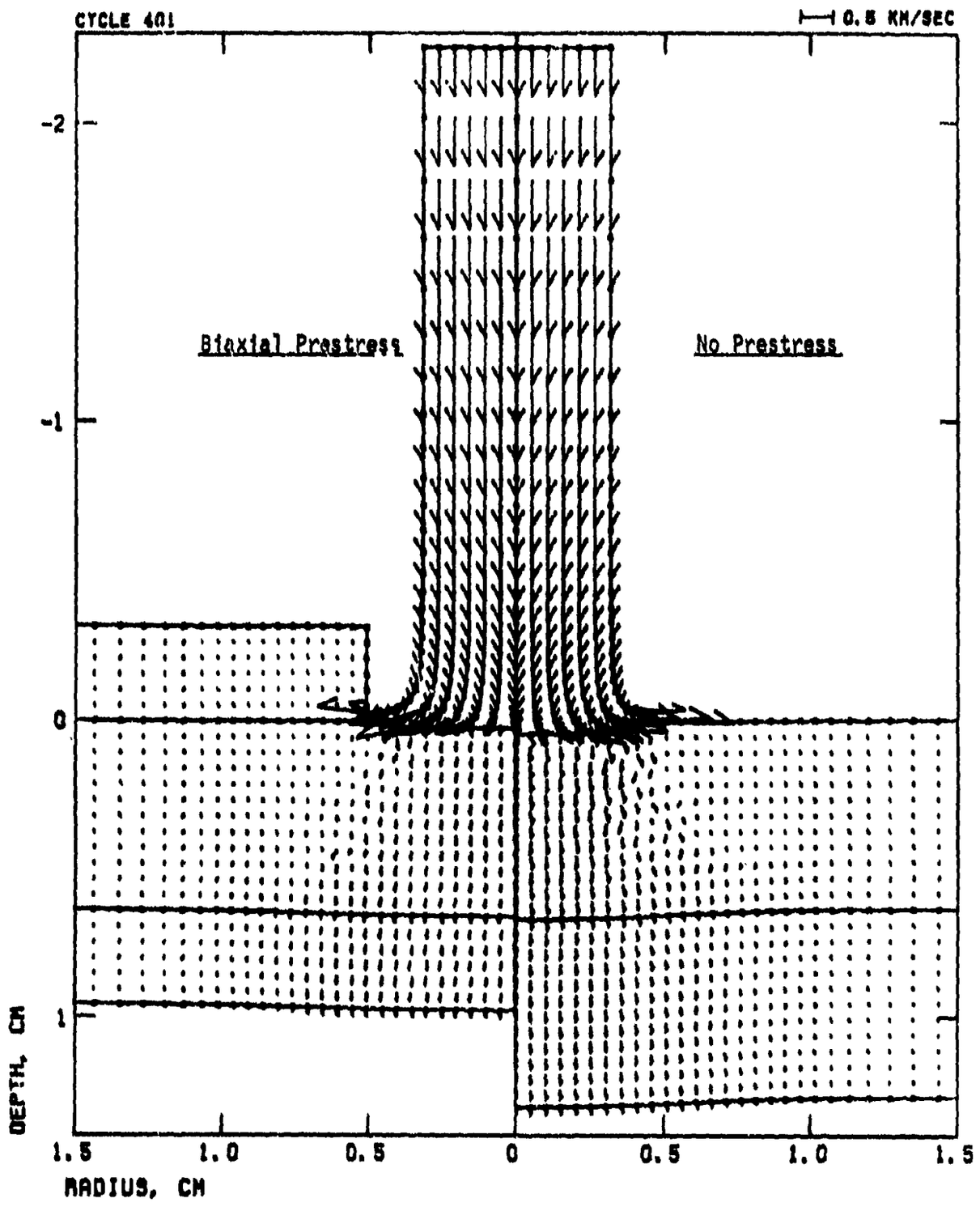

Figure 4.7. Velocity Field in a Prestressed Kevlar/Ceramic/Kevlar Concept Compared to Ceramic/Kevlar Plate at t = 6.5 μsec.

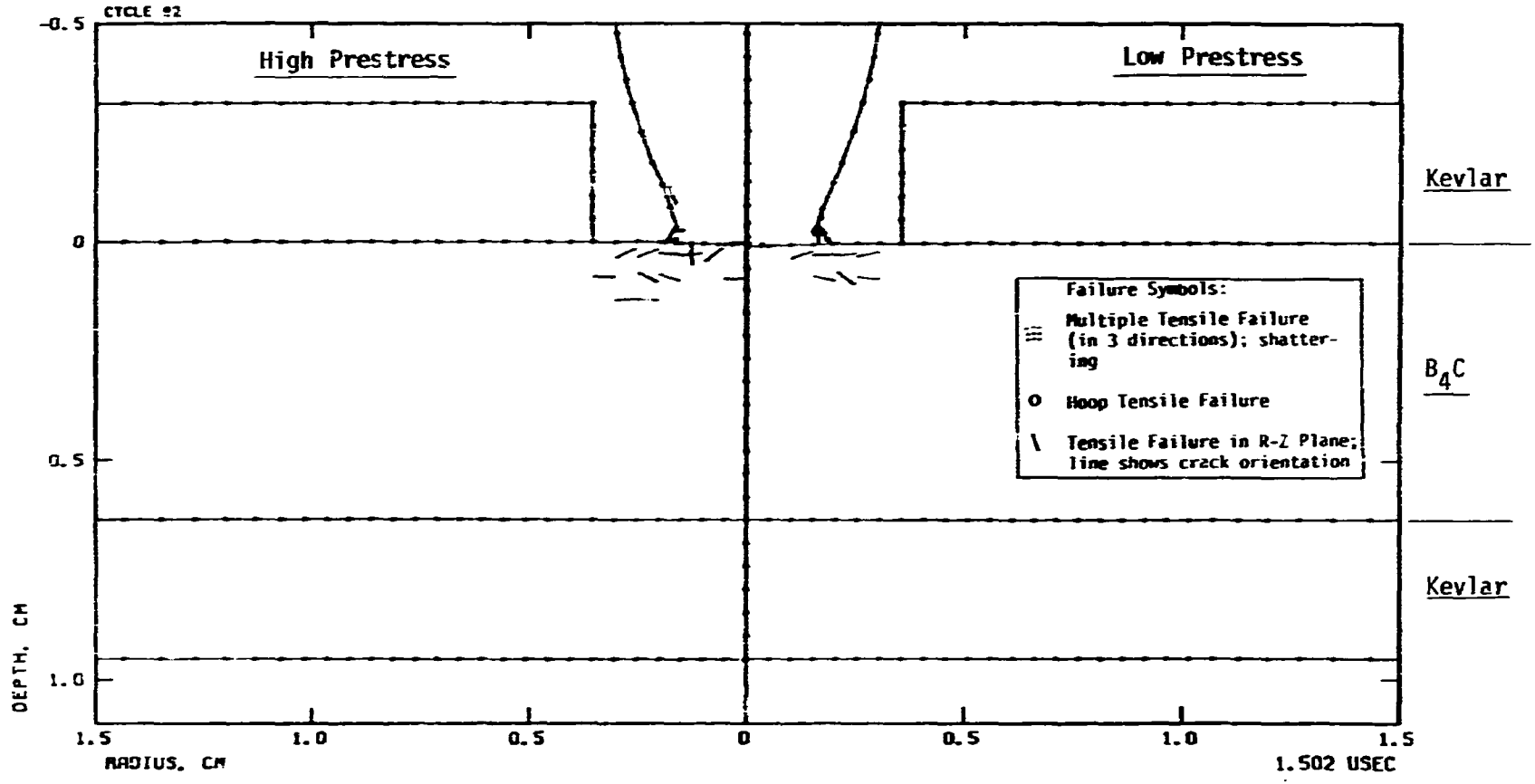

Figure 4.8. Comparison of Damage in High and Low Prestressed Kevlar/Ceramic/Kevlar Cocepts at t = 1.5 μsec.

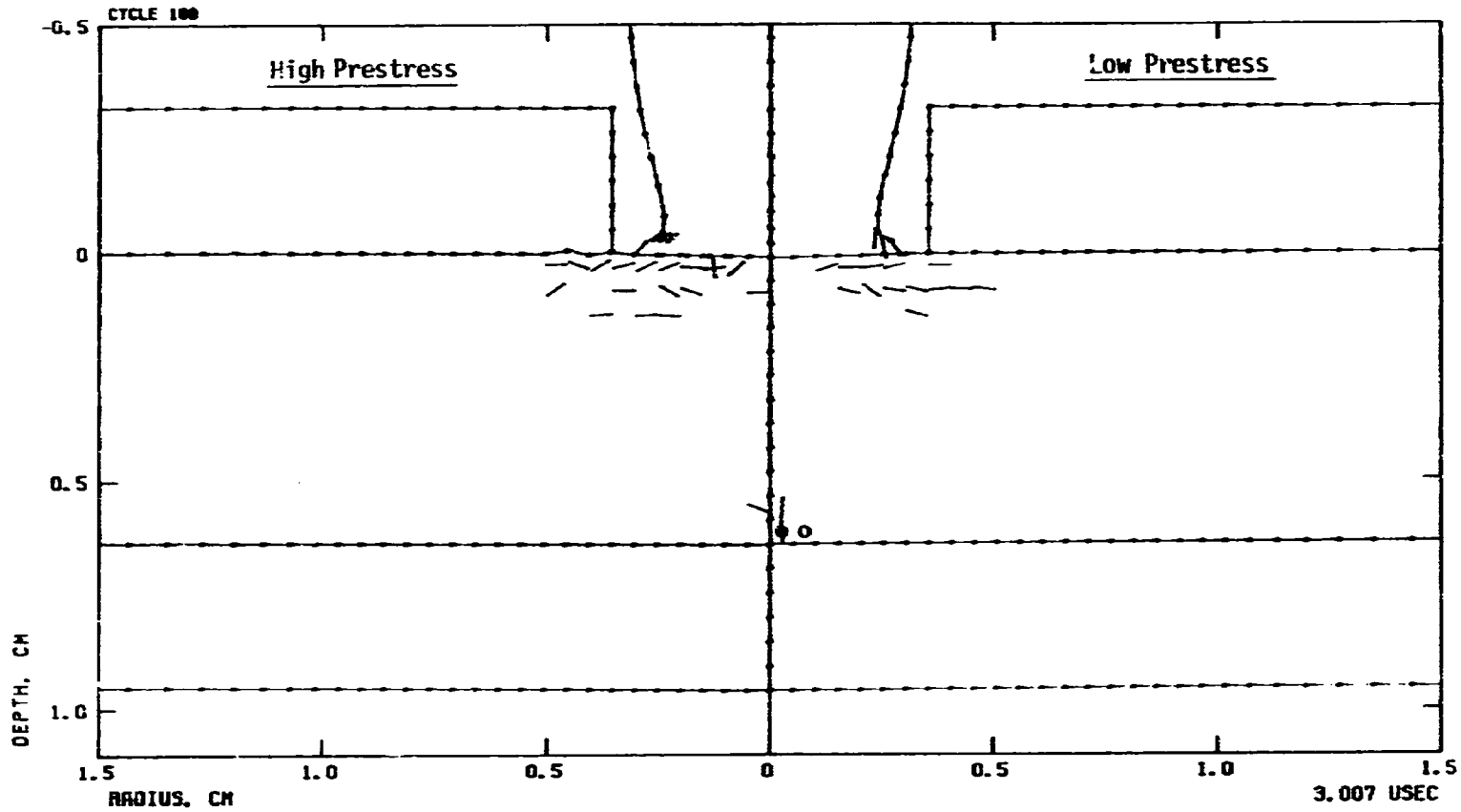

Figure 4.9. Comparison of Damage in High and Low Prestressed Kevlar/Ceramic/Kevlar Concepts at t = 3.0 μsec.

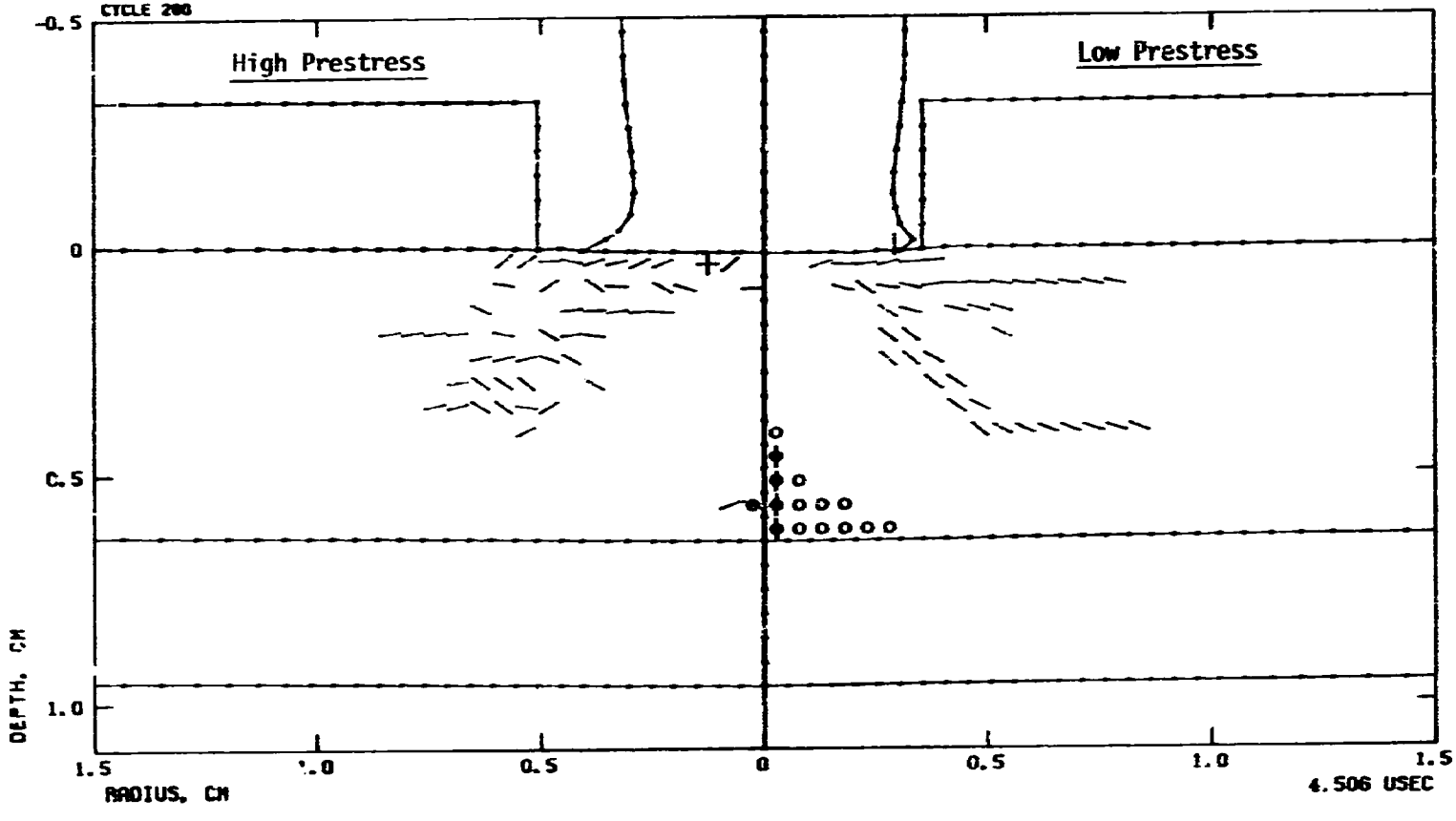

Figure 4.10. Comparison of Damage in High and Low Prestressed Kevlar/Ceramic/Kevlar Concepts at t = 4.5 μsec.

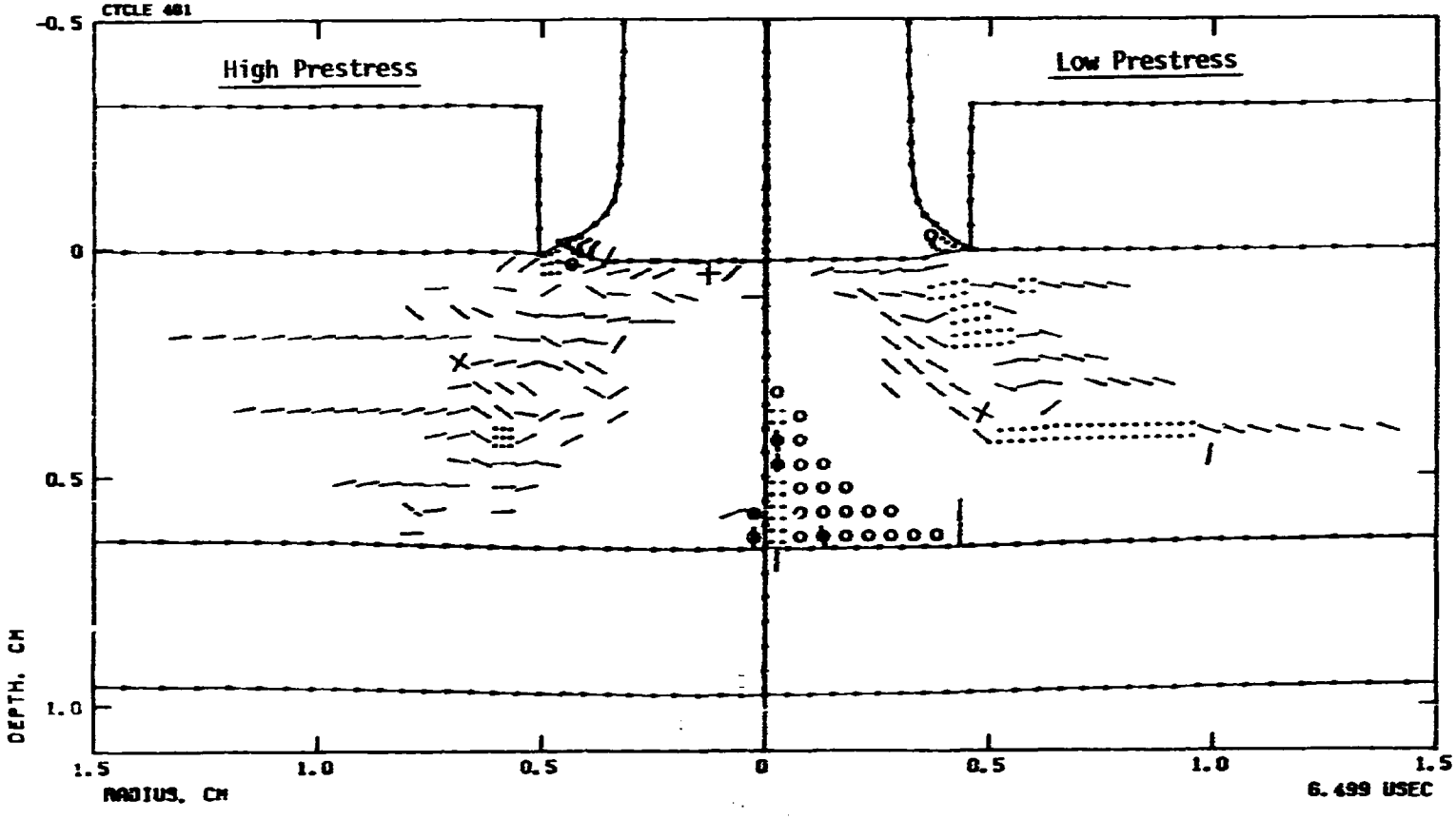

Figure 4.11. Comparison of Damage in High and Low Prestressed Kevlar/Ceramic/Kevlar Concepts at t = 6.5 μsec.

By 4.5 μsec the conoid failure progression turns and proceeds in a horizontal direction, in alignment with the prestress field as seen in Figures 4.10. Although this turn in the direction of crack propagation delays the conoid breakout at the back surface, the target integrity is compromised. The concentration of shearing forces leads to extensive yielding through the remaining uncracked depth of ceramic. By 6.5 μsec, Figure 4.11, rear surface failures have almost coalesced with the fracture conoid to form a shear plug. The velocity field (Figure 4.12), at this time is similar to the high prestress case despite the different mode of failure.

Kevlar failure initiates at 8.5 μsec about one projectile radius from the impact centerline. This is caused by the motion of the ceramic plug below the blunted projectile. Complete through failure of the Kevlar backing occurs by 10.5 μsec, Figure 4.13. The well-defined plug of ceramic is salient in the velocity field shown in Figure 4.14. It is evident that biaxial prestress delays but can not prevent the formation of a narrow ceramic plug, which is difficult for the Kevlar backing to arrest.

Comparison with Test Data

Several test shots of prestressed Kevlar wrapped ceramic targets were performed by BRL. From examination of post-test ceramic targets, it clear that ceramic plug damage predicted by the analyses was the dominant failure mechanism. The BRL test shots and extrapolations of the numerical solutions indicate a very high residual projectile momentum to exist following target penetration. A residual velocity equal to 80% of the impact velocity was measured experimentally. The value extrapolated

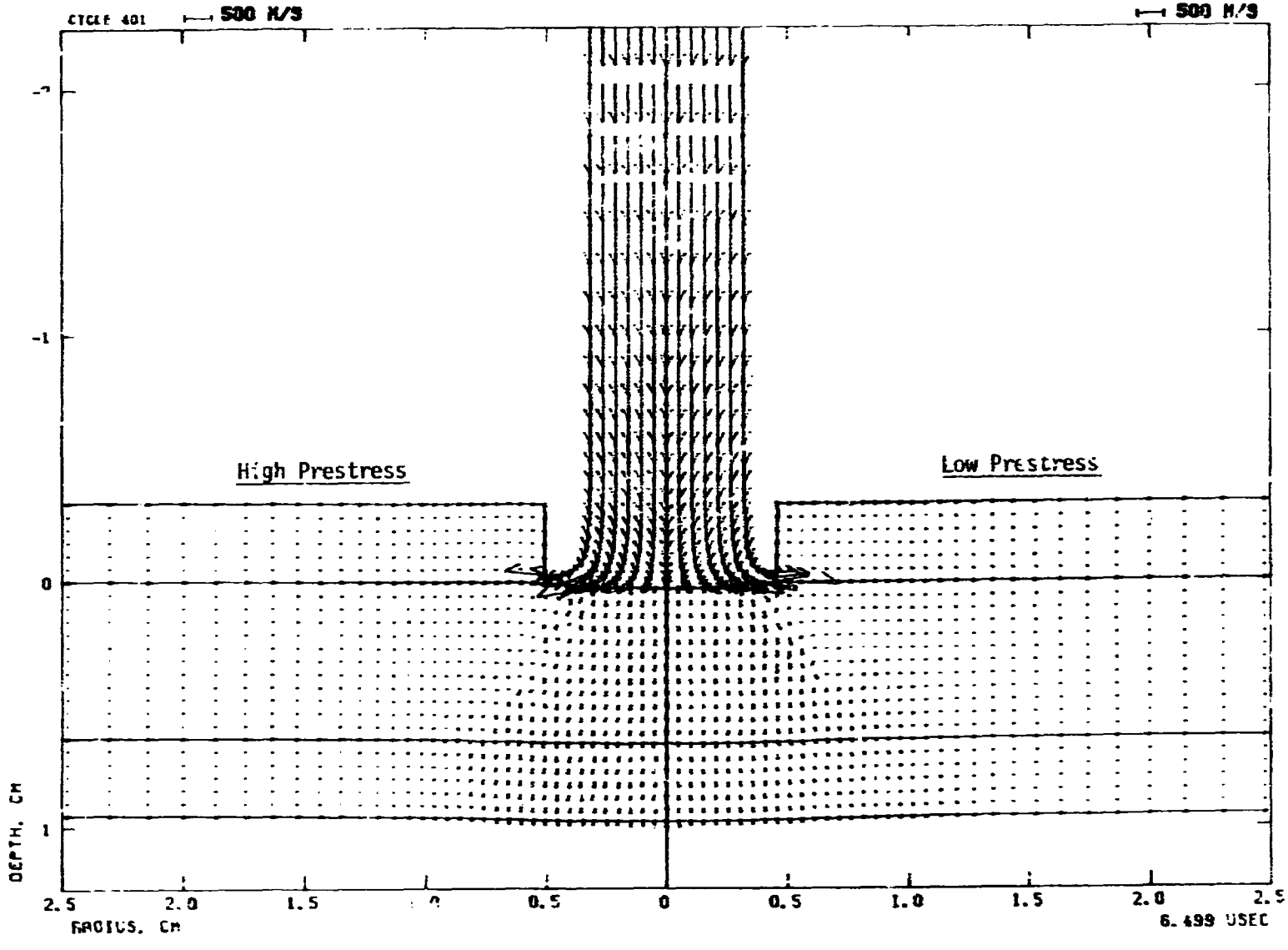

Figure 4.12. Velocity Field Comparison in High and Low Prestressed Kevlar/Ceramic/Kevlar Concepts at t = 6.5 μsec.

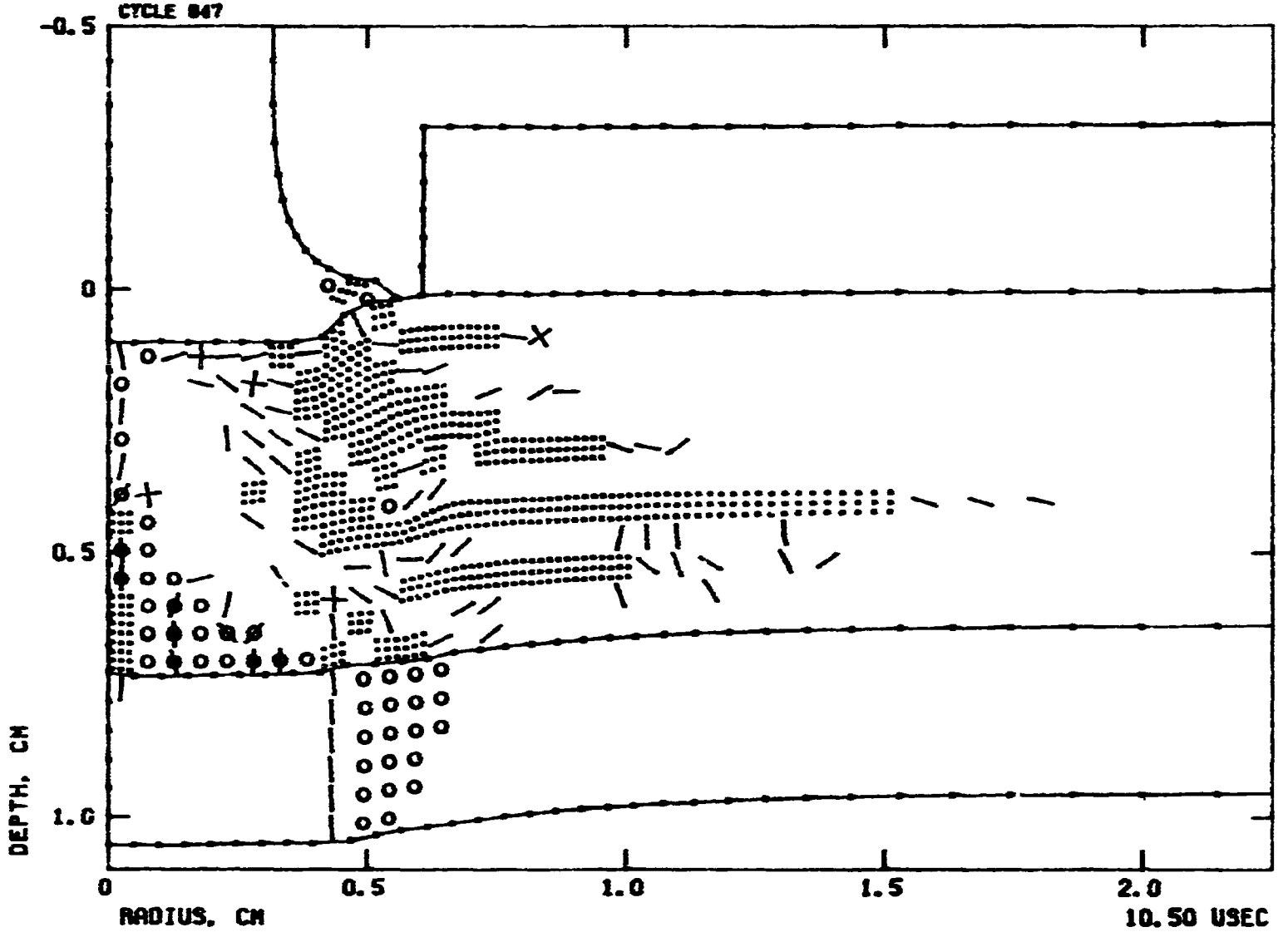

Figure 4.13. Damage in Low Prestressed Kevlar/Ceramic/Kevlar Concept at t = 10.5 μsec.

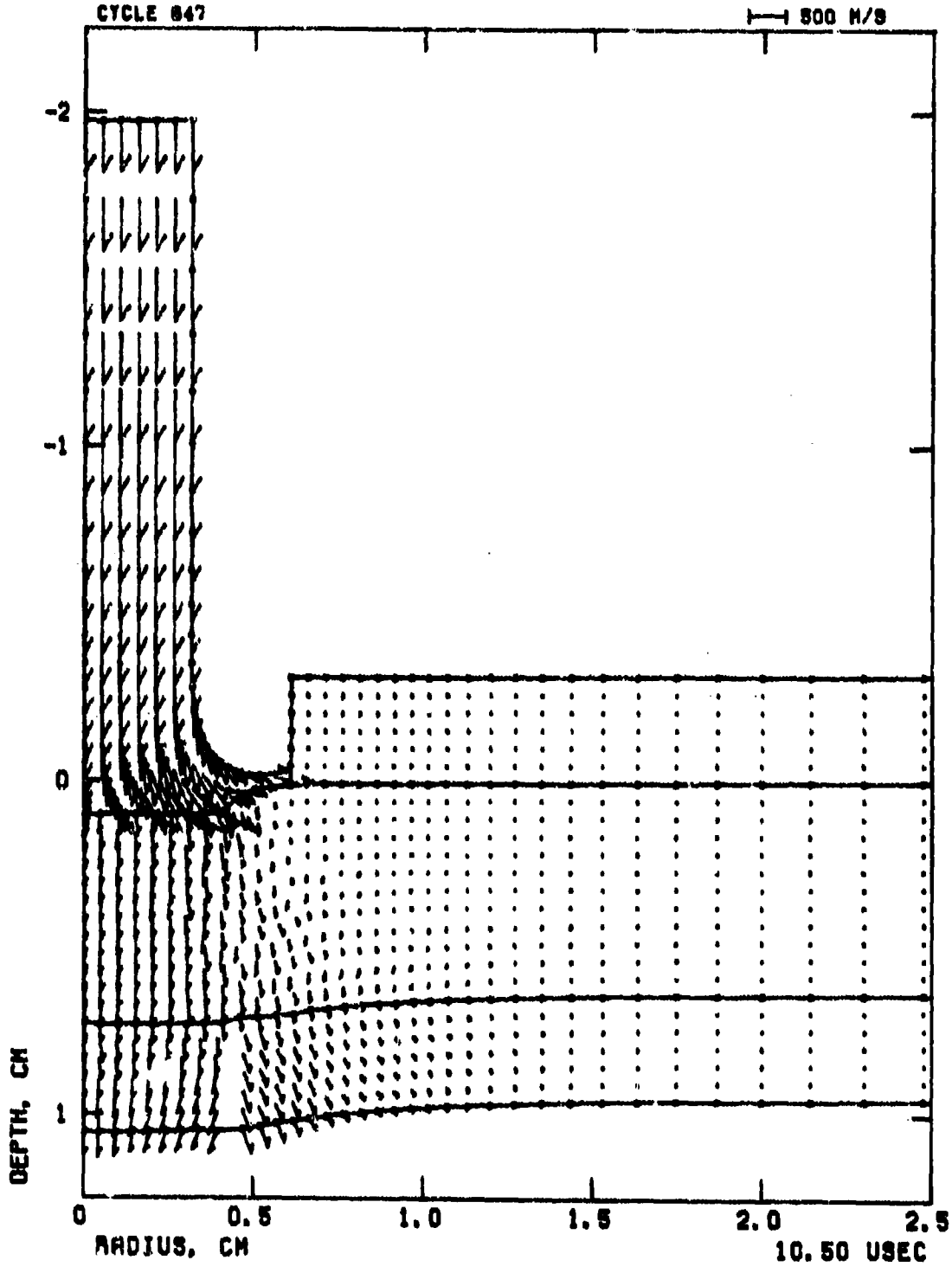

Figure 4.14. Velocity Field in Low Prestressed Kevlar/Ceramic/Kevlar Concept at t = 10.5 μsec.

from the analysis is 70% for high prestress and 75% for low prestress. The nominal ceramic plug size seen in the photographs of experimental targets and that predicted from the calculated failure patterns were in general agreement.

Assessment

It is apparent from both the test and analysis that biaxial prestressing does not significantly improve the performance of 5 psf ceramic armor. Although large amounts of prestress may inhibit the development of classic tensile failure patterns, it appears that it may also heighten the shock environment within the ceramic and produce strata failure. The resulting target degradation is substantial. However, the high prestress was sufficient to overcome the magnitude of tensions generated on the ceramic rear surface during impact.

In summary, the use of biaxial prestress, does not uniformly strengthen the material and in the final analysis serves only to slightly alter early time failure mechanisms. Tensile strength enhanced in the unprestressed direction would be required to provide substantial improvement in armor resistance.

4.2 SPHERICAL INCLUSIONS

A means for bringing more mass into the impact process might be to lump the mass into spherical shapes and thereby concentrate the momentum transfer capabilities of the front phase. Such spherical masses might also blunt the projectile and possibly cause large lateral and/or rotational motions in the projectile during impact. This concept leads to the investigation of composite front plates containing hardened spherical inclusions.

Analysis

To develop some insight into the mechanics of momentum transfer and projectile motion during impact with spherical inclusions a series of simplified analyses were performed involving the impact of a (blunted) projectile with one and two body systems of hard spheres of various sizes. The analysis was conducted using a discrete element code PROBS [10] which is capable of tracking the motion of individual blocks throughout the impact.

These analyses showed that if the inclusions were of sufficient mass, significant momentum transfer and projectile deflection and rotation would occur. However, this would require areal densities on the order of 10 psf. At 5 psf a single layer of ceramic spheres with a diameter approximately twice the caliber of the projectile could reduce impact velocity by at least 15% and cause a major tumbling action, see Figure 4.15. On the otherhand two layers of one caliber spheres does not possess sufficient mass to cause any major changes in projectile flight path, see Figure 4.16.

Comparison with Test Data

These results were confirmed qualitatively by a series of tests conducted by BRL using targets made with hardened ceramic balls of various caliber, assembled in different arrangements and imbedded in several matrix materials. In most lightweight tests at 5-10 psf, the projectile simply smashed through the target, with little velocity reduction. In several tests, significant rotation and angular velocity was noted following target

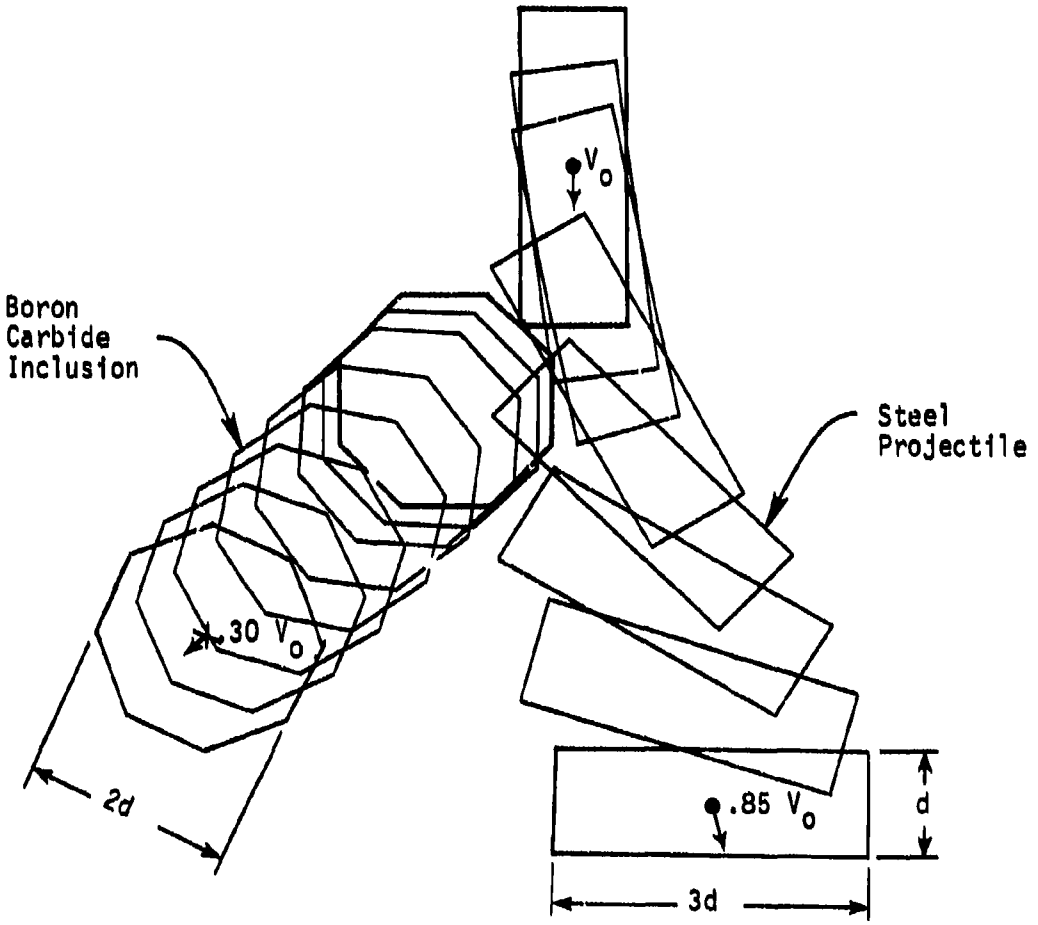

Figure 4.15. Effect of Two Caliber Ceramic Inclusion on Penetration Path.

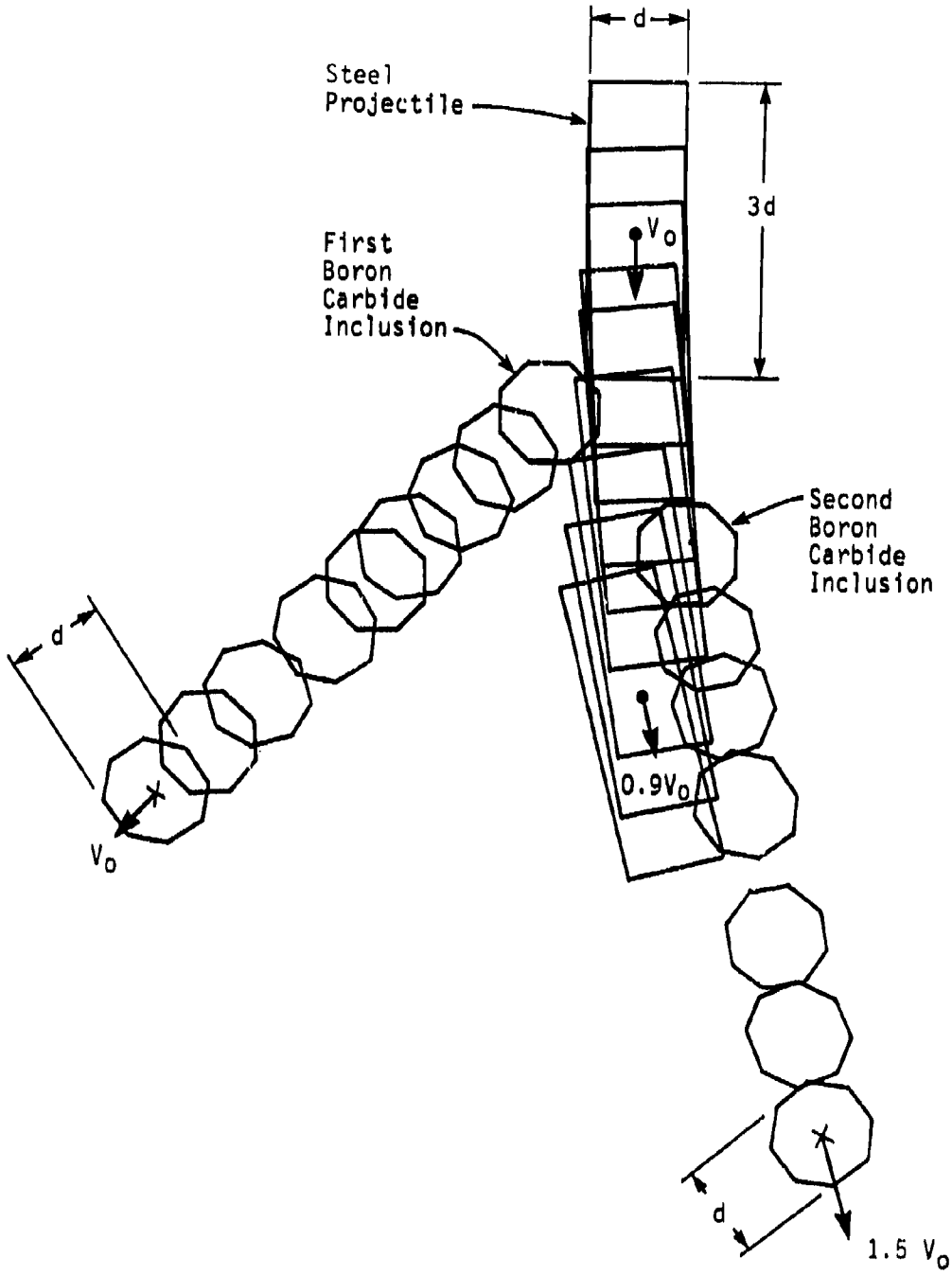

Figure 4.16. Effect of Two-Layer One Caliber Ceramic Inclusions on Penetration Path.

penetration. Also, rubber-like matrix materials provided enhanced multi-hit capabilities.

Assessment

Both the simplified PROBS analysis and the experimental data showed a key fact: The only way of arresting the projectile is by developing a target capable of bringing sufficient mass into the impact process. However, the use of hard spherical inclusions with sufficient mass to have a significant effect on the analysis is not feasible at the 5 psf level.

These results suggest a concept which combines the effects of the rigid inclusions with the lightweight 5 psf design objective, namely the use of small platelets in the form of disk type structures. These platelets have an areal mass which is low but a total mass which is sufficiently great to effectively resist projectile impact. This type of front phase concept is considered next.

4.3 CERAMIC PLATELETS

As noted previously, the conical failure pattern which has been seen to develop at early times in impacts on continuous ceramic plates immediately limits the momentum transfer capability to the mass within the conical region. The reason for this early failure is that the mass outside the failure region in effect requires more force to be accelerated than can be transmitted by the ceramic due to its limited tensile strength. In a continuous plate concept, this material outside of the failure region is inertially constrained from moving freely by the plate material further away from the point of impact.

A means for bringing more target mass into the impact process might be to divide the front phase into platelets, thereby limiting the effect of outlying material. In this manner the tensile forces required to accelerate material outside the fracture conoid could be decreased. An added benefit, as in the spherical inclusion concept, could be improved multi-hit resistance.

Analysis

To investigate possible platelet benefits, a numerical simulation of the 2500 fps impact of the caliber .25 steel-cored threat on a 5 psf ceramic platelet was performed. The nominal platelet dimensions were .39-in. thickness and .93-in. diameter. The calculated failure patterns are compared to the solution of a continuous plate of the same areal density in Figures 4.17 to 4.20.

As expected, the initial failures are identical in both cases. By 3.5 μsec, Figure 4.18, reflections from the free boundary cause the platelet cracking to differ from the continuous plate. However, the differences at this time are insignificant.

By 5.75 μsec, Figure 4.19, conoid cracking has progressed about halfway through both targets. The conoid in the platelet has developed at a steeper angle, with crack surfaces oriented more toward the free edge tensile source. This development means that less target material has been included from the impact in the platelet case, at this time.

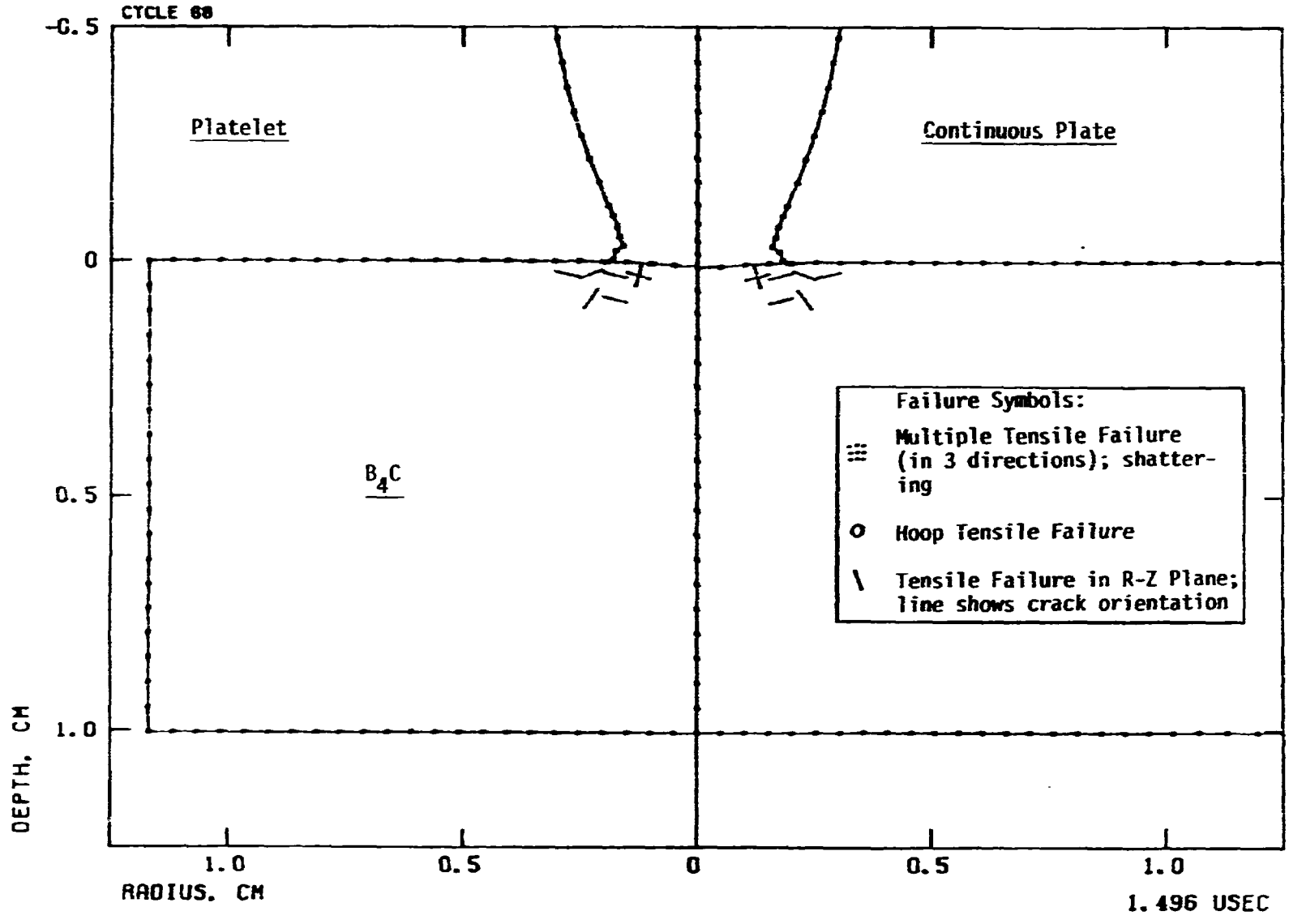

Figure 4.17. Comparison of Damage in Ceramic Platelet and Continuous Plate Targets at t = 1.5 μsec.

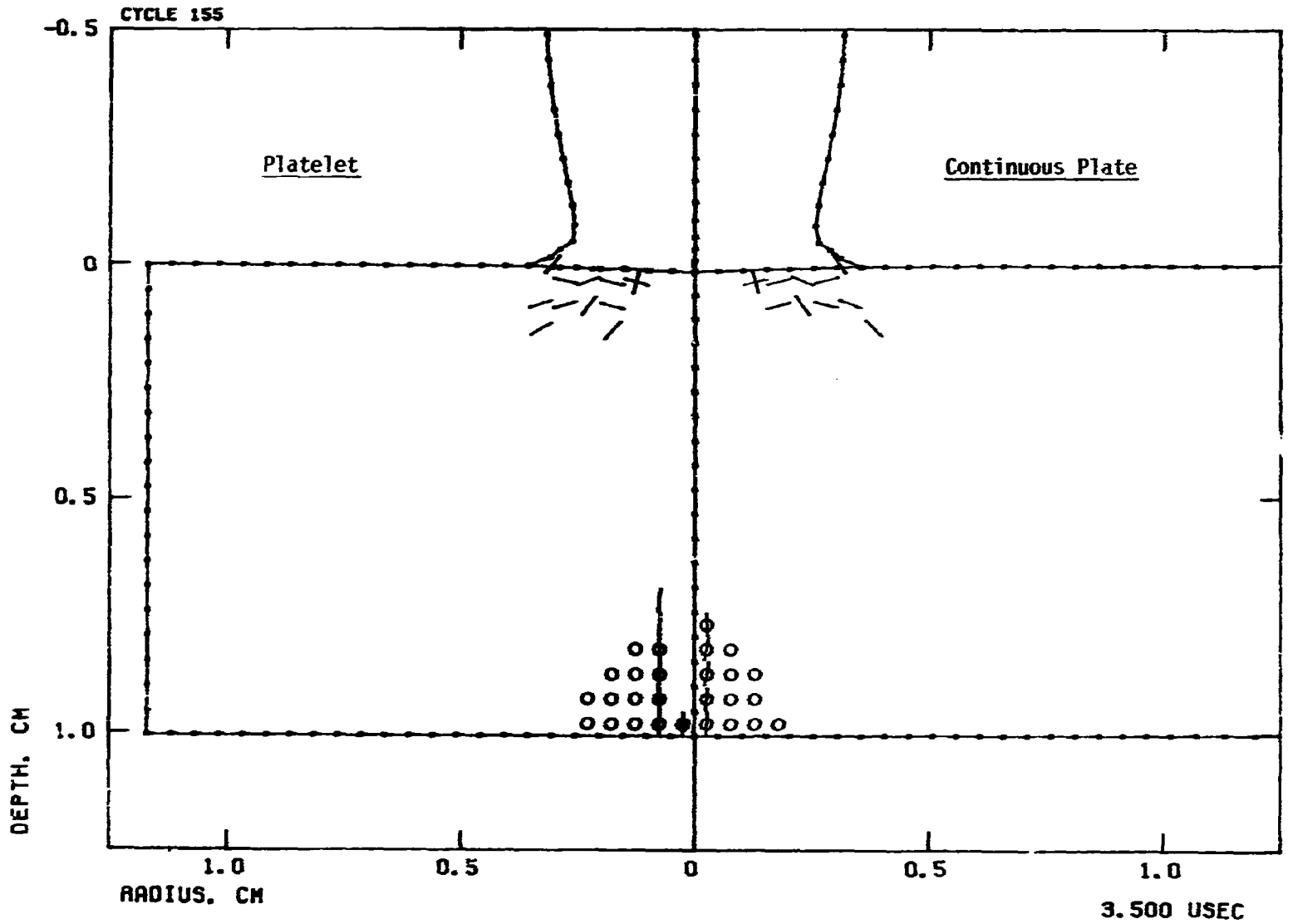

Figure 4.18. Comparison of Damage in Ceramic Platelet and Continuous Plate Targets at t = 3.5 μsec.

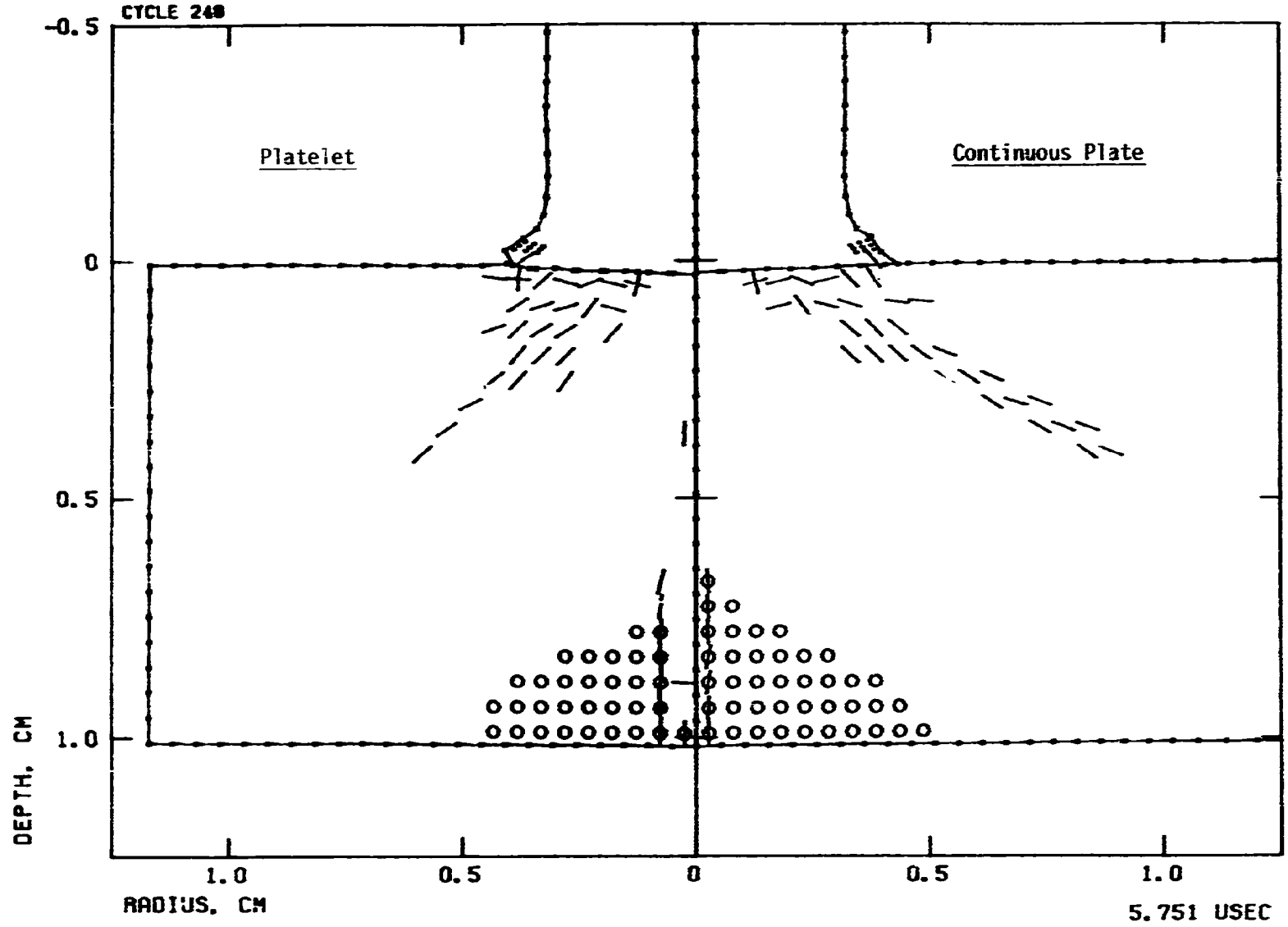

Figure 4.19. Comparison of Damage in Ceramic Platelet and Continuous Plate Targets at t = 5.75 μsec.

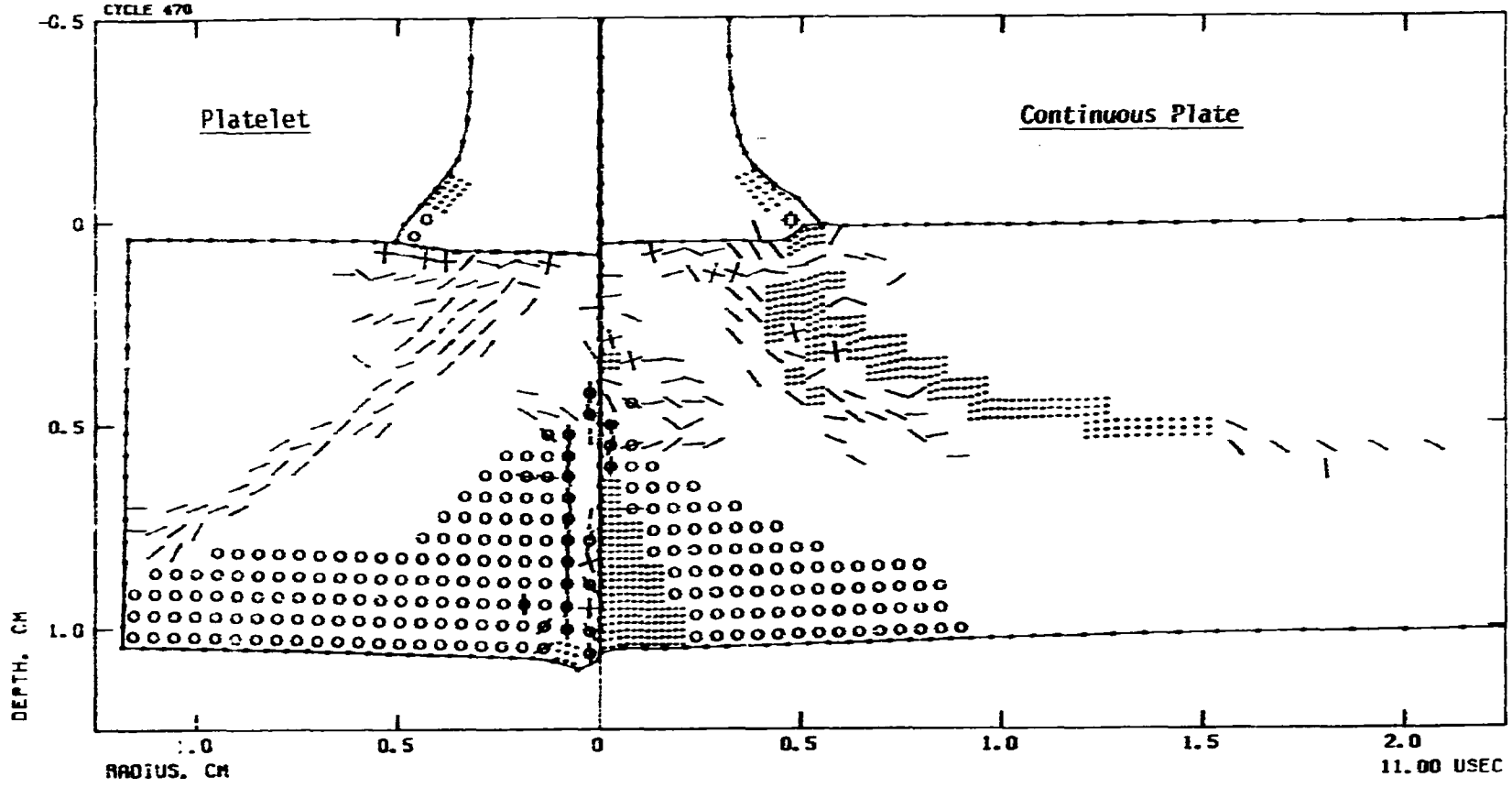

Figure 4.20. Comparison of Damage in Ceramic Platelet and Continuous Plate Targets at t = 11.0 μsec.

The conoid breaks out of the platelet at 11.0 μsec, Figure 4.20. The maximum projectile momentum which could be transfered would result in a residual velocity of 1725 fps.

At this time cracks in the continuous plate extend out to a .8-in. radius and the conoid region and rear surface cracking has intensified inward. The continuous plate has a narrow plug break out of the back surface at 12 μsec.

Comparison of velocity fields at 11 μsec, Figure 4.21, demonstrates that more target material has been able to respond in the platelet case before conoid breakout. The discontinuous drop in velocity across the conoid is very visable here.

Assessment

Conoid failures progressed at just as high a rate in the platelet solution as in the continuous plate solution, and at a poor orientation from the standpoint of mass included. The reason that the removal of inertial fixity did not improve the tensile environment appears to stem from the fact that this relief also allowed material within the conoid to accelerate more freely as seen in the velocity field comparison, Figure 4.21. Thus, counteracting mechanisms affected the platelet failures.

Material above the developing conoid requires less force because it need not, in turn, accelerate as much surrounding material. This is verified by the higher velocity attained in this region compared to the continuous plate solution. Opposing this improvement is the higher acceleration required to maintain target integrity across the conoid because the material within the conoid is able to respond faster in the platelet case.

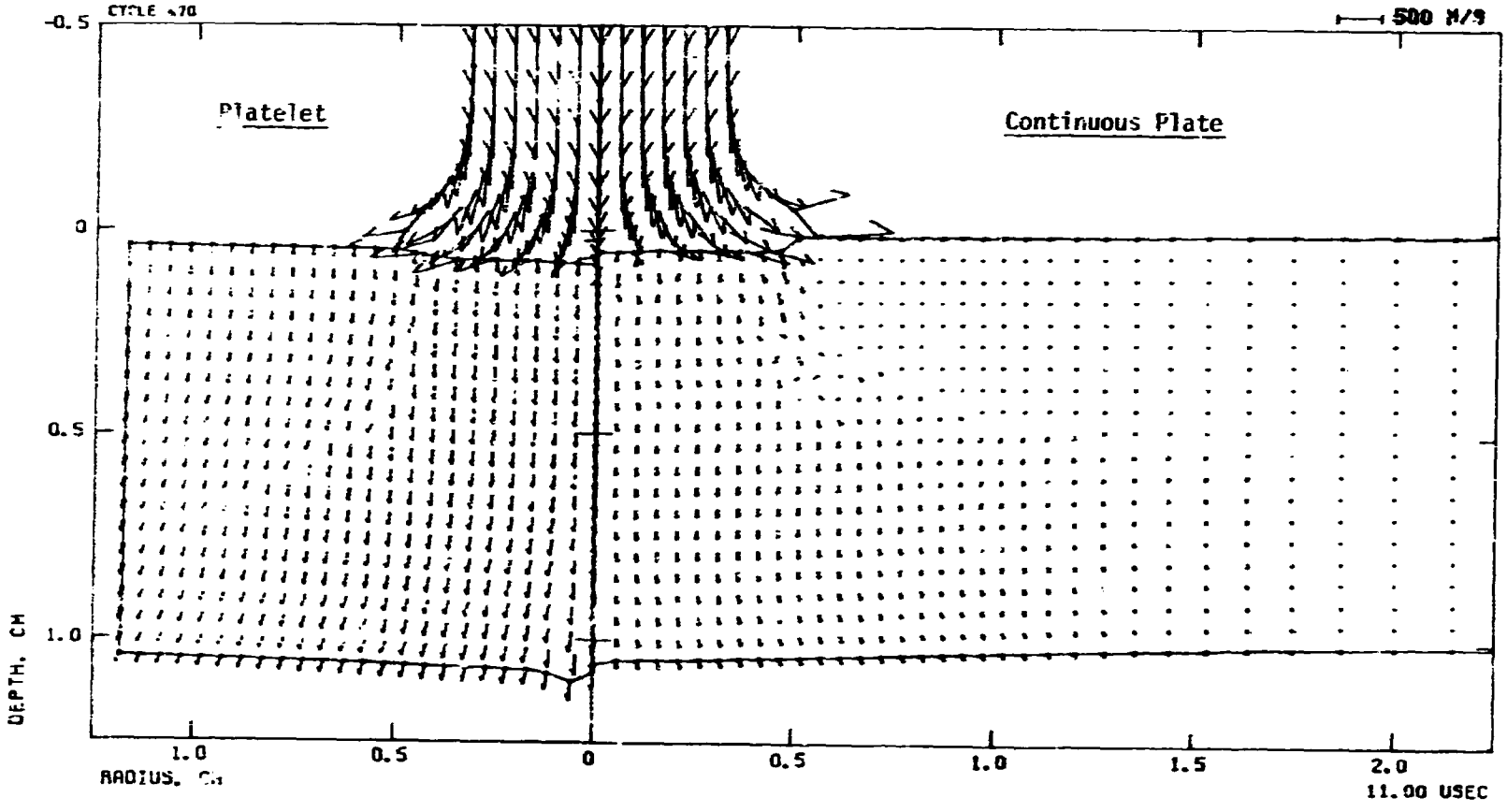

Figure 4.21. Comparison of Velocity Fields in Ceramic Platelet and Continuous Plate Targets at t = 11.0 μsec.

In summary, the benefit derived from the application of ceramic platelets appears to be improved multi-hit resistance. Damage could be confined to no more than adjacent platelets (in the case of a impact in the seam). Possible degradation in ballistic performance against hits near a platelet edge has not been assessed in the current study.

4.4 ENCHANCED MATERIALS

In the previous subsections, several methods for improving the performance of lightweight armor using available state-of-the-art materials were investigated. None of the 5 psf concepts evaluated significantly delayed ceramic failures, which in turn prevented adequate engagement of target mass in the impact. As a result, residual fragment velocity remained high and the impact footprint remained narrow. The basic problem which could not be overcome by the 5 psf concepts evaluated was the large discrepency between the forces (especially tensions) generated during the high velocity impact and the ceramic tensile strength.

Thus, the success of the refined concepts was still limited by the maximum available material strength properties. In this section, several analyses will be presented which help estimate the degree of improvement in ceramic strength properties which would be required in order to attain a successful 5 psf armor front phase. More specifically, the objective of this analysis will be to define the required increases in ceramic tensile strength and/or ductility.

Enhanced Tensile Ductility

In the first analysis the effect of increased tensile strength and ductility in a 5 psf ceramic platelet (.39-in. thick, .93-in. diameter) is considered. The tensile strength was increased to 80 ksi for this analysis, and in addition, plastic strains were allowed to accumulate at this stress level, which prohibited cracking. In this way the amount of ductility sustained during the impact could be determined. This value provides an estimate of the required ductility in an otherwise ceramic-like material if platelet integrity is to be insured. Compressive strength properties were unchanged.

The velocity/stress field at 18 μsec is shown in Figure 4.22. The entire platelet is seen to be moving with a uniform velocity of 600 fps and still accelerating. Because tensile stresses have unloaded to below ultimate by this time, peak tensile plastic strains have already been attained. In Figure 4.23 plastic strain contours depict the level of sustained tensile damage. As seen in the figure, ∿1% ductility is needed (with 80 ksi tensile strength) to surpress all tensile failures.

By using extrapolation, the residual velocity of projectile and platelet is found to be 880 fps. The footprint on a back layer consists of the entire .93-in. diameter platelet. This amount of residual momentum could be arrested by one psf of Kevlar backing [8] due to the large diameter footprint.

Significant improvements in material performance could be achieved with less than the 1% ductility required to suppress all tensile failures. Because conoid failures are critical to a the momentum transfer capability of the platelet, surpressing them

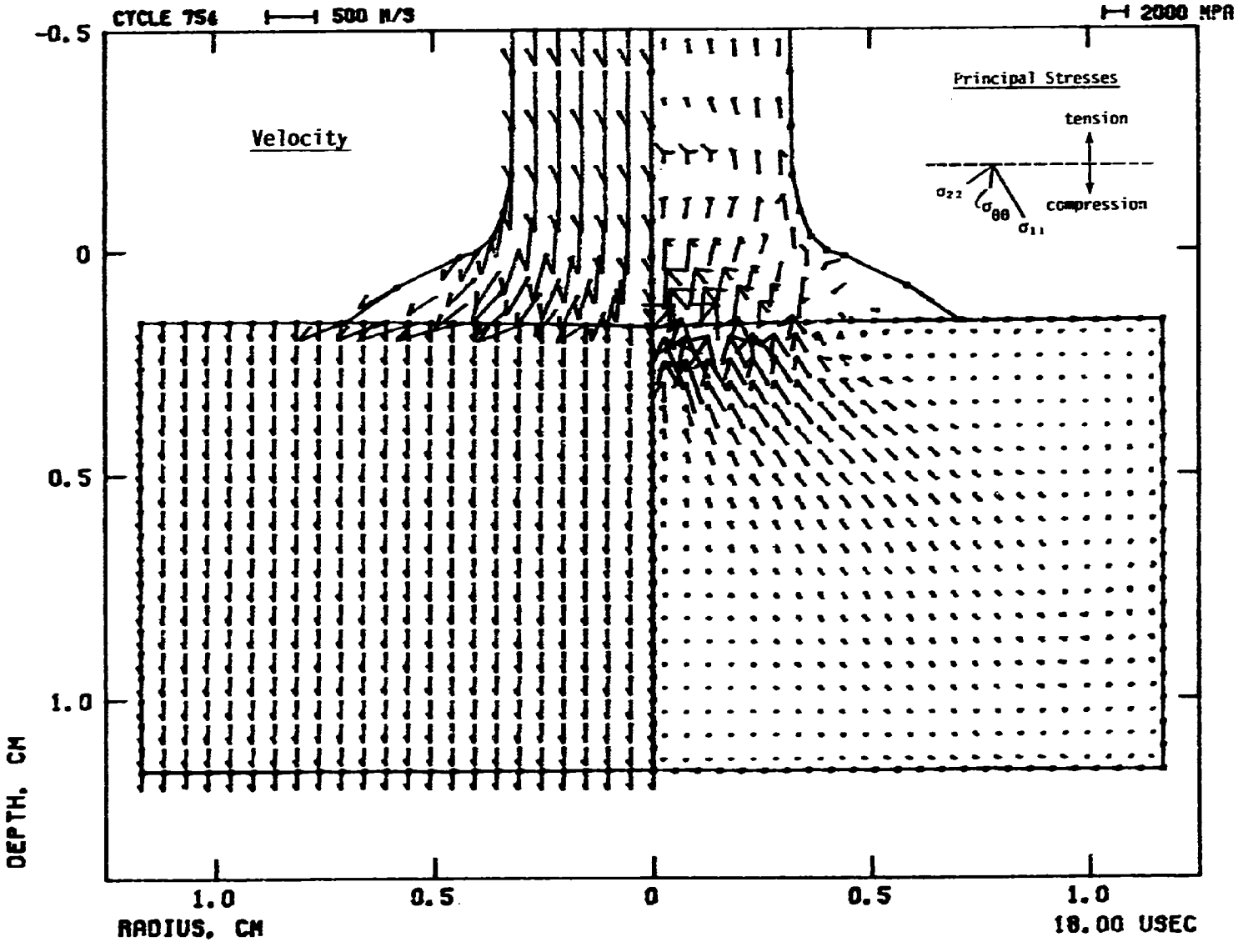

Figure 4.22. Velocity and Stress Fields in Enhanced Ductility Ceramic Platelet at t = 18.0 μsec.

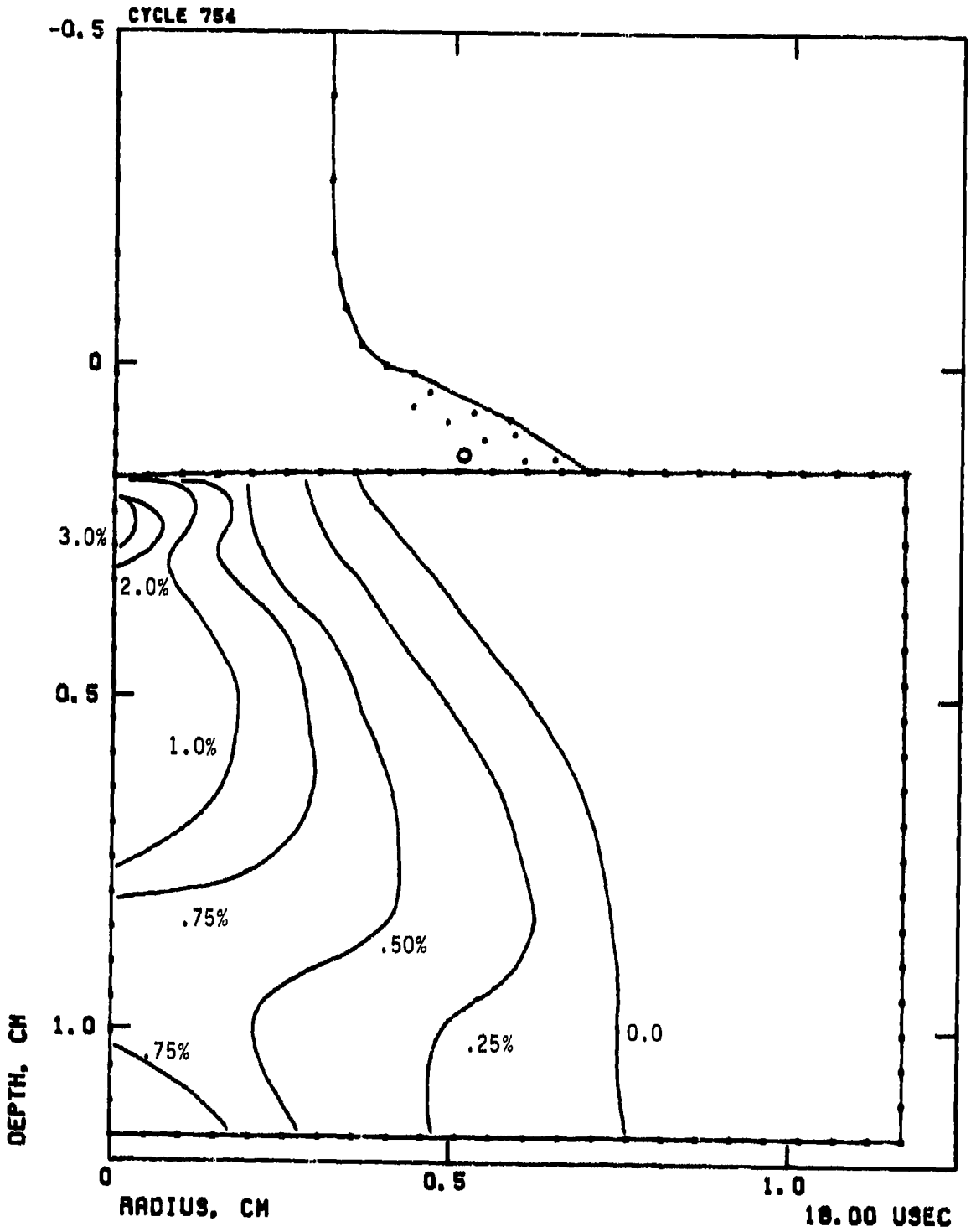

Figure 4.23. Accumulated Generalized Plastic Strain Contours in Enhanced Ductility Ceramic Platelet at t = 18.0 μsec.

alone should prove beneficial. This would require a ductility (with 80 ksi tensile strength) on the order of .25 to .50 percent.

A second analysis was performed which utilized the same enhanced material model. The target for this case consisted of a .25-in. thick, .93-in. diameter platelet, with .25-in. Kevlar backing which results in a 5 psf armor system. The tensile environment was expected to be more severe on the platelet back surface than in the previous case due to the decreased ceramic thickness.

Evidence of increased back surface tension can be seen in the large amount of plastic strains sustained in the calculation, Figure 4.24. Over six times the strains have accumulated at this time compared to the .39-in. platelet, and the tension has not yet unloaded.

The explanation for this large increase relative to a less significant change in thickness is two fold. First, it should be recalled from the discussion in Section 3.2 that the impulse per unit of front area of the shock wave decays with the square of the distance traveled from the point of impact. This means that the wave reaches the back surface of a .25-in. platelet with roughly 2.5 times the intensity as in a .39-in. platelet. Thus, the tensions generated (on the back surface) are expected to increase correspondingly. A second cause of this increase is the addition of Kevlar backing. This relatively flexible material adds inertial resistance to the motion of the platelet extremities without providing a corresponding increase in the target's capability to transmit vertical momentum radially

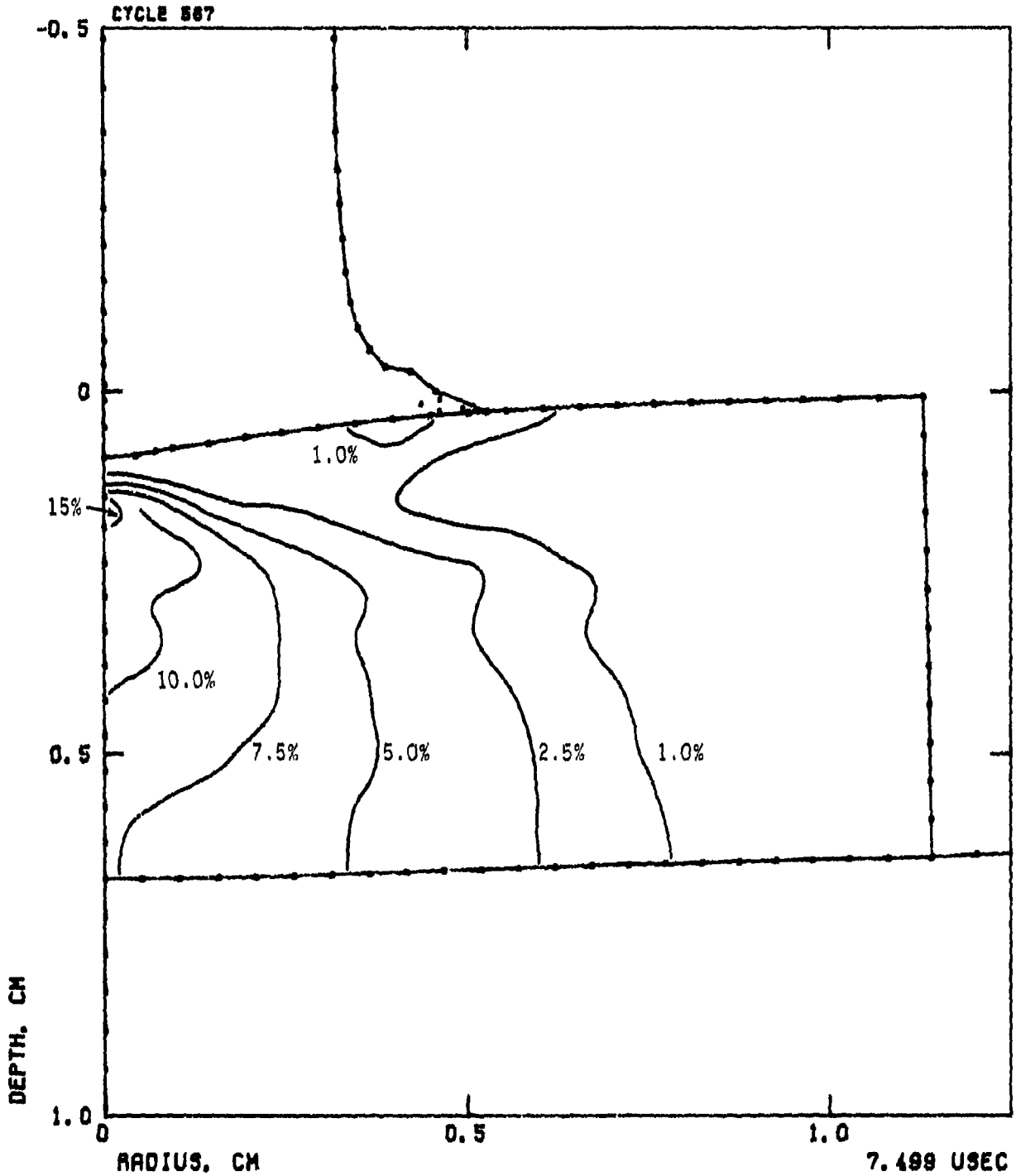

Figure 4.24. Accumulated Generalized Plastic Strain Contours in Enhanced Ductility Ceramic Platelet at t = 7.5 μsec Strain Values.

outward, which results in increased platelet bending, and thus, rear surface tensile loading.

This bending tendancy is apparent in the velocity field at 7.5 μsec, Figure 4.25. Here the center of the platelet is traveling much faster than the extremities. For this reason tensile strains would continue to accumulate if the solution were continued, probably in excess of 10%. Ductility requirements to surpress conoid formation are on the order of five percent.

Enhanced Tensile Strength

In order to determine the peak tensile stresses developed during impact on a 5 psf (.25-in. ceramic, .25-in. Kevlar) target, an additional enhanced material analysis was performed. The front phase for this analysis was again a .93-in. diameter platelet. The platelet material properties emulated B_4C except that tensile cracking was prohibited. In this manner peak tensions attained could be monitored directly, and brittle tensile strength requirements estimated.

The velocity/stress field at 7.5 μsec is shown in Figure 4.26. This figure corresponds in time to the previous case, Figure 4.25. In this case the entire platelet and associated Kevlar backing have been accelerated uniformly. In order for this to occur, material on the impact axis at the platelet back surface was forced to carry high tensile stresses. The stress-time history for this location, Figure 4.27, reveals a peak tensile stress of 450 ksi. The peak tensions attained throughout the platelet are given in Figure 4.28.

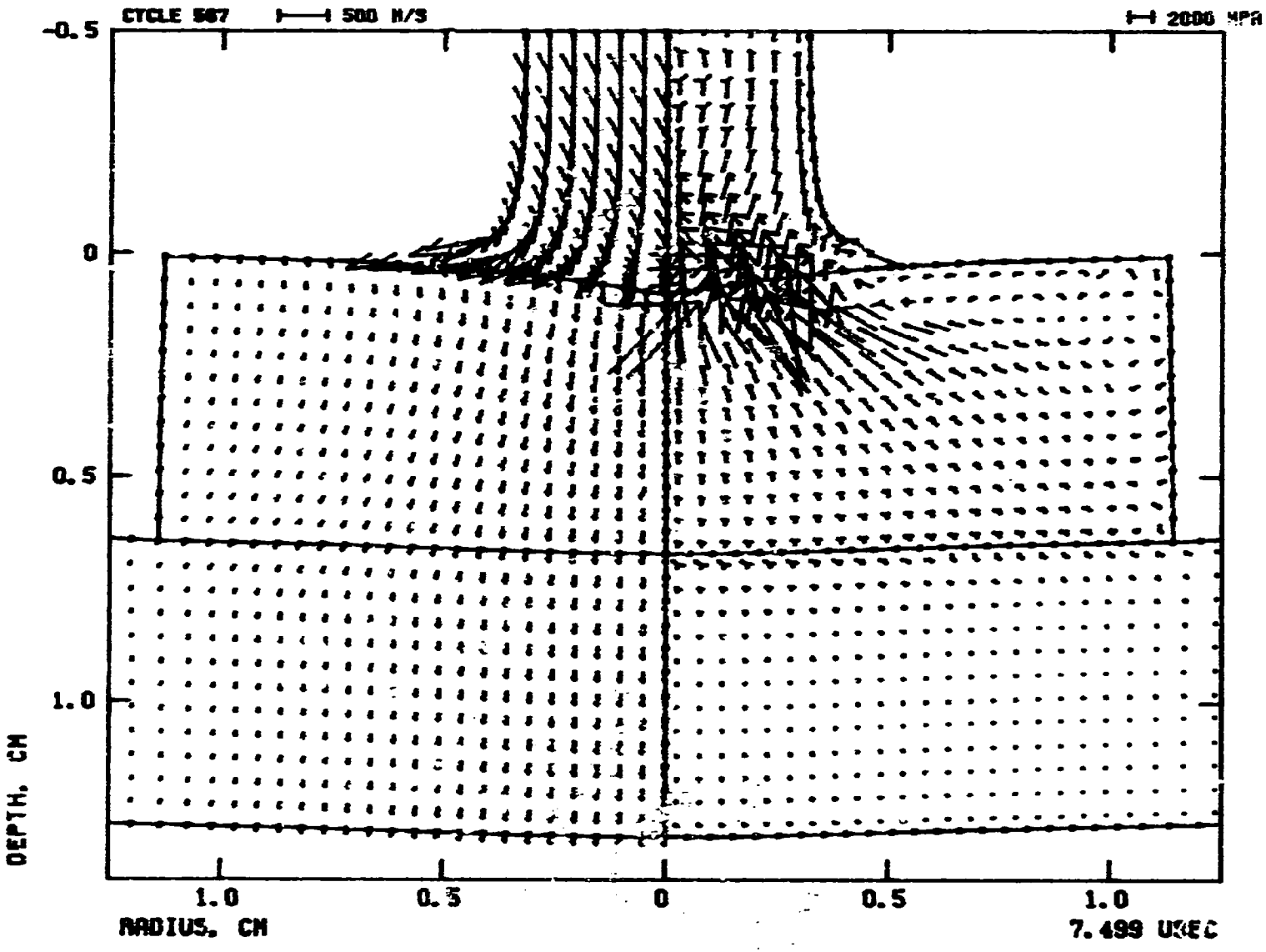

Figure 4.25. Velocity and Stress Field in Enhanced Ductility Ceramic/Kevlar Target at t = 7.5 μsec.

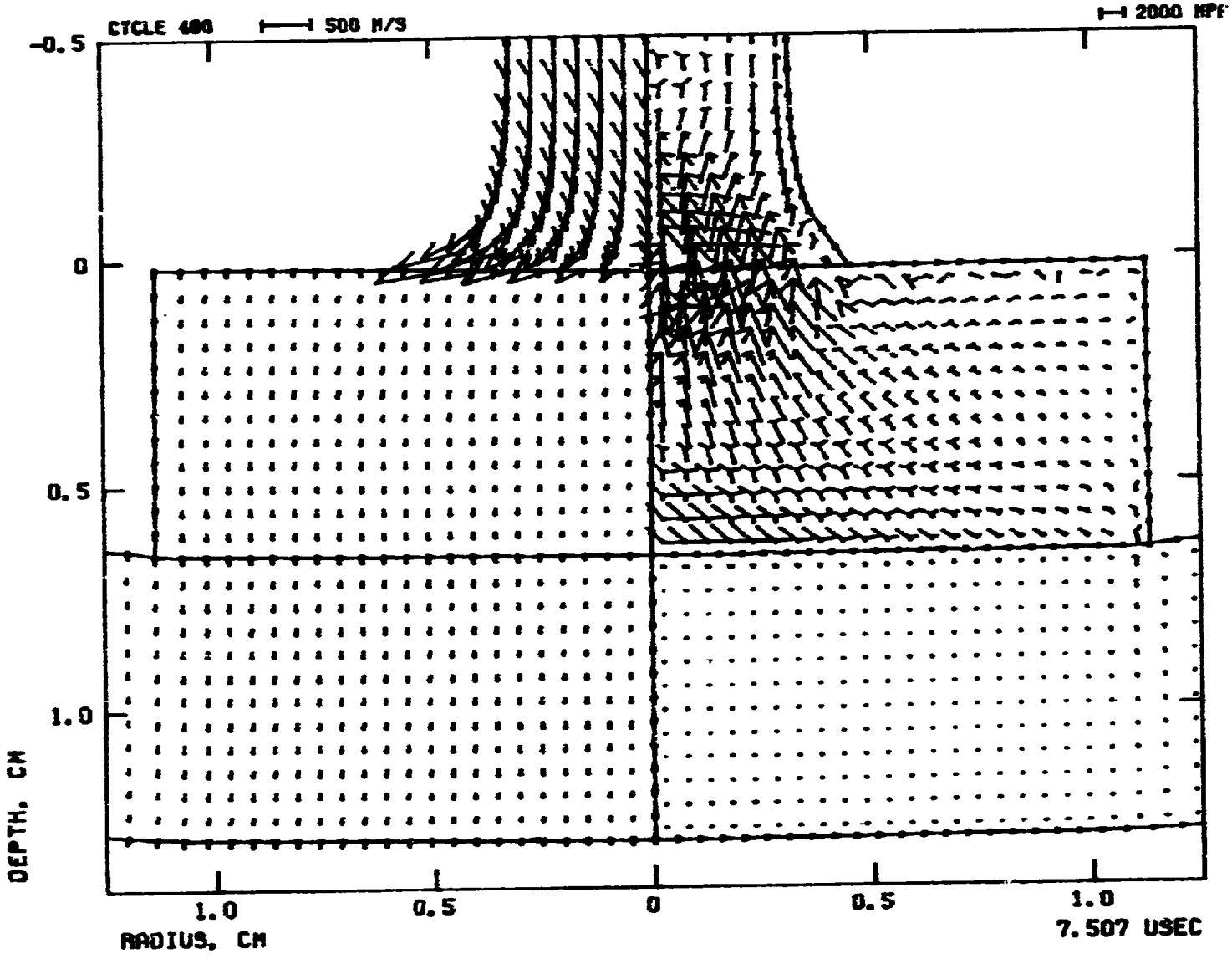

Figure 4.26. Velocity and Stress Fields in Enhanced Tensile Strength Ceramic/Kevlar Target at t = 7.5 μsec.

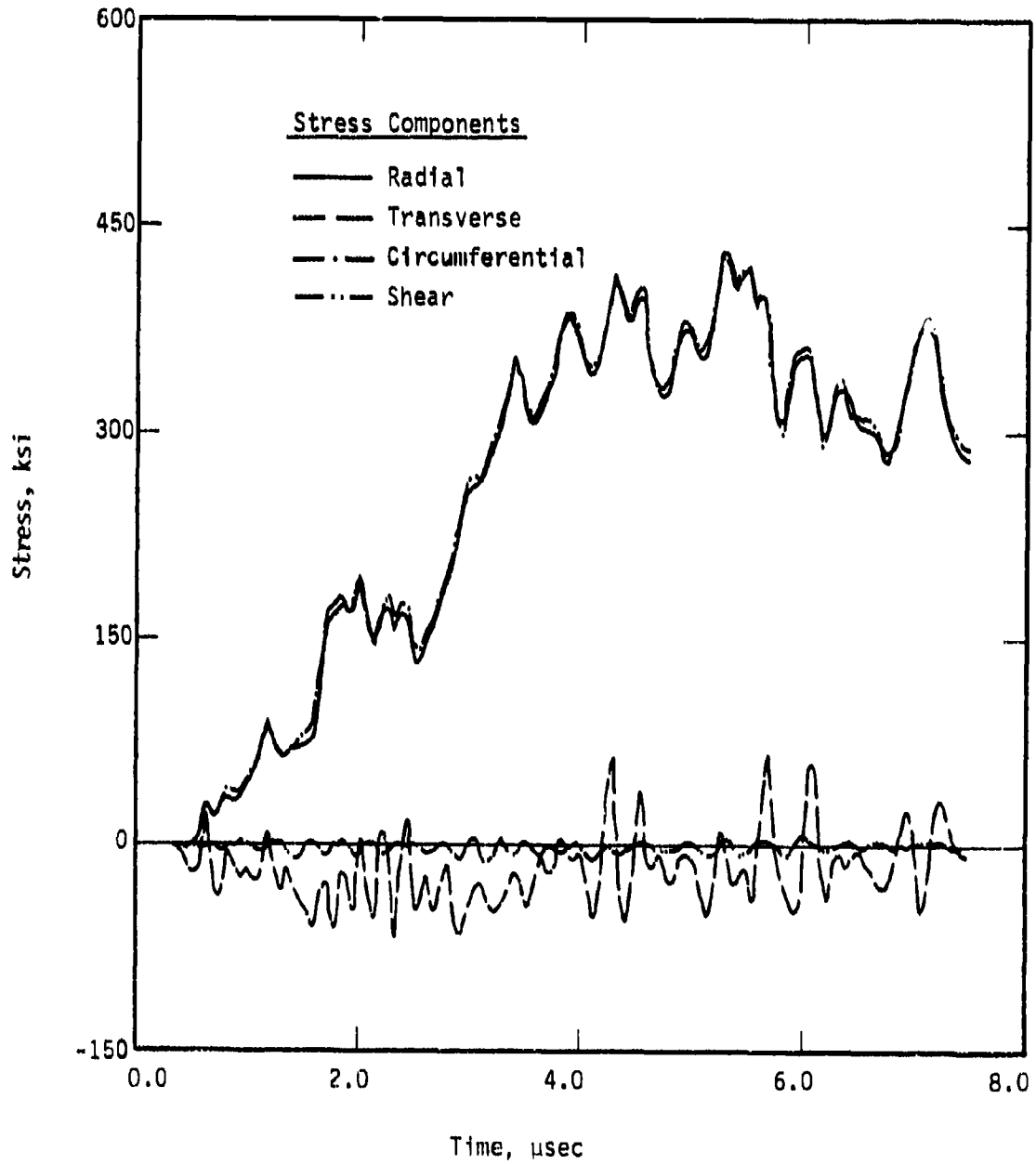

Figure 4.27. Stress-Time History on Impact Axis at Back Surface of Enhanced Tensile Strength Ceramic Platelet/Kevlar Target.

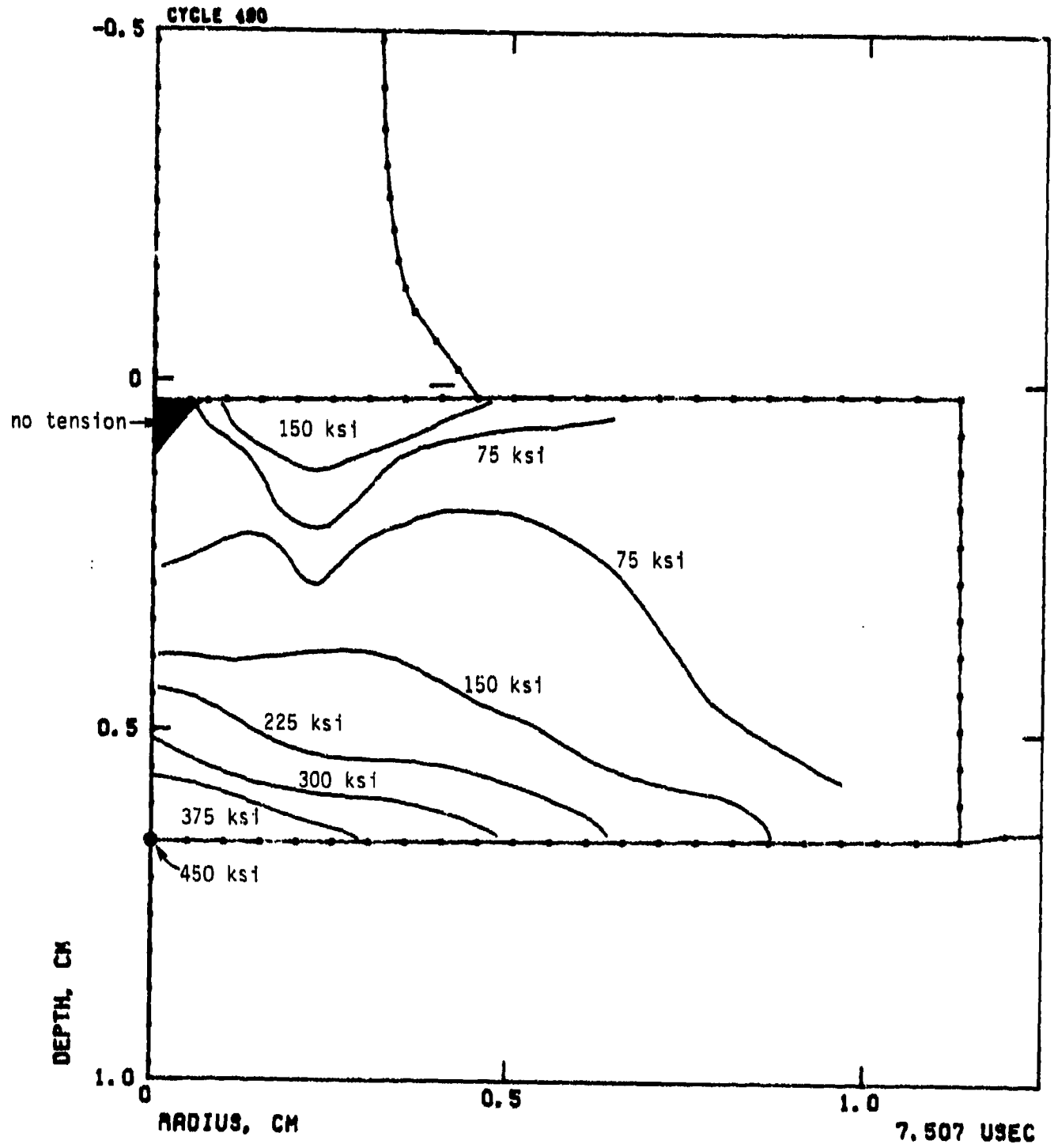

Figure 4.28. Peak Tensile Stress Contours in Enhanced Tensile Strength Ceramic/Kevlar Target at t = 7.5 μsec.

Thus, the .25-in. ceramic platelet is severely overmatched by the threat. It would require an order of magnitude increase in tensile strength to prevent back surface failures. In the conoid region, a somewhat milder 150 ksi must be sustained.

Again, because conoid failures directly affect momentum transfer capabilities of a target more strongly than back surface failures, an increase in brittle tensile strength to this 150 ksi level would be quite beneficial. Furthermore, following the back surface crack initiation which would occur at this strength level, tensile stresses in the conoid region would tend to be relieved, possibly reducing the tensile strength requirements necessary to surpress conoid tensile failures.

Assessment

Although the three analyses discussed above by no means constitute a comprehensive study of 5 psf armor material requirements, they do provide valuable insight into the level of improvement needed relative to state-of-the-art materials. A material exhibiting the desirable qualities of Boron Carbide, i.e., lightweight and high compressive strength, must also possess enhanced tensile strength. Alternatively, tensile ductility on the order of several percent is required. Either of these alternatives would require major advances in ceramic technology, or perhaps the development of a new composite material.

An important factor to note is the large decrease in tensile strength required with the addition of ductile behavior. A ductile material is able to sustain tensile stresses at its ultimate strength level longer than a brittle material.

SECTION V

EVALUATION OF REAR PHASE CONCEPTS

Containment of residual momentum of degraded projectiles and fragments which penetrate front armor layers is the primary role of the rear-most layer in the generic multi-phase lightweight armor concept. Both rigid and flexible concepts could be employed in the rear layer application. Rigid back layers diminish back surface deflections thus providing decreased effective armor thickness. Considerable impact testing and wide application to lightweight body armors indicate flexible membranes to be more weight efficient in absorbing momentum than rigid concepts [5]. Because weight-efficient stopping capability is the primary back layer function, a flexible back layer concept has been adopted as the base for generic back layer study.

This section will examine the mechanisms which enable light-weight ballistic materials to absorb residual momentum. Computer simulated impacts will be used to illustrate this process and to evaluate the effects of changes in material and geometry parameters. From these parametric studies, mechanisms for improving the state-of-the-art in weight sensitive ballistic back layer concepts will be identified.

Kevlar 29 fabric is widely regarded as the state-of-the-art in flexible lightweight armor materials [5]. As a stand-alone armor system, layers of Kevlar fabric weighing under 2 psf have resisted a wide variety of handgun threats [8]. High velocity projectiles, however, with high hardness and sharp nose contouring are able to defeat these systems by weave perforation and fiber shearing [5]. Since these fabric defeating projectile

qualities are assumed to be degraded during front layer penetration, Kevlar fabric was selected as the flexible back layer material for numerical study.

The mechanical properties of Kevlar are very unusual. While extremely light, Kevlar 29 fibers possess mechanical properties more typical of structural metals, namely a nominal tensile strength of 410 ksi and an elastic modulus of about 9.5×10^6 psi [9].

A dense, plain weave (Figure 5.1) fabric consisting of 1500 denier Kevlar 29 fibers, 24 x 24 per square inch, was selected as a baseline back layer material. The high fabric density (.067 psf/ply) improves resistance to penetration by fiber spreading. Because of weave crimp, the fabric is approximately 3% heavier and 3% more flexible than is calculated from fabric properties. Figure 5.2 shows the stress-strain curve of both Kevlar 29 fibers and the baseline Kevlar fabric.

5.1 KEVLAR FABRIC RESPONSE

The purpose of back layer numerical impact simulation is two-fold: First, to gain an understanding of the response of membrane fabric targets subjected to projectile impacts; and second, to undertake a parametric study of variations in geometry, fabric properties and threat level to identify mechanisms for improving the Kevlar fabric back layer concept. In order to meet these objectives, it is necessary to model the constituents with enough detail to effectively simulate the physical effects of the fabric/projectile properties. To enable

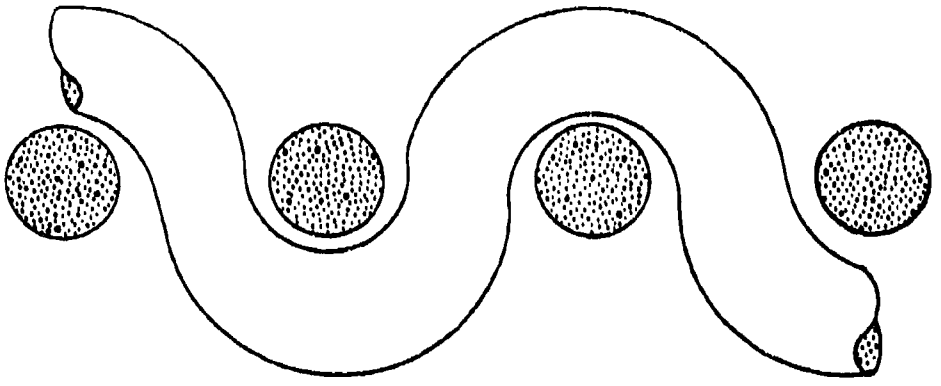

Figure 5.1. Plain Weave Geometry.

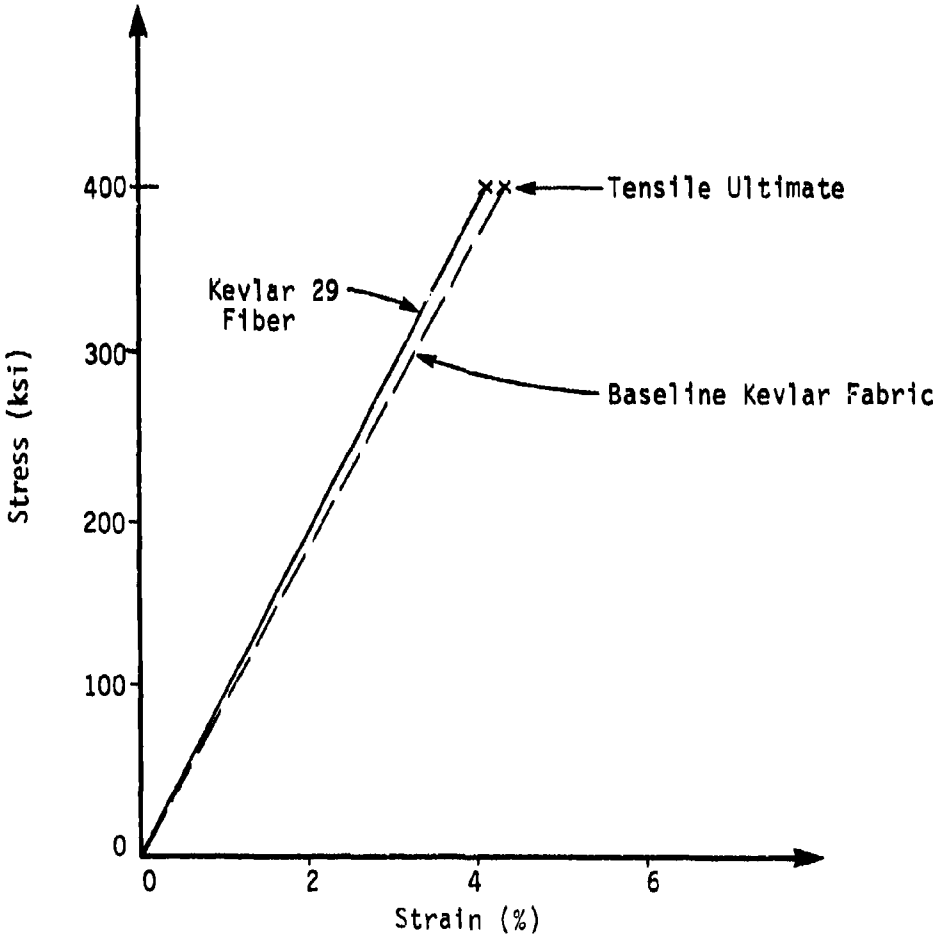

Figure 5.2. Stress-Strain Curve for Kevlar 29 Fiber and Baseline Kevlar Fabric.

the undertaking of a parametric study involving many analyses, the analytical model must be economical and easy to modify and to check for each analysis.

CALSAP [11], a non-linear finite element code, is particularly well-suited for analysis of fabric impacts within these contraints. This code is capable of modeling the dominant uniaxial fiber properties, including large rotations in a simple manner. Because of the flexible target and low residual impact velocity, high contact stresses which would demand modeling of components as a continuum do not exist. Variations in geometry and materials are easily conducted in CALSAP.

An axisymmetric fabric model was developed for use in computer simulation of projectile/fragment impacts on fabric targets. Axisymmetric modeling allows analysis of fabric impacts with a minimum of solution expense. This is accomplished by dividing the fabric into concentric ring regions about the impact point. As seen in Figure 5.3, this approach assumes that the motion of all points lying on a concentric circle is identical. Thus, axisymmetric modeling reduces the degrees of freedom necessary to model the problem by constraining the motion of many points to a single mode of deformation. Although axisymmetric calculations are approximate (due to these assumptions), they should provide qualitative insight into the response of Kevlar fabric and the effects of material and geometry variations.

The analytical model developed employs two truss finite elements to represent a ring region of fabric; one to model radial fabric stiffness and the other hoop stiffness. To define the truss element properties, the Axisymmetric Cartesian Equivalent (ACE) computer program was developed. The ACE program

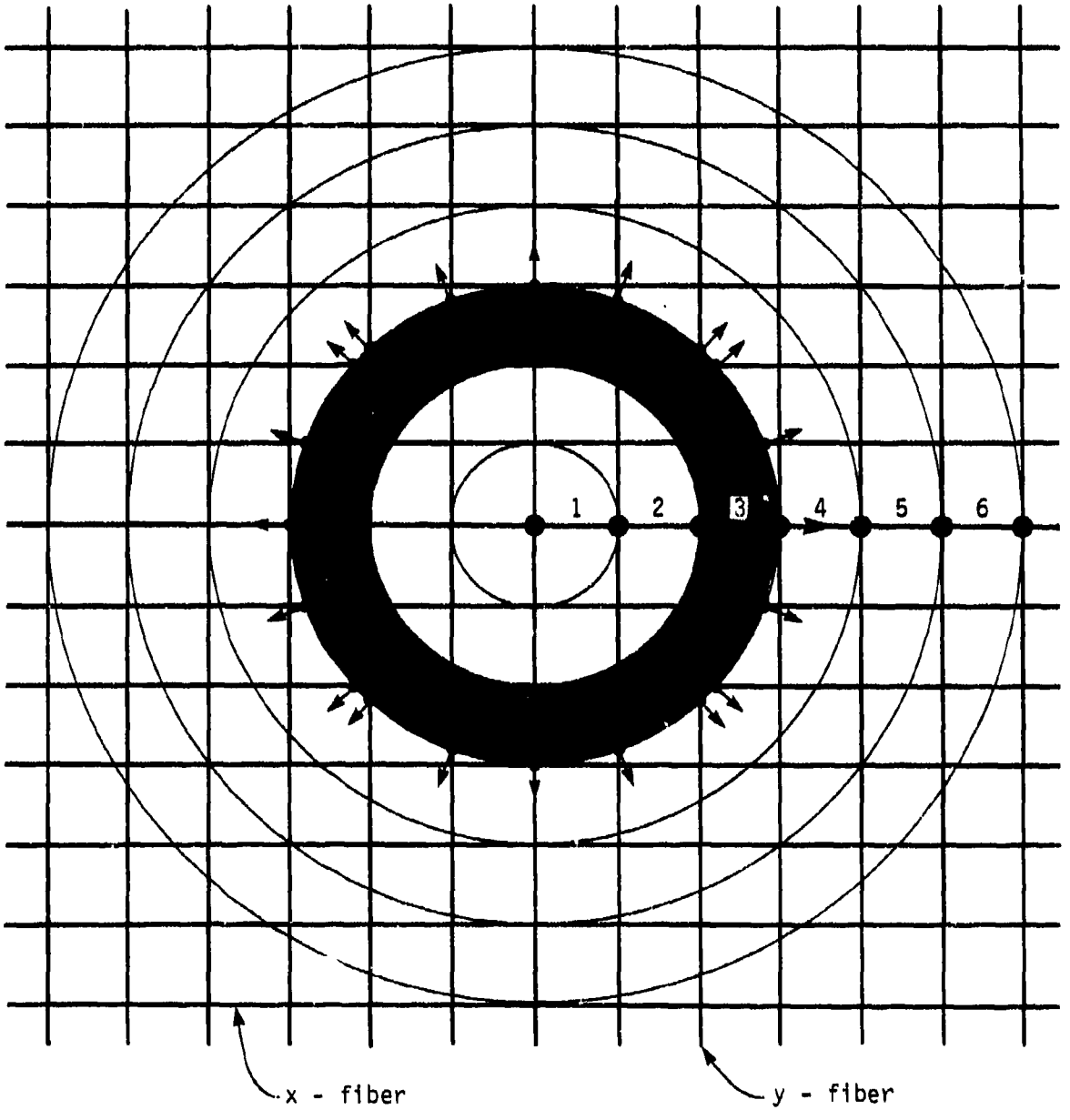

Figure 5.3. Ring Regions for Axisymmetric Modeling of Fabric. (Mode of Deformation On Outer Edge of Ring Region 3 (Shaded) is Depicted By Arrows.)

calculates the radial and hoop truss stiffnesses necessary to represent the fabric resistance to the assumed deformation modes. ACE also applies the mass of each ring region to the proper truss elements.

The projectile threat for CALSAP solutions was intended to simulate ejecta emanating from the back surface of the front armor layer. Several rigid elements were employed to model a caliber .60 compact fragment with a radius of curvature of .50 in. The projectile mass was .018 lbm.

Seven gap/contact elements were used to simulate contact and sliding between the projectile and fabric. Gap elements close when interpenetration is detected during a solution. A closed gap element prevents further penetration normal to the contact surface, but allows unrestricted sliding to occur. There is no mass associated with gap/contact elements.

The entire CALSAP finite element model is depicted in Figure 5.4. It consists of 65 finite elements: 14 rigid trusses to model the projectile, 51 trusses to model the fabric target, and 7 gap/contact elements. Due to axisymmetric modeling and course zoning away from the point of contact, only 61 degrees of freedom were necessary to model an 8-in. circular fabric target.

Two baseline numerical solutions of a simulated blunted fragment impacting a Kevlar fabric target were conducted. Projectile velocities of 600 fps and 900 fps were selected to represent the residual velocity following front layer penetration. The target model stiffness and mass were scaled to represent 18 fabric plys resulting in a 1.2 psf target.

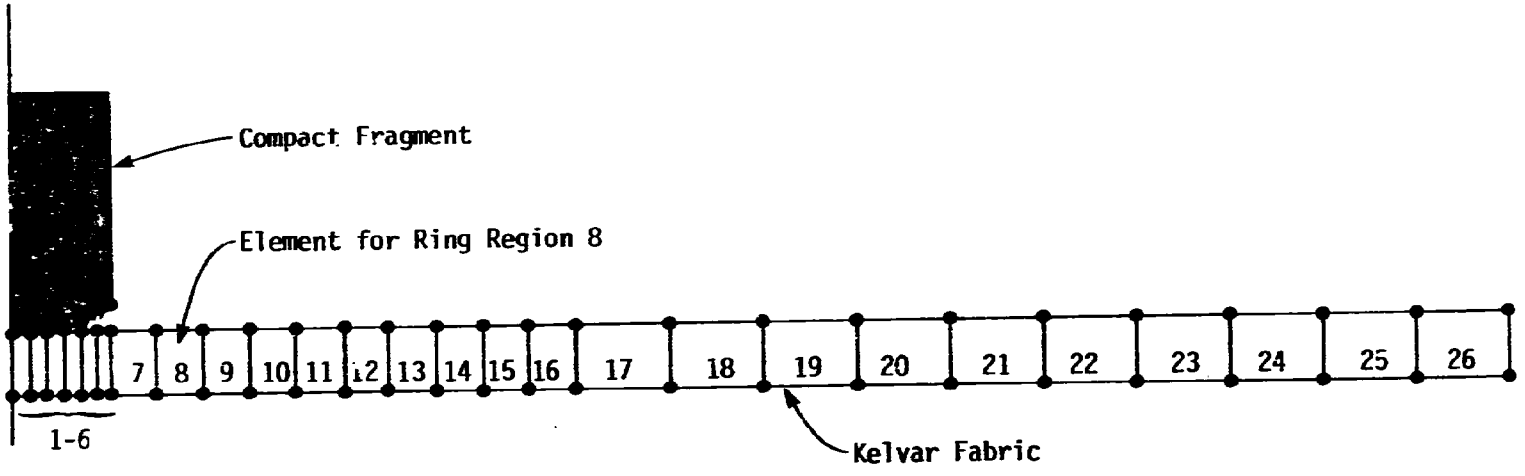

Figure 5.4. CALSAP Finite Element Model For Analysis of Fabric Impact Response. (The Ring Regions (Numbered) Are Expanded Away From The Point of Contact For Solution Efficiency).

Figures 5.5 and 5.6 show the deformed target at several points in time following a 600 fps impact. At the projectile's first contact, the fabric at the point of impact is quickly accelerated to the impact velocity. Only a small amount of projectile momentum is lost in this process, since so little fabric is involved at this time. Because the fabric at the point of contact is stretched as transverse deflection occurs, tensile fiber stresses develop. These stresses propagate radially outward in the target, accelerating encountered fabric horizontally toward the point of contact. As fabric moves horizontally, the fiber stretching (and thus stress) is relieved. Fabric inertia, however, resists this motion, and prevents stress relief from keeping pace with stretching demanded by the center deflections. This causes stresses to build. During these early times, fabric stresses do not effectively resist projectile motions since the target is virtually horizontal.

As seen at later times in Figure 5.6, the fabric at the outer most point of contact with the projectile is no longer horizontal, and therefore has a component of its tensile stresses which decelerate the projectile (Figure 5.7). The higher the fabric tension at the point of contact and the more vertically aligned the fabric there, the more rapidly will the projectile be decelerated.

As the projectile is decelerated by the vertical component of fabric stresses at the point of contact, so is the horizontal fabric at the edge of the transverse wave accelerated downward by similar forces. This leads to an expansion of the wave front (Figure 5.8). Thus, as the impact event progresses, the initial projectile momentum is spread to an increasing area of fabric much more massive than the projectile.

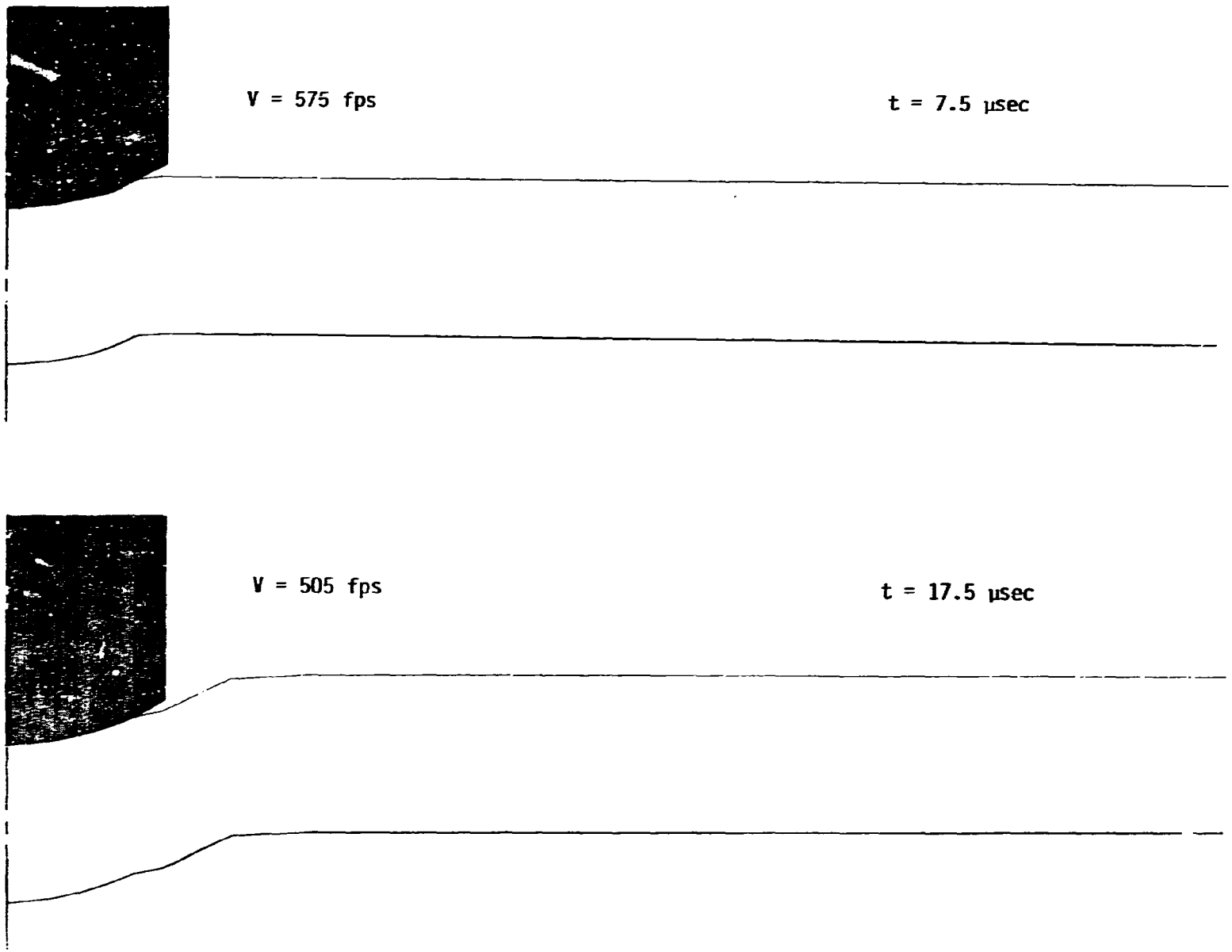

Figure 5.5. Early-Time Response of 18-Ply Fabric to 600 fps Impact.

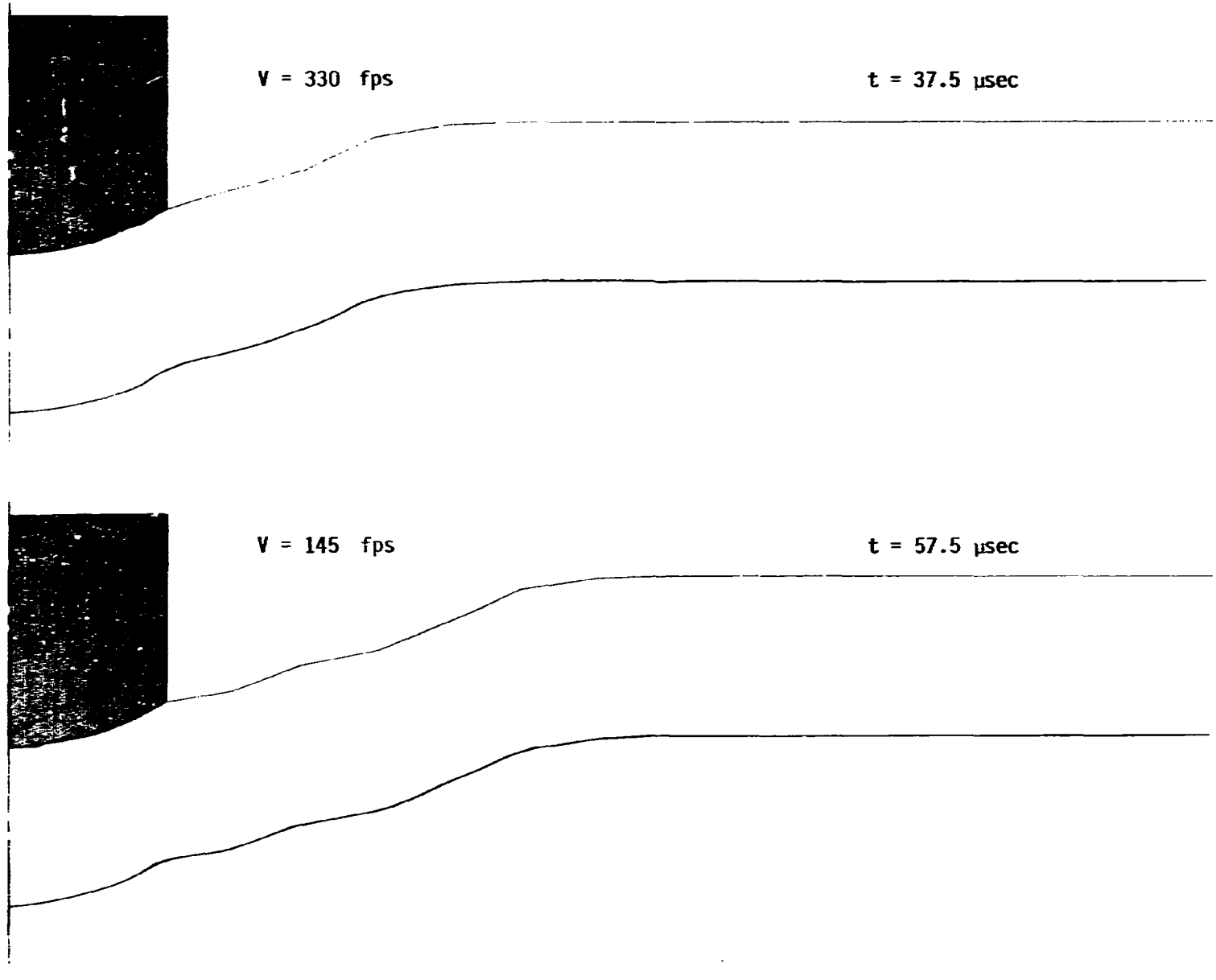

Figure 5.6. Late-time Response of 18-ply Fabric to 600 fps Impact.

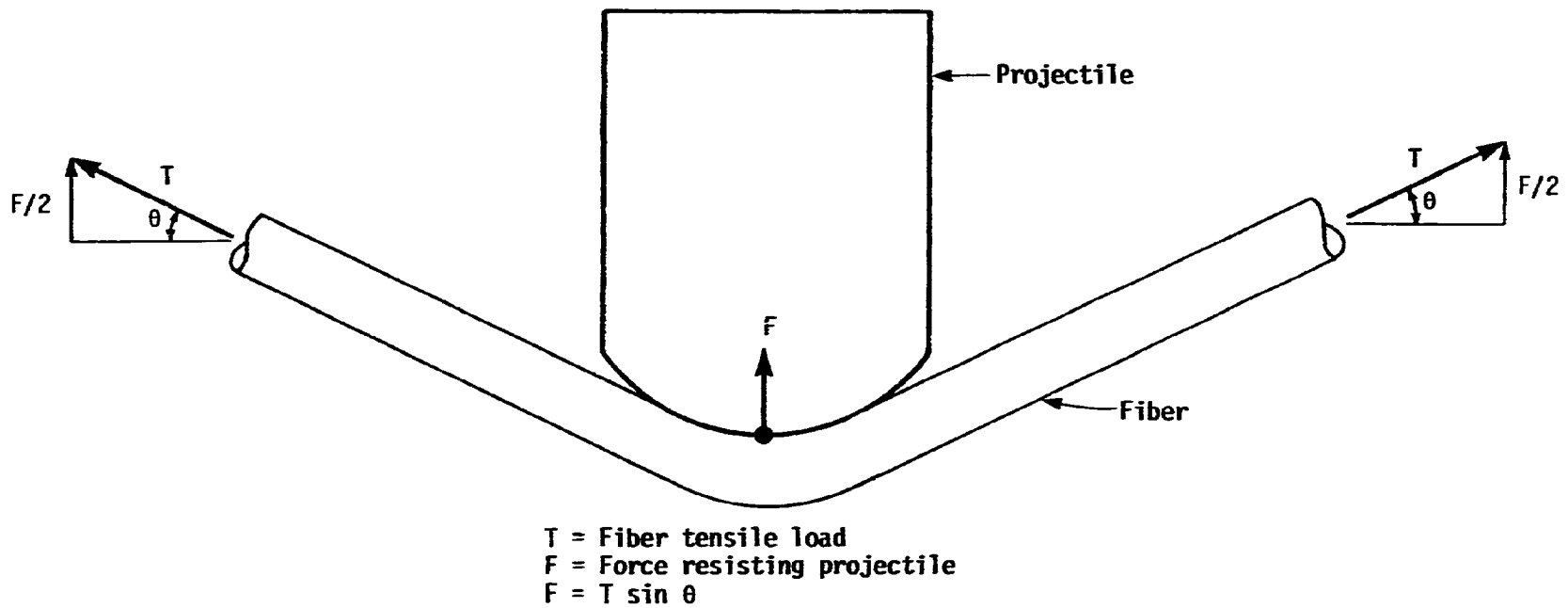

Figure 5.7. Relationship of Fiber Tension To Force Resisting Projectile.

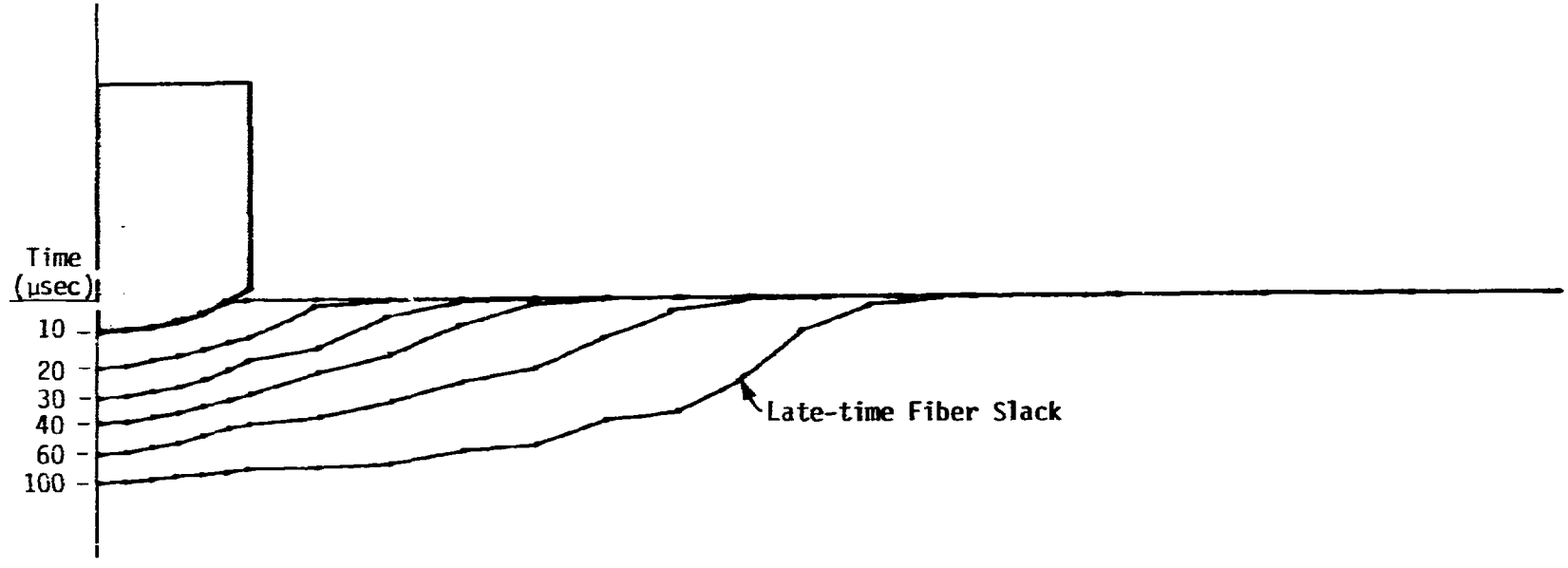

Figure 5.8. Response of 18-ply Target To 600 fps Impact.

Without any support of the fabric, a projectile would never be completely stopped, but would approach zero velocity as the transverse wave front involves more fabric. Because the CALSAP model is finite in size and simulated an unsupported target, the projectile is decelerated to a small non-zero final velocity. In a back layer design, some support at the fabric edges or soft backing would be provided. Figure 5.9 shows the projectile velocity time history and notes the effect of the finite model. Figure 5.10 gives the projectile displacement time history.

As the projectile slows and the transverse center deflection grows, the rate at which further fabric stretching is demanded decreases. This enables the fabric response to finally catch up to the projectile motion and begin to relieve the stresses. As seen in Figure 5.11, the fiber stress at the point of contact peaks at about 40 μsec. It is at this location where the highest stresses are obtained in the target.

The peak fiber stress of 460 ksi, while above the tensile ultimate for Kevlar 29, is not indicative of armor failure. Because of compliance between fabric plys, the response of underlying plys is softened, resulting in lower stresses. The CALSAP simulations, by modeling a multi-plyed armor as 1-layer of adjusted stiffness and mass, assume all plys to respond identically to the front. Therefore, the calculated peak stress indicates only the possibility of localized failures in the top plys.

Figures 5.12 and 5.13 depict the target response to a 900 fps impact. Displacement, velocity and stress time histories of 600 fps and 900 fps are compared in Figures 5.14 - 5.16. As

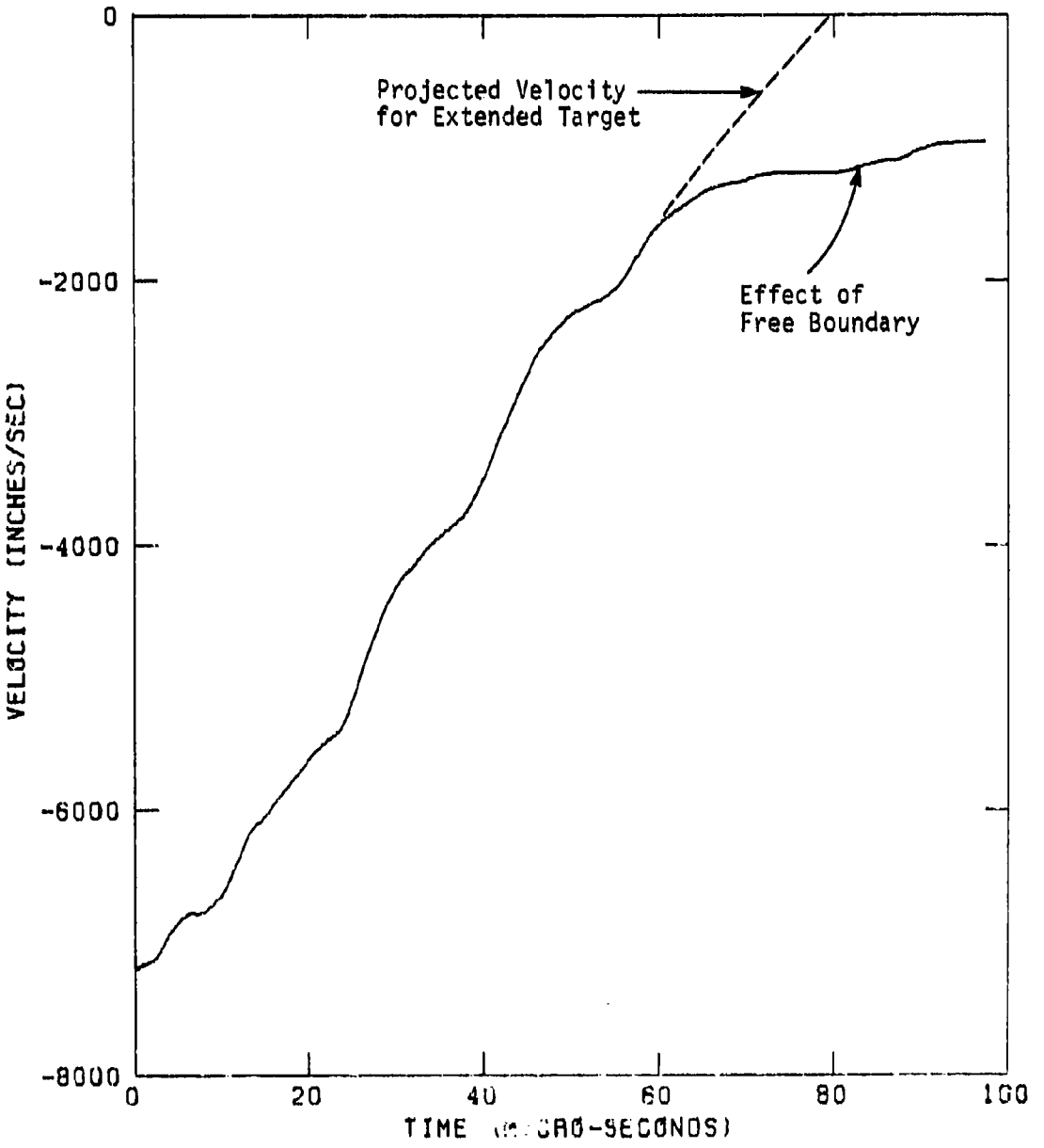

Figure 5.9. Velocity-time History of 600 fps Fragment Following Impact on 18-ply Fabric Target.

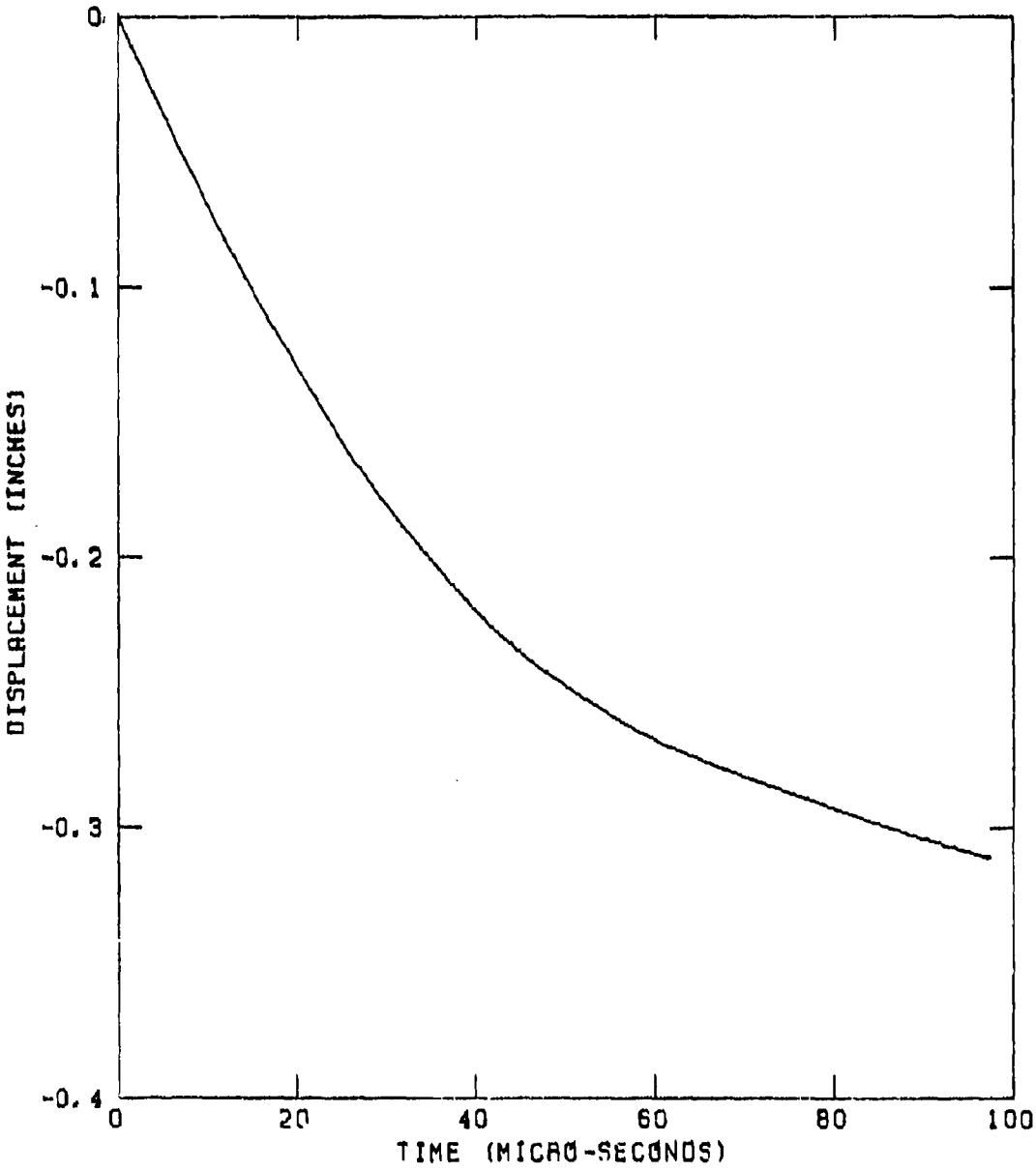

Figure 5.10. Displacement-time History of 600 fps Fragment Following Impact On 18-ply Fabric Target.

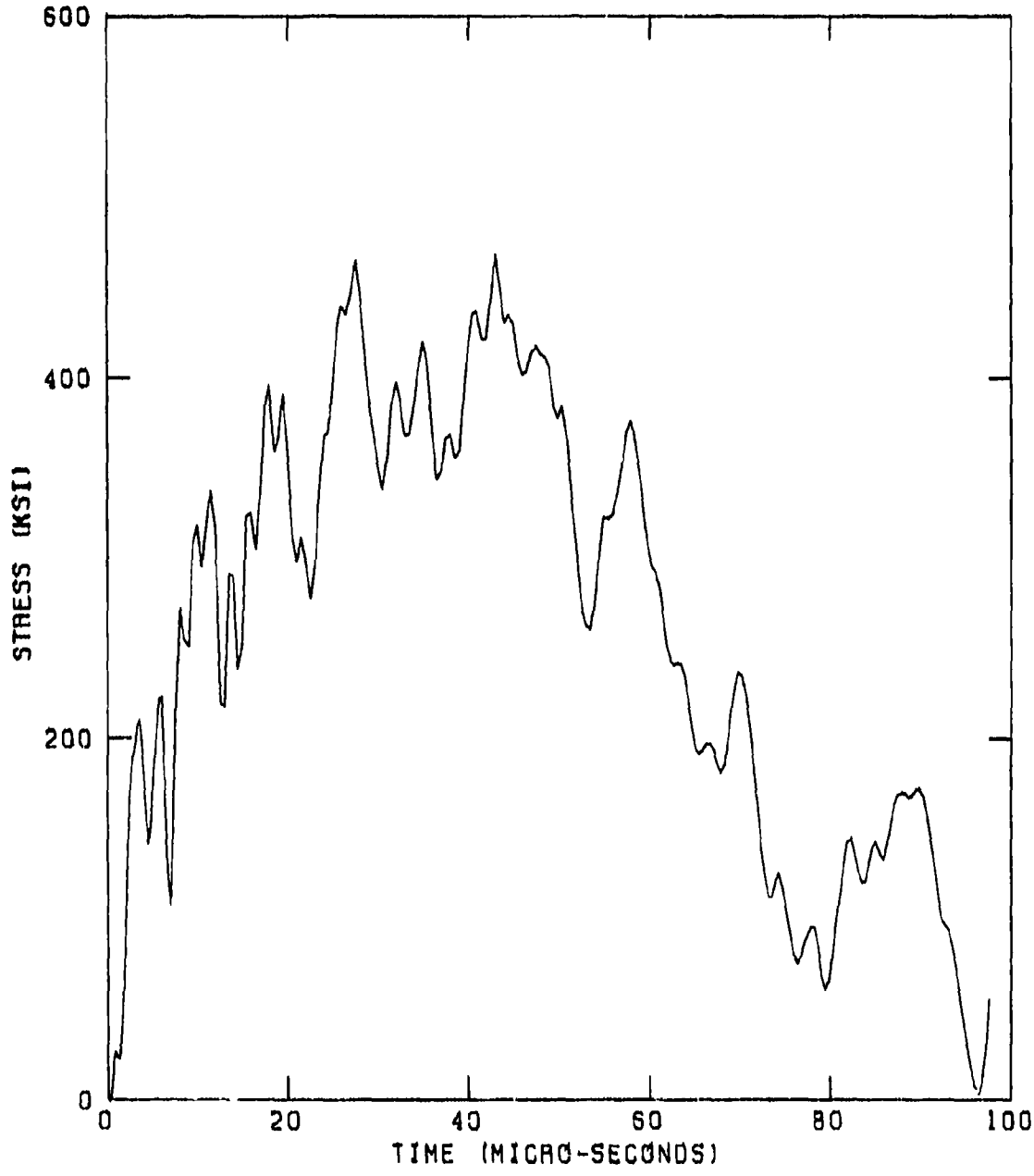

Figure 5.11. Stress-time History of Fiber at Impact Point of 600 fps Fragment on 18-ply Fabric Target.

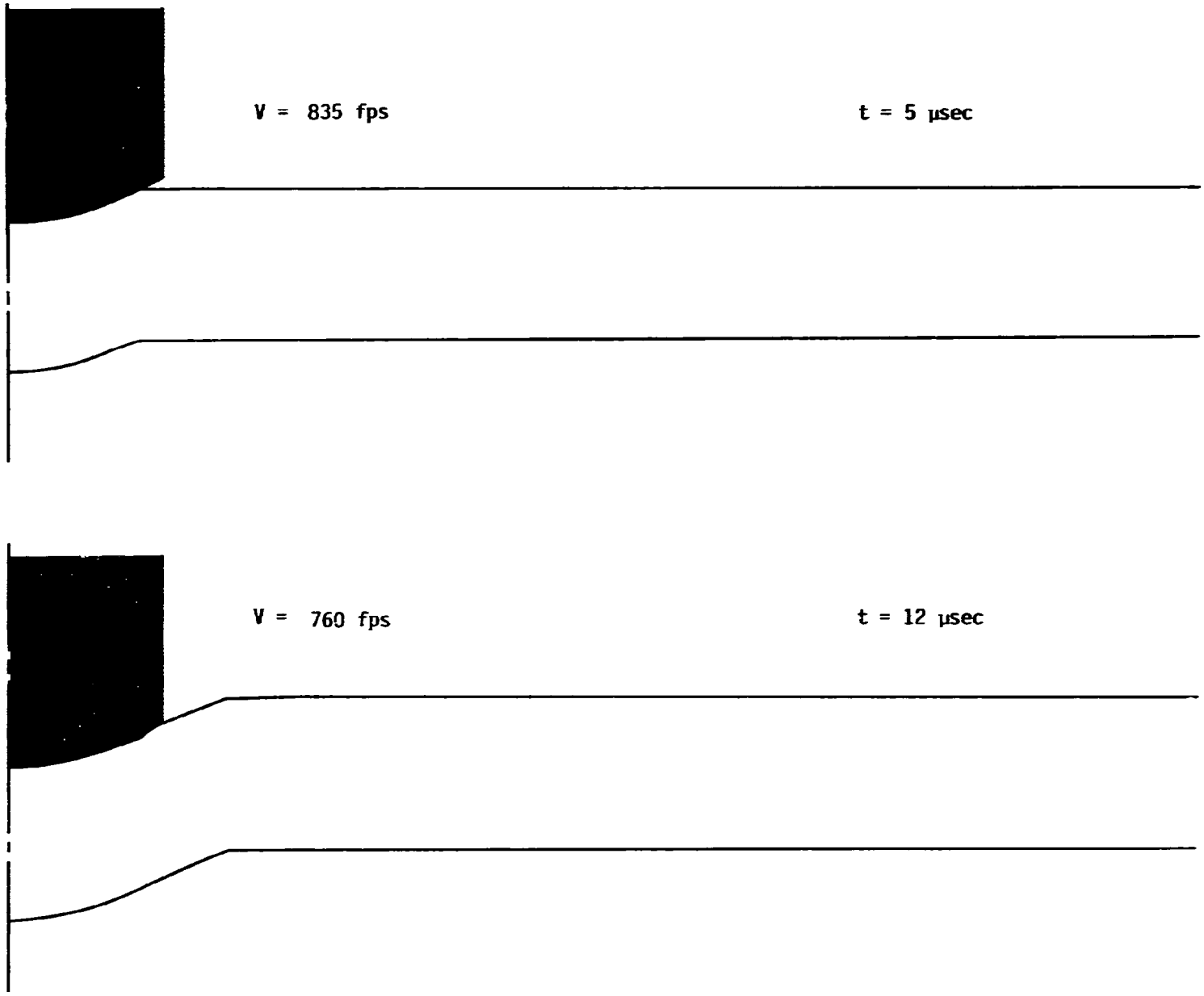

Figure 5.12. Early-time Response of 18-ply Fabric to 900 fps Impact.

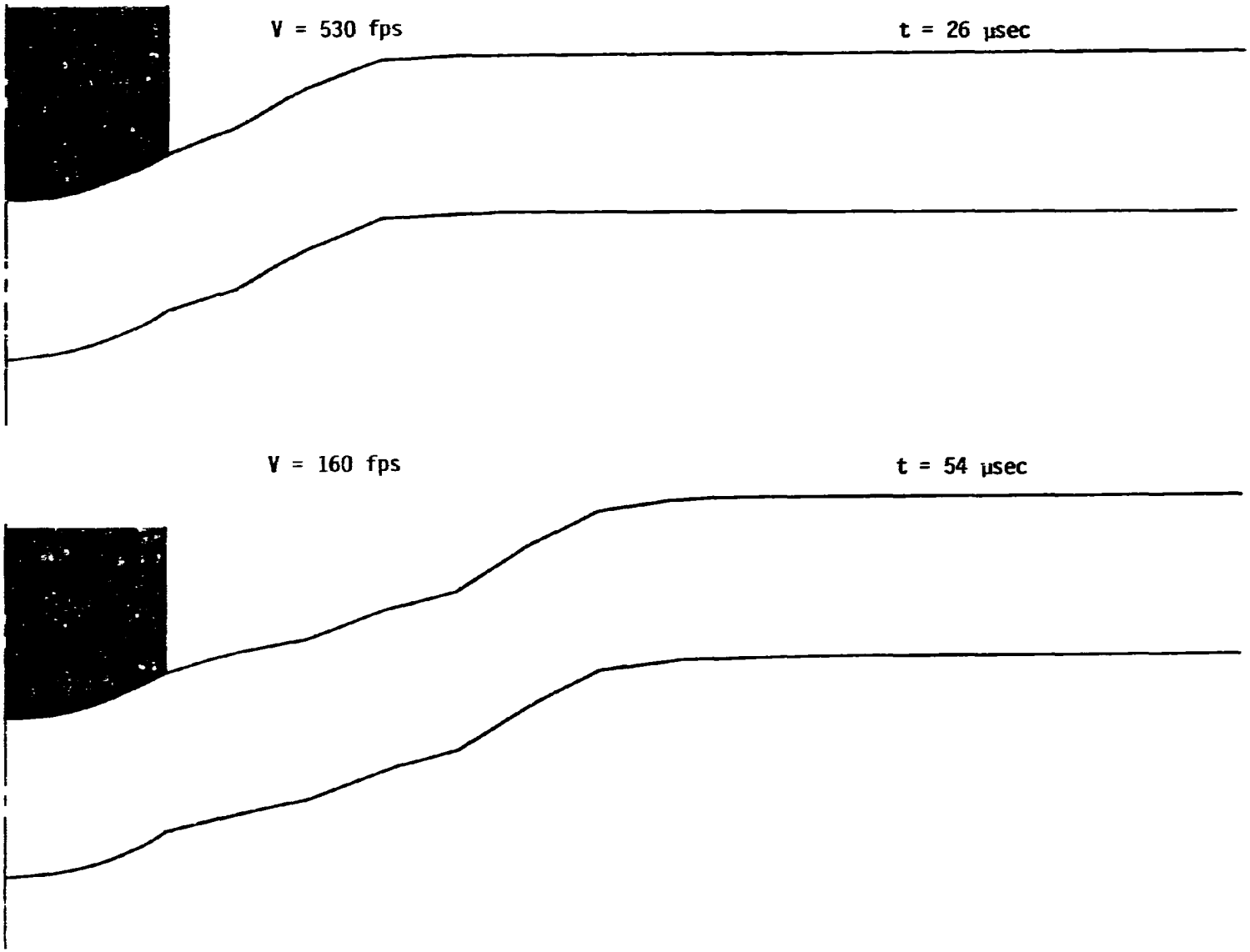

Figure 5.13. Late-time Response of 18-ply Fabric to 900 fps Impact.

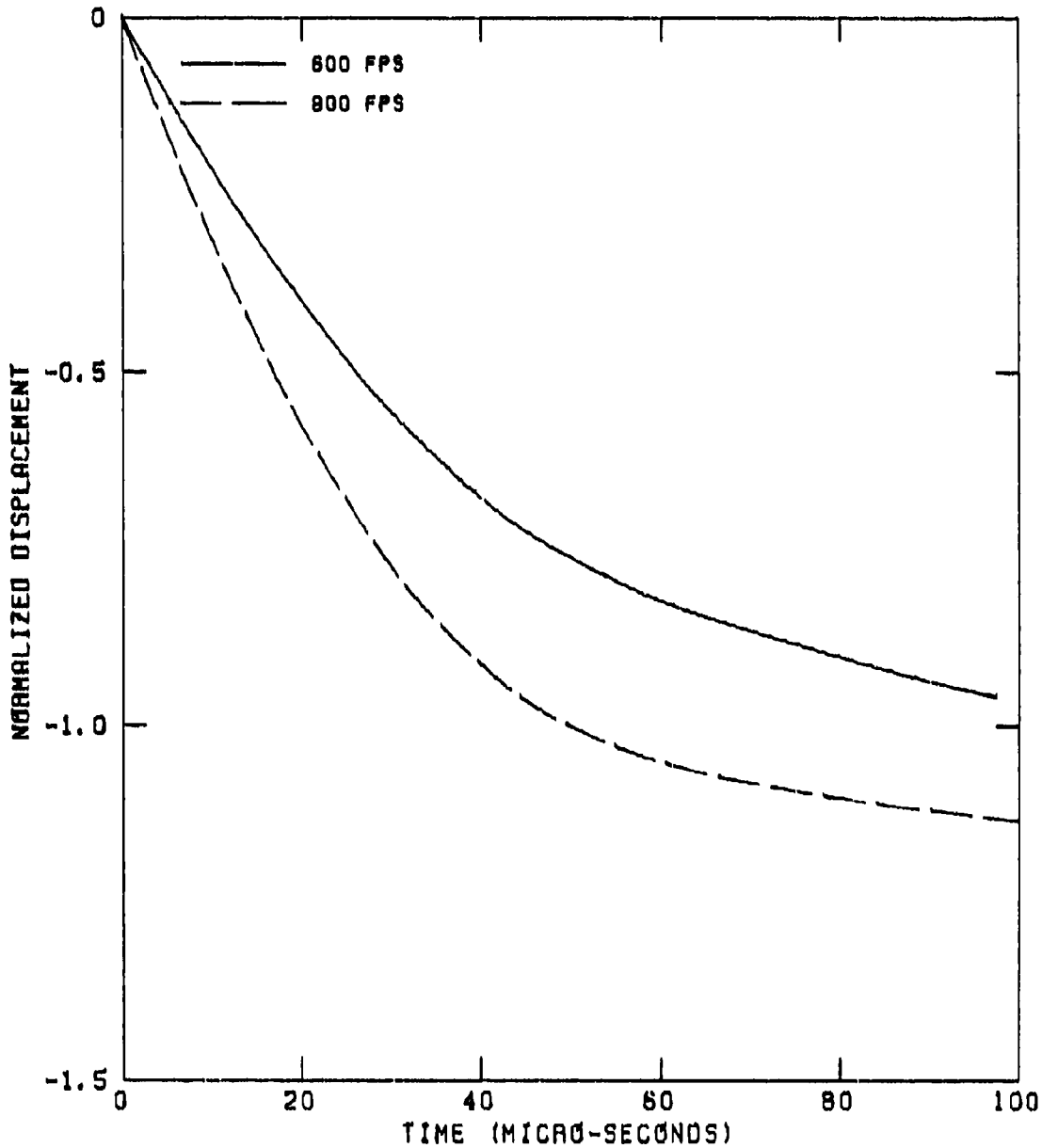

Figure 5.14. Comparison of Displacement-time Histories; 600 fps vs 900 fps Impacts on 18-ply Fabric. (Displacement Normalized to 18-ply, 600 fps Solution).

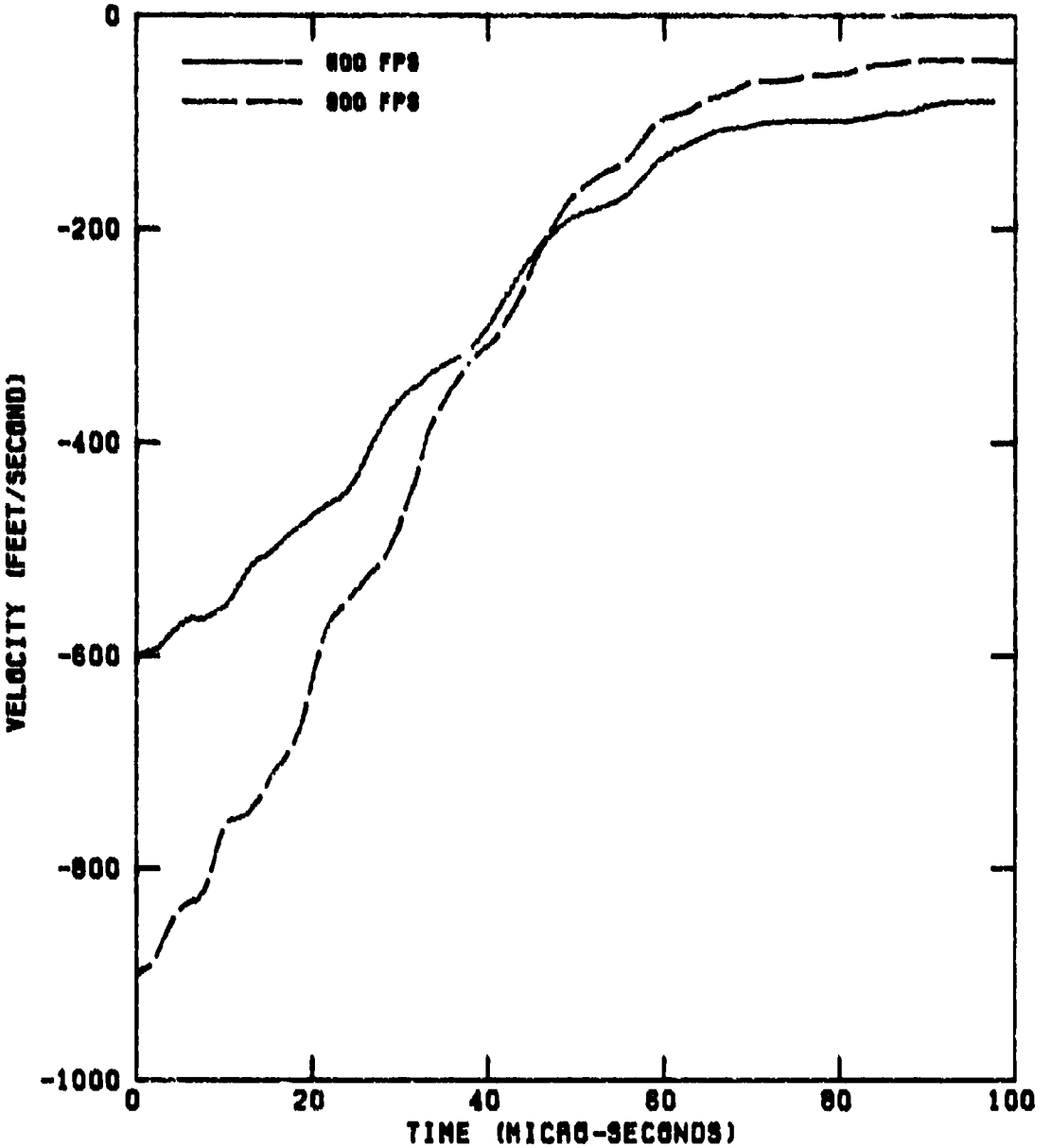

Figure 5.15. Comparison of Fragment Velocity-time Histories; 600 fps vs 900 fps Impacts On 18-ply Fabric.

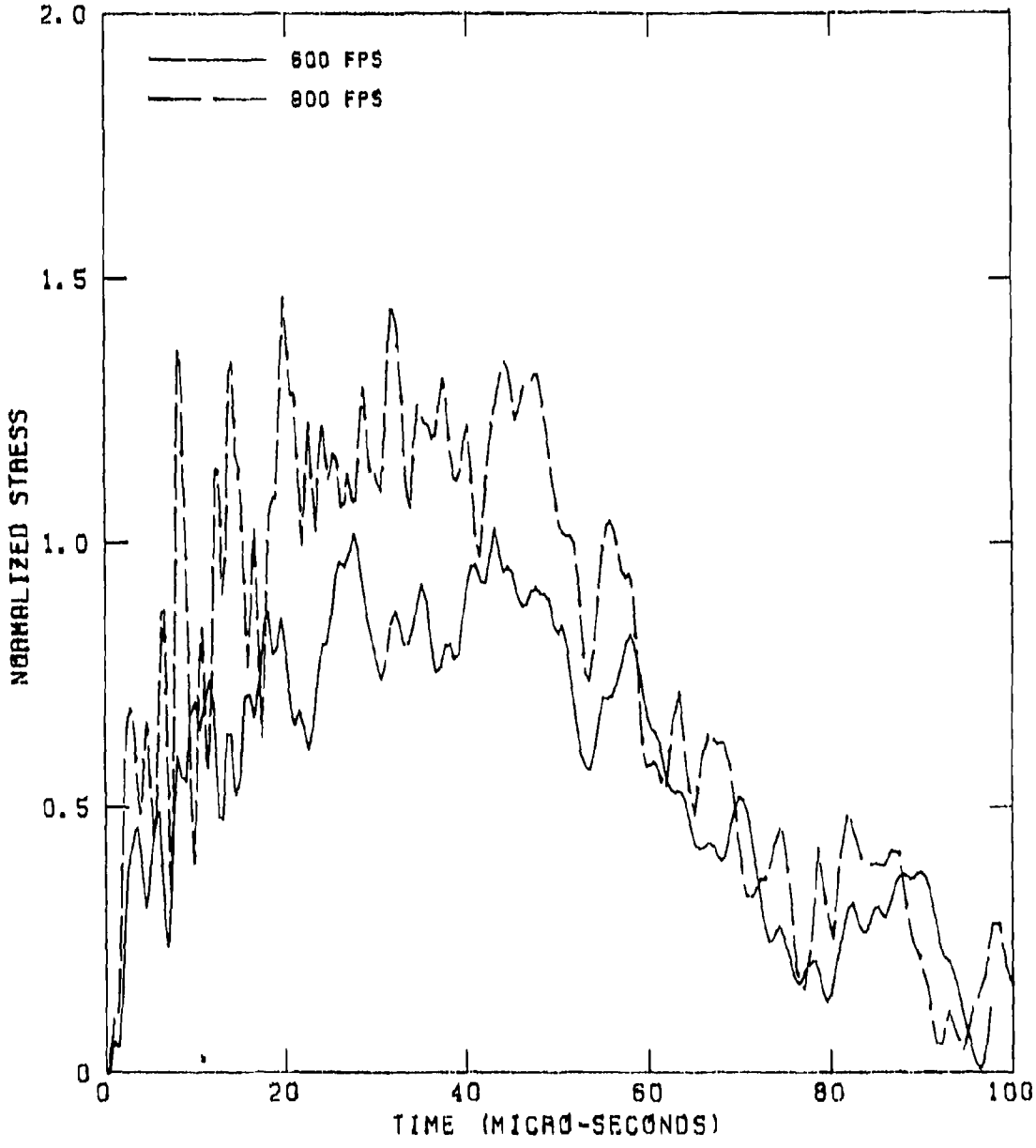

Figure 5.16. Comparison of Stress-time Histories; 600 fps vs 900 fps Impacts on 18-ply Fabric. (Stress Normalized to 18-ply, 600 fps Solution).

expected, these figures show increased impact velocity to result in higher displacement and stress. The prolonged sustainment of above ultimate tensile stress predicts severe front ply failures and possible target perforation from a 900 fps impact.

Fiber stresses and deflections at the point of contact are the two measures by which parametric variations will be evaluated.

5.2 EFFECT OF FABRIC THICKNESS

A logical method of increasing ballistic capability of a fabric back layer is to increase the number of fabric layers and, therefore, weight. In the development of a lightweight generic armor concept, it is desirable to understand more quantitatively the trade-off of improved ballistic performance versus added weight. To investigate this relationship, numerical simulations of 600 fps and 900 fps on double thick (36-ply) targets were performed.

As expected, these analyses show 36-ply targets initially to absorb projectile momentum at approximately twice the rate of 18-ply targets (Figures 5.17 and 5.18). Figures 5.19 and 5.20 depict the reduction in center deflections from the additional fabric plys. These analyses, however, indicated only a small improvement in peak stresses when the target thickness was doubled. Figures 5.21 and 5.22 compare the stress time histories of 18-ply and 36-ply targets subjected to 600 fps and 900 fps impacts, respectively.

The small sensitivity of peak stresses to thickness can be explained by the mechanics of fabric membrane response. As

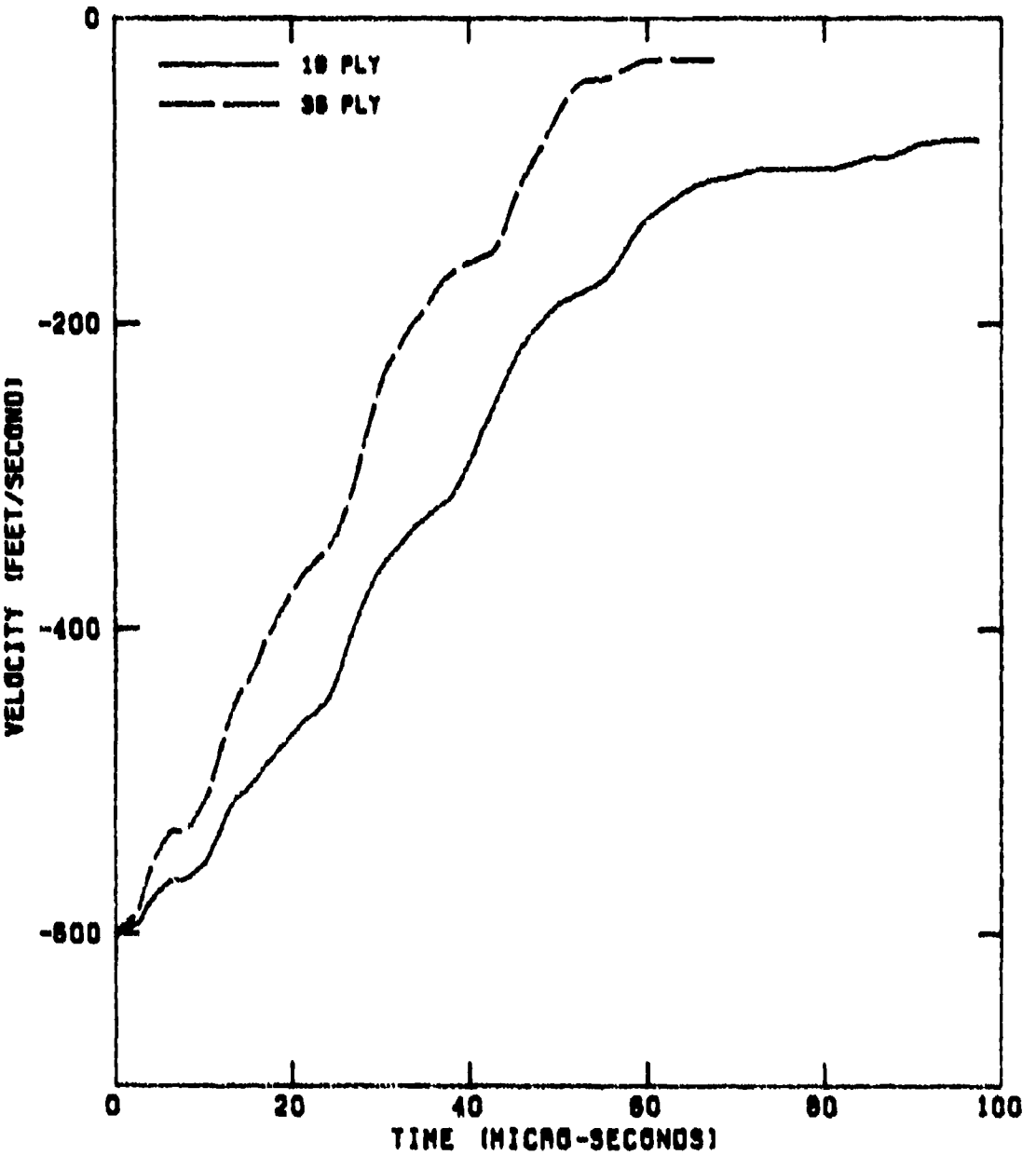

Figure 5.17. Comparison of Fragment Velocity-time Histories; 18-ply vs 36-ply Fabric, 600 fps Impact.

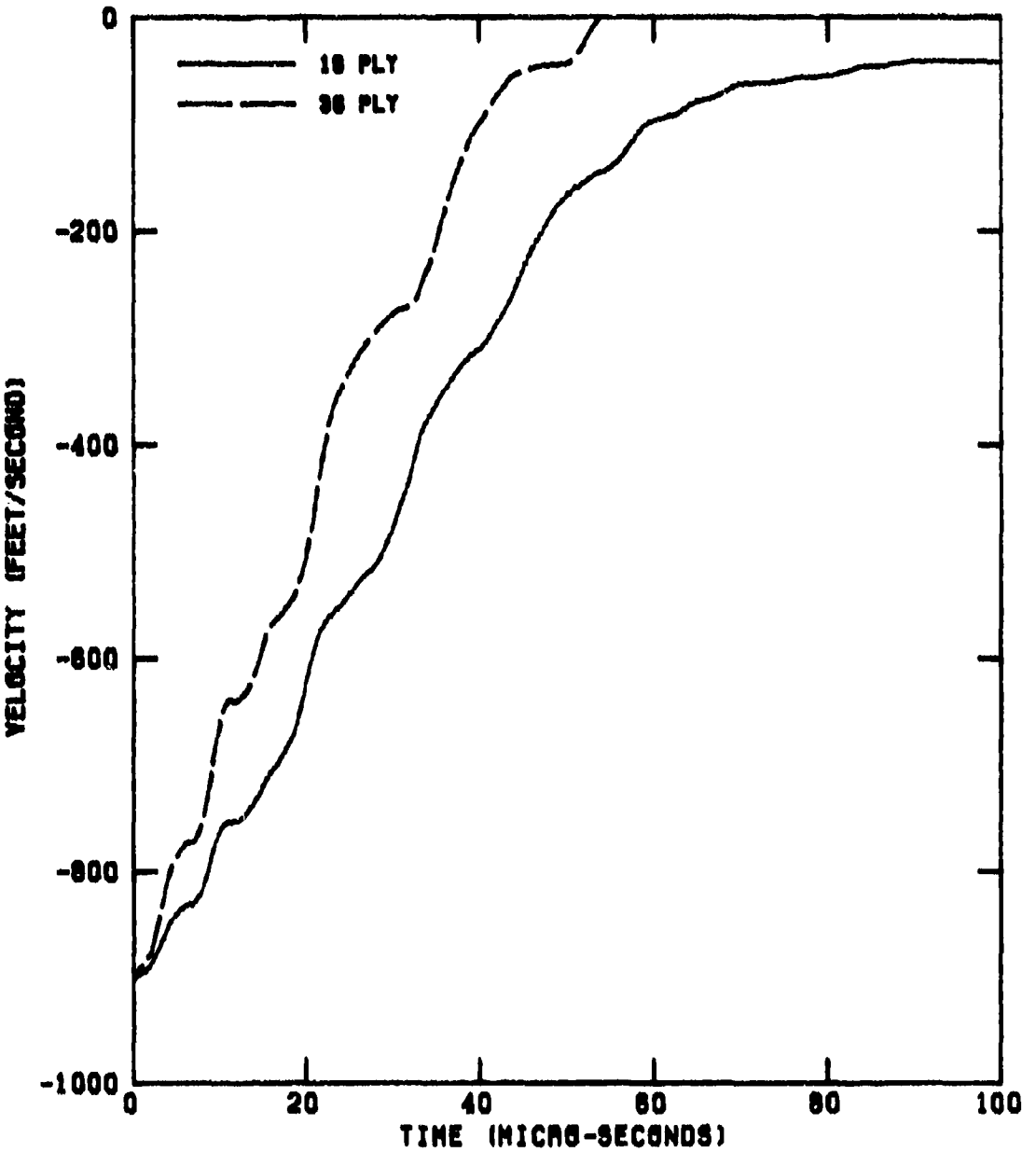

Figure 5.18. Comparison of Fragment Velocity-time Histories; 18-ply vs 36-ply Fabric, 900 fps Impact.

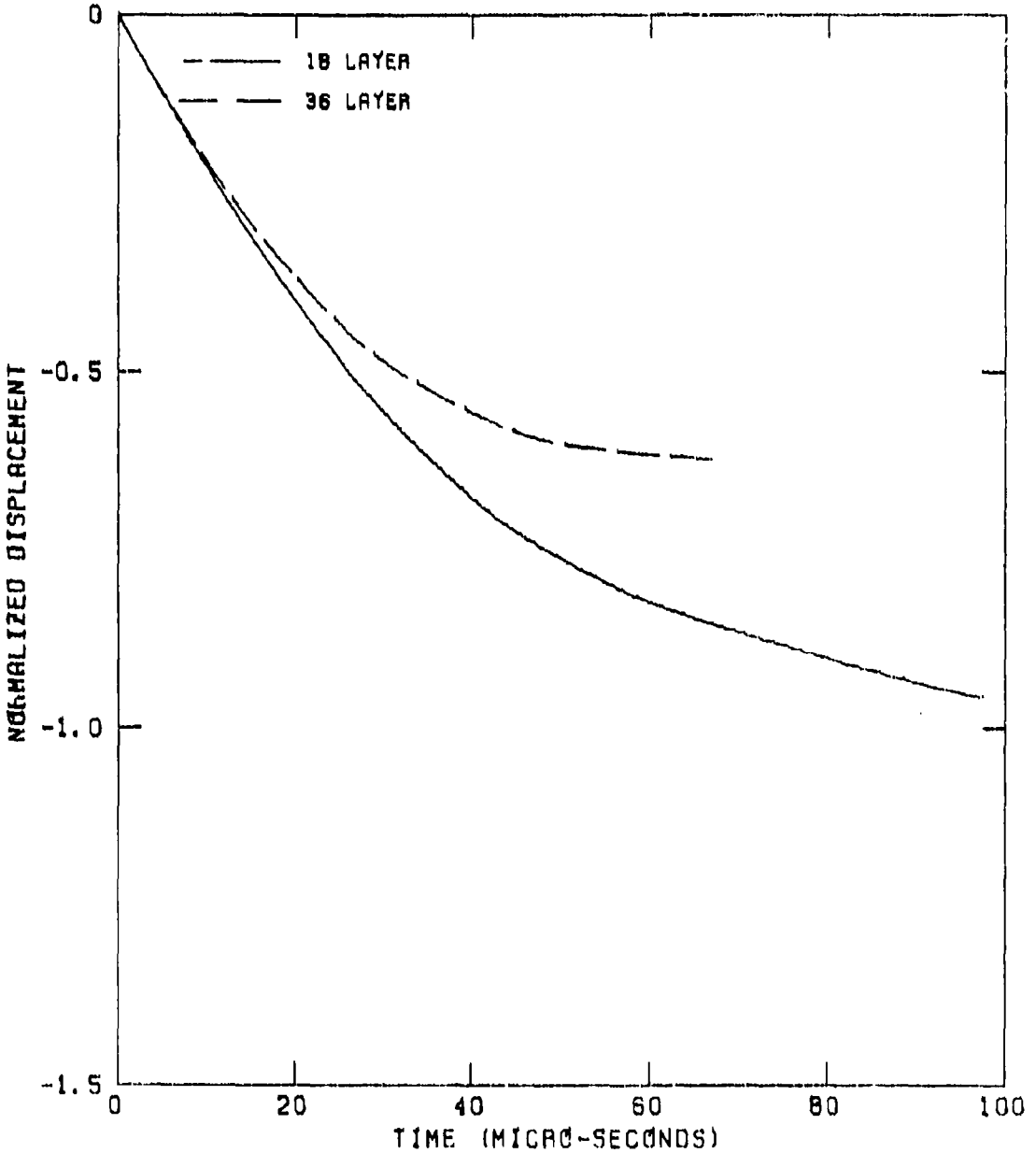

Figure 5.19. Comparison of Center Displacement-time Histories; 18-ply vs 36-ply Fabric, 600 fps Impact. (Displacement Normalized to 18-ply, 600 fps Solution).

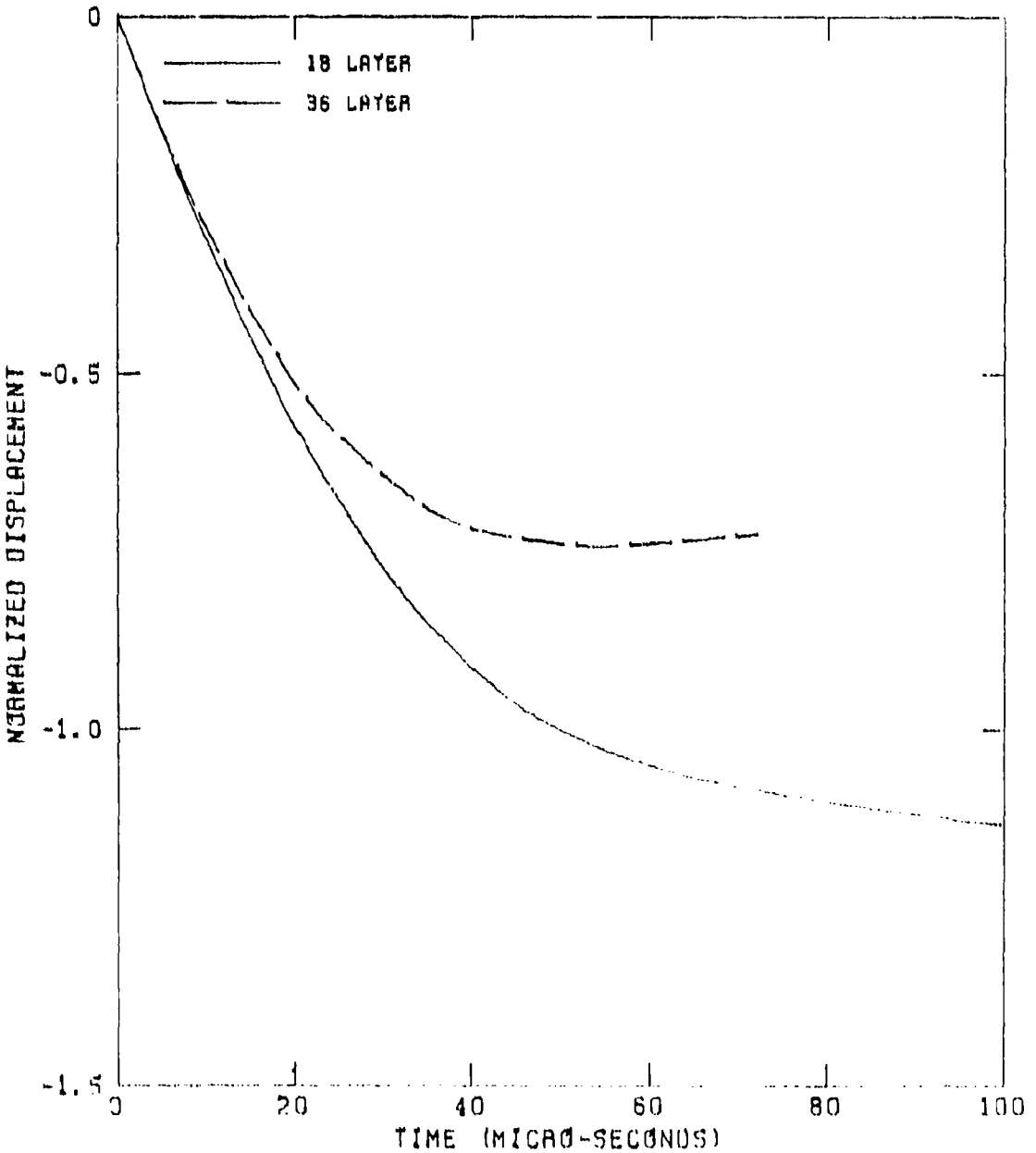

Figure 5.20. Comparison of Center Displacement-time Histories; 18-ply vs 36-ply Fabric, 900 fps Impact. (Displacement Normalized to 18-ply, 600 fps Solution).

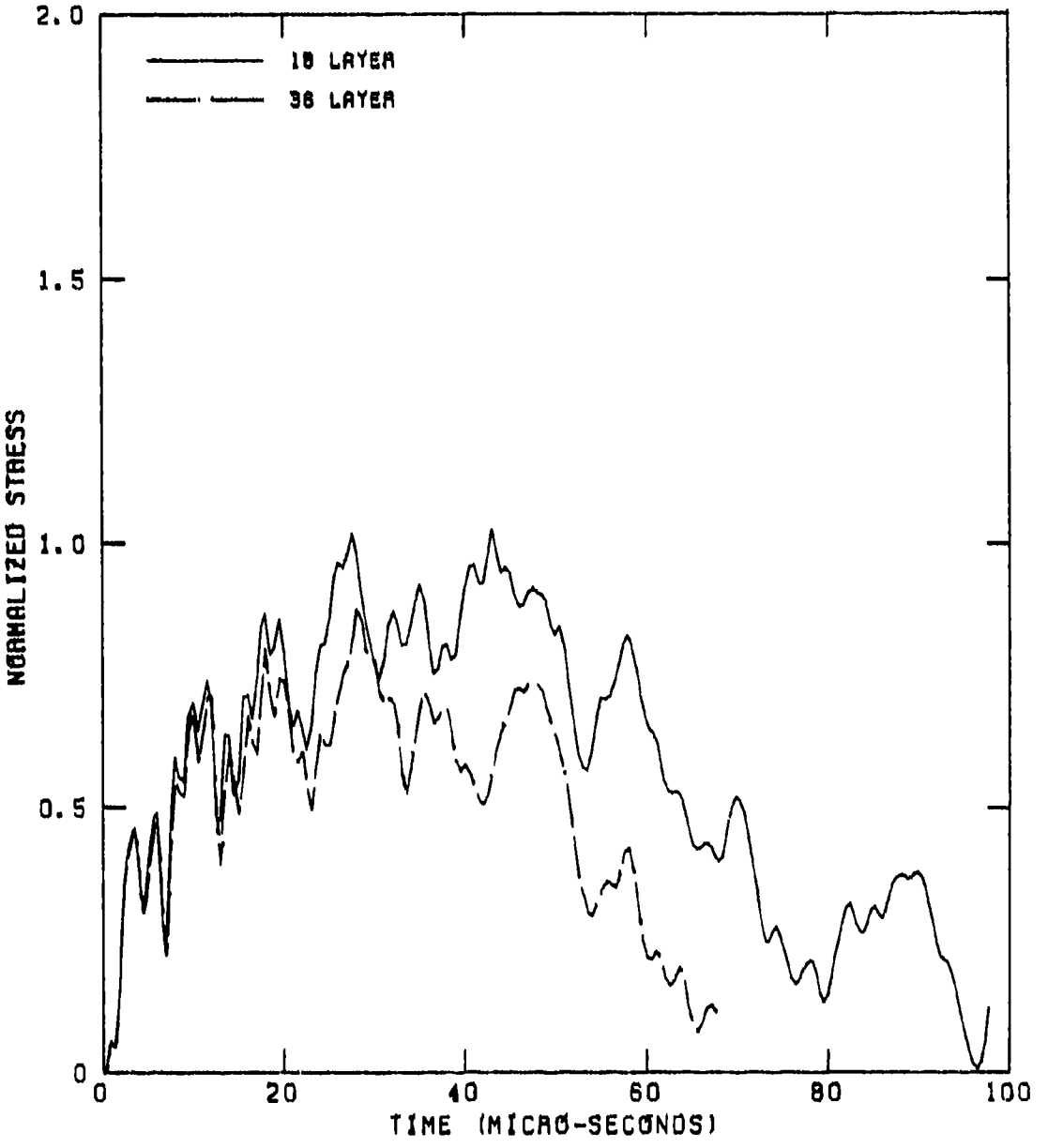

Figure 5.21. Comparison of Stress-time Histories; 18-ply vs 36-ply Fabric, 600 fps Impact. (Stress Normalized to 18-ply, 600 fps Solution).

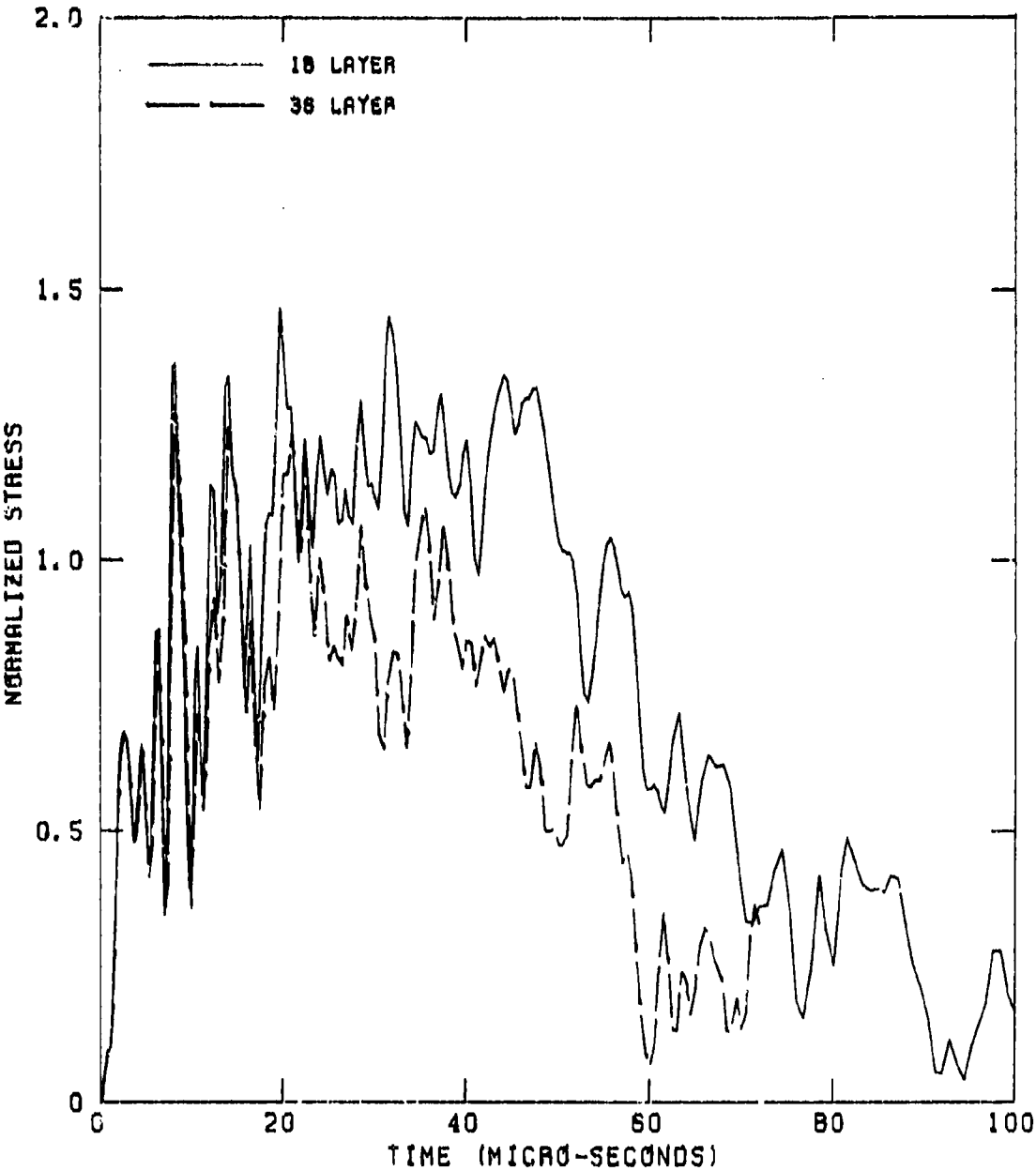

Figure 5.22. Comparison of Stress-time Histories; 18-ply vs 36-ply Fabric, 900 fps Impact. (Stress Normalized to 18-ply, 600 fps Solution).

initial contact is made on the 36-ply target, fabric at that point is accelerated to the projectile velocity as in the case of the 18-ply target. Because twice the fabric mass is involved in the 36-ply case, twice as much projectile momentum is absorbed. However, since the involved target mass in either case is small compared to the projectile mass, the projectile velocity remains virtually unchanged at this early time. Thus, during early times the rate of transverse deflection is nearly identical for 18- and 36-ply targets.

Under dynamic conditions, the stress developed in fibers is a function of how rapidly they are pulled, and the fiber stiffness and mass. Because the targets are deflected at the same rate at early times, and since the increase in target thickness affects the target stiffness and mass equally, the early time stresses of the two targets are expected to be about the same. These arguments suggest that impact velocity is the dominant factor in predicting peak target stresses, if they occur at early times.

The small sensitivity of decreased fiber stresses to additional fabric plys indicates this method of increasing back layer performance is not weight efficient.

5.3 EFFECT OF FABRIC SHEAR STIFFNESS

Impregnation of Kevlar fabric plys with epoxy matrix material provides in-plane and interlaminar shear stiffness. While decreasing flexibility, this allows a fabric target to resist transverse deflections while completely horizontal. to investigate the effect of shear stiffness on multi-plyed fabric

response, an axisymmetric CALSAP model has been developed and applied to several numerical simulations.

The analytical modeling for shear-stiffened fabric is similar to that previously described for unimpregnated fabric. Because correct transverse location is necessary for the shear-stiffened problem, individual fabric plys were modeled explicitly. To capture the shear stiffness effect provided by the epoxy matrix, axisymmetric continuum elements were superimposed on the fabric grid. The shear modulus of the continuum elements was 220 ksi. The density of these elements reflected the epoxy density and a volume fraction of 40%. The finite element model is shown in Figure 5.23. Impregnated 18-ply and 9-ply cases, representing 1.8 psf and .9 psf systems, respectively, were analyzed.

Explicit fabric plys and modeling of interply compliance by continuum elements allowed the recognition of failures in the shear-stiffened analyses. During the solutions, fabric truss elements which attained tensile ultimate stress (410 ksi) were automatically failed so they could no longer sustain any load.

Figure 5.24 shows the response of an impregnated 18-ply target to a 600 fps impact. The shear stiffness can be seen to effectively suppress the transverse wave development which is prominent in nonimpregnated target response. Despite this transverse stiffness, the impregnated 18-ply target was less effective in momentum absorption than the nonimpregnated target (Figure 5.25). One reason for this was the interply compliance (not modeled in the plain fabric analyses) which was provided by the continuum elements. The flexibility delayed activation of the lowerplys into the problem, whereas in the earlier analyses,

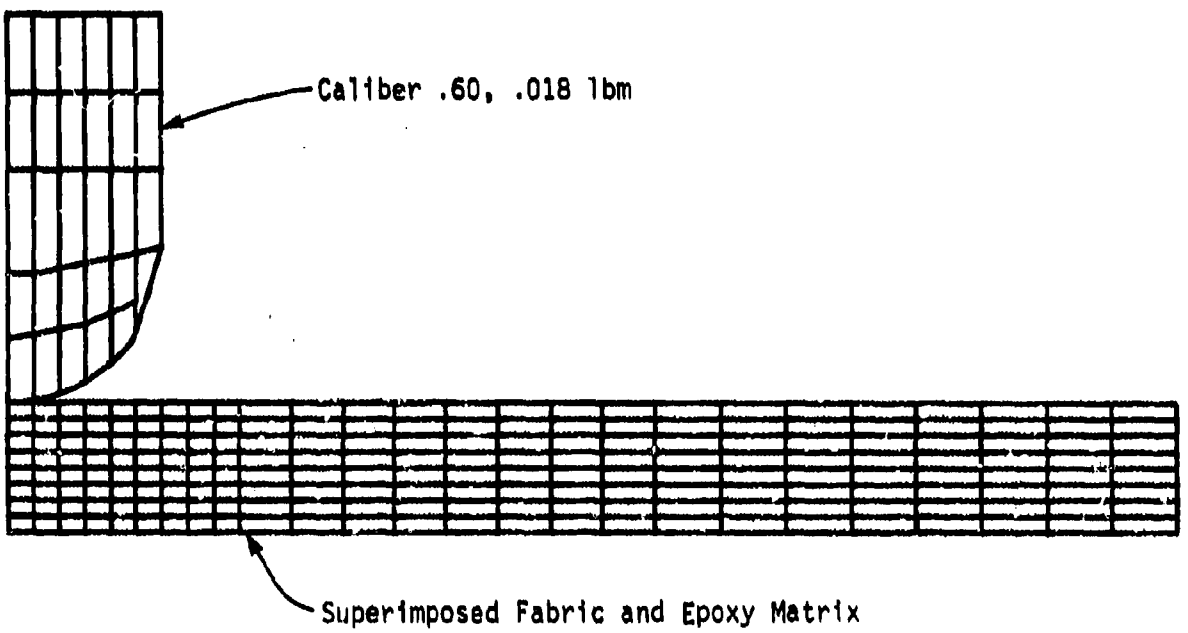

Figure 5.23. Finite Element Model For Analysis of Impact on Shear Stiffened Fabric Targets. (18-ply Model Shown).

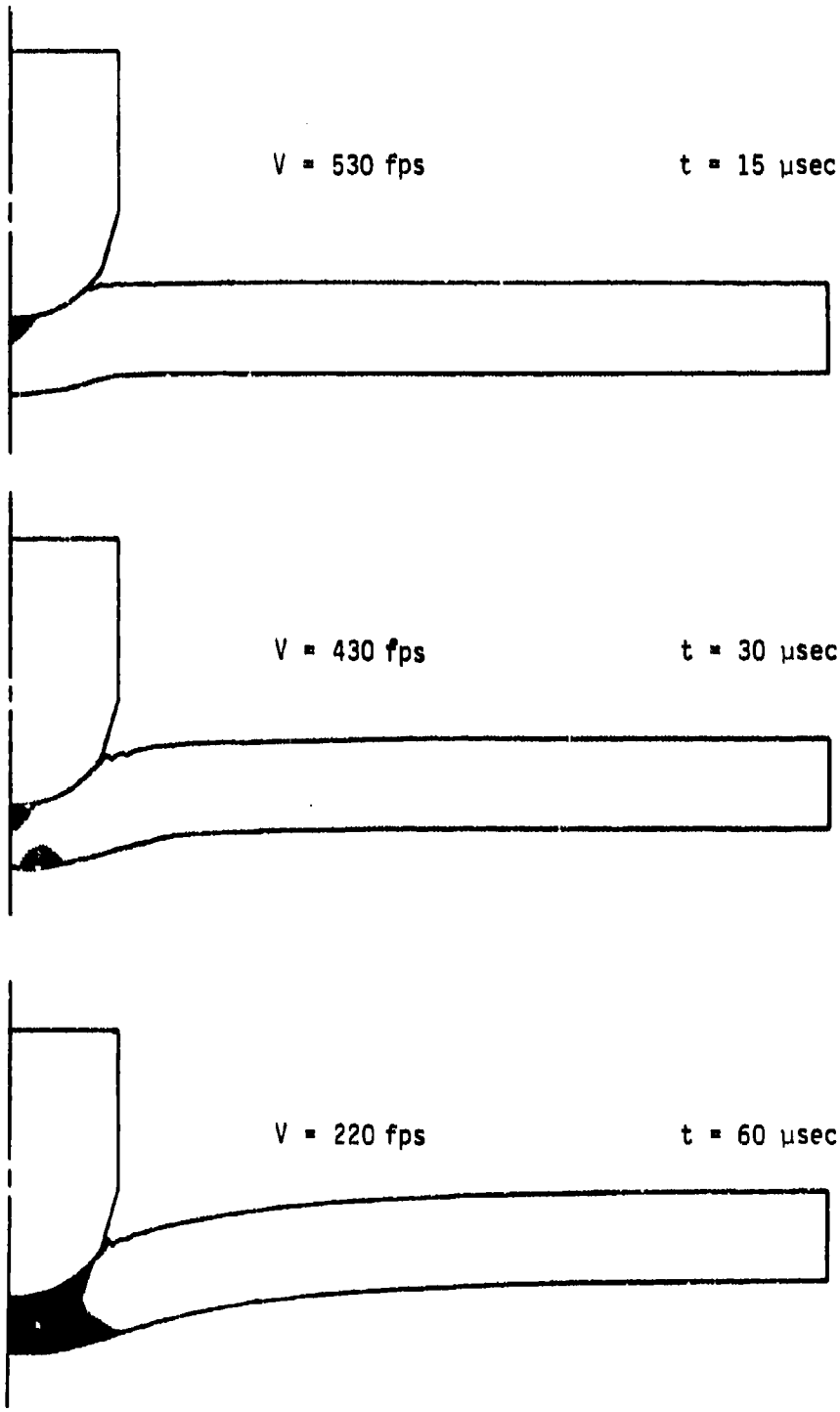

Figure 5.24. Response of 18-ply Shear Stiffened Target To 600 fps Impact. (Shaded Areas Indicate Fiber Failures.)

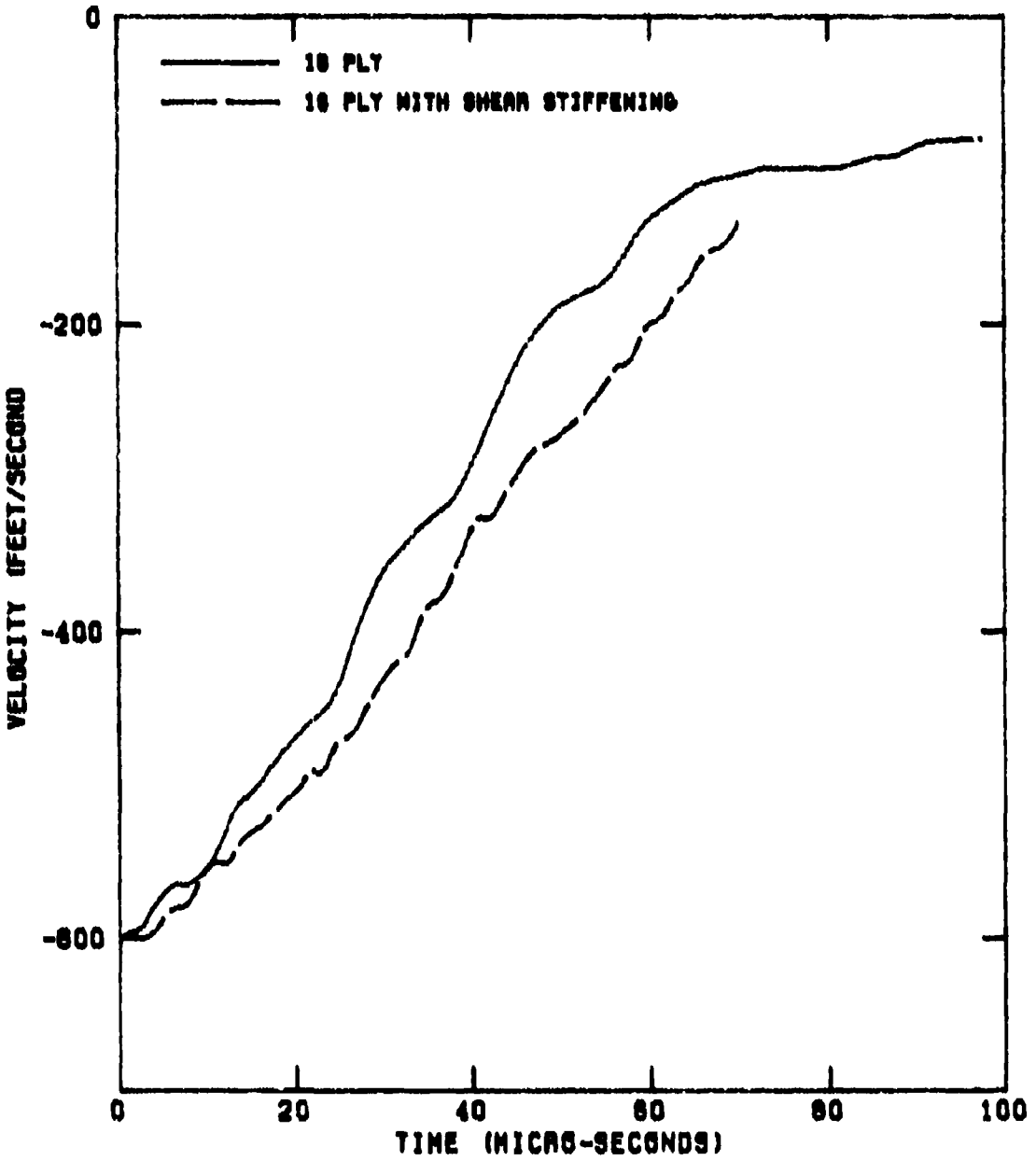

Figure 5.25. Comparison of Velocity-time Histories; 18-ply vs Shear Stiffened 18-ply Targets, 600 fps Impact.

all plys were encountered by the fragment instantaneously. Fiber failures also softened the impregnated target. As seen in Figure 5.24, these failures coalesced to complete target perforation by 60 μsec. The residual fragment velocity was 200 fps. The fiber failures, which propagated from the target's back surface, were due to bending stresses developed as a result of shear stiffness.

The impregnated 9-ply target response to a 300 fps impact was similar (Figure 5.26) through failures developed leading to penetration with a 50 fps residual projectile velocity.

The extensive bending failures induced by shear stiffness at the additional expense of added weight underscore the deliterious effect of fabric rigidity on weight-sensitive ballistic performance.

5.4 EFFECT OF FABRIC WEAVE

As discussed previously, the rate of projectile deceleration is dependent on the vertical component of fabric stresses. By increasing the fabric tensile strength, a target's capacity for decelerating a projectile is improved since a corresponding larger vertical component of these stresses can be attained. The same improvement can be obtained without increasing fabric strength, if the fabric at the area of contact is oriented so a larger vertical component of the stresses exists. Incorporating initial slack in the weave allows a fabric to re-orient in this manner before any stresses are developed.

Two simulations were performed to study this effect on 18-ply targets, one with an initial weave slack of 1% and the

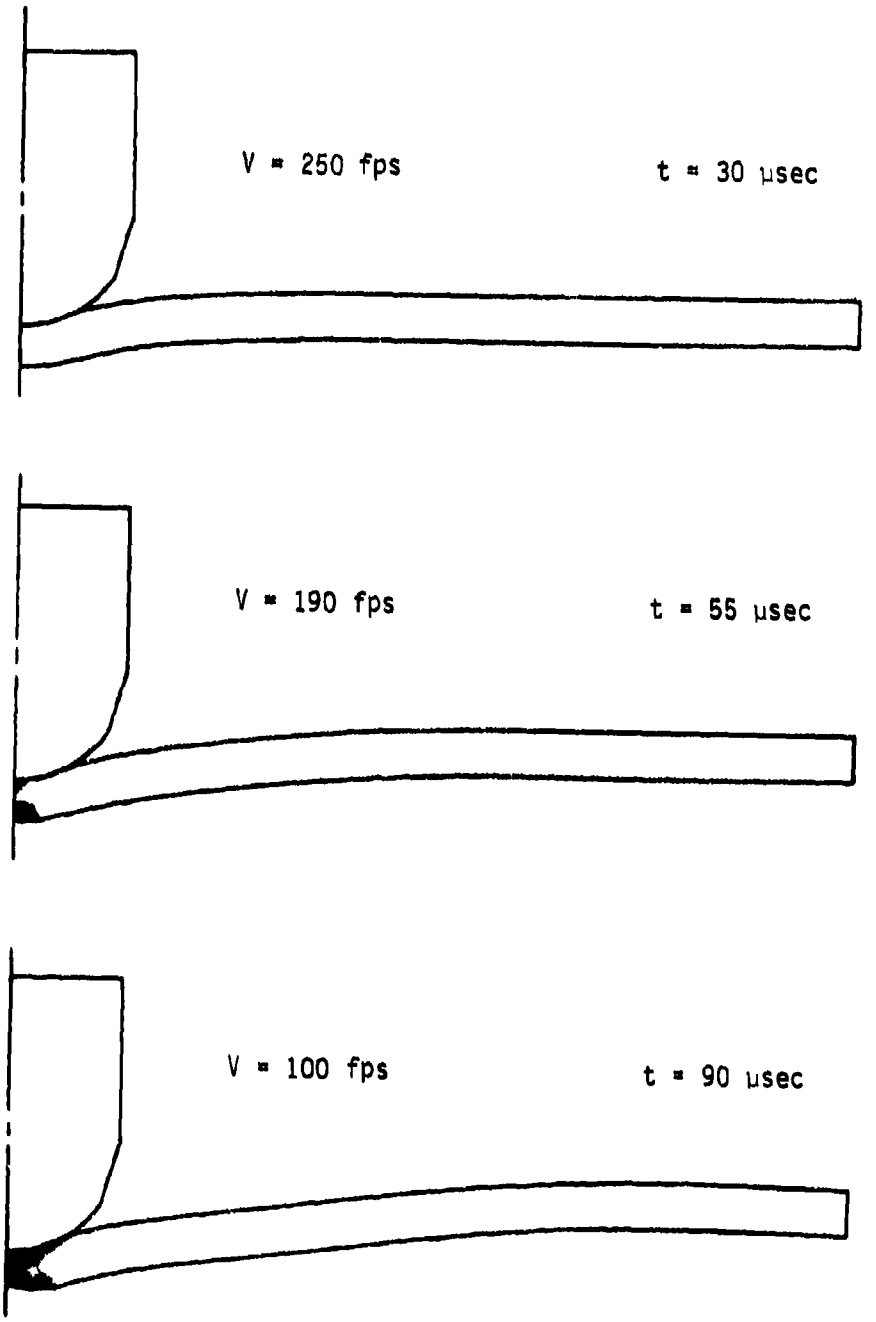

Figure 5.26. Response of 9-ply Shear Stiffened Target to 300 fps Impact. (Shaded Areas Indicate Fiber Failures.)

other 4%. Initial slack was incorporated into the CALSAP solutions by employing the fiber stress-strain relations shown in Figure 5.27. Both initial slack cases modeled 600 fps projectile impacts. Not considered in this analysis is the decreased fabric resistance to fiber spreading induced by initial slack.

Figure 5.28 highlights the dramatic reduction in stresses obtained in these two solutions. Figure 5.29 compares the response of the 4% initial slack target to the baseline target. The concentration of deformation which results in the desirable fiber orientation can be seen in this figure. Although stresses are reduced, initial fiber slack allows greater center deflections. Figures 5.30 and 5.31 compare the deflection and velocity time histories, respectively, of baseline, 1%, and 4% initial slack cases.

These solutions indicate initial weave slack as a promising means of increasing fabric back layer performance at the cost of increased deflections.

5.5 EFFECT OF HONEYCOMB BUFFER

The previous subsection demonstrated the benefit of deforming fabric out-of-plane before stresses are developed. In the case of initial weave slack, this was accomplished by adjusting the fabric stress-strain relationship. Alternatively, or in conjunction with weave slack, a buffering system could be designed to force the fabric to respond slowly before contact with the projectile. A low rate of transverse deflection prior to projectile contact provides fabric time to respond in-plane, thereby preventing excessive stress buildup. An additional benefit of a buffer material is to provide a soft coating to a

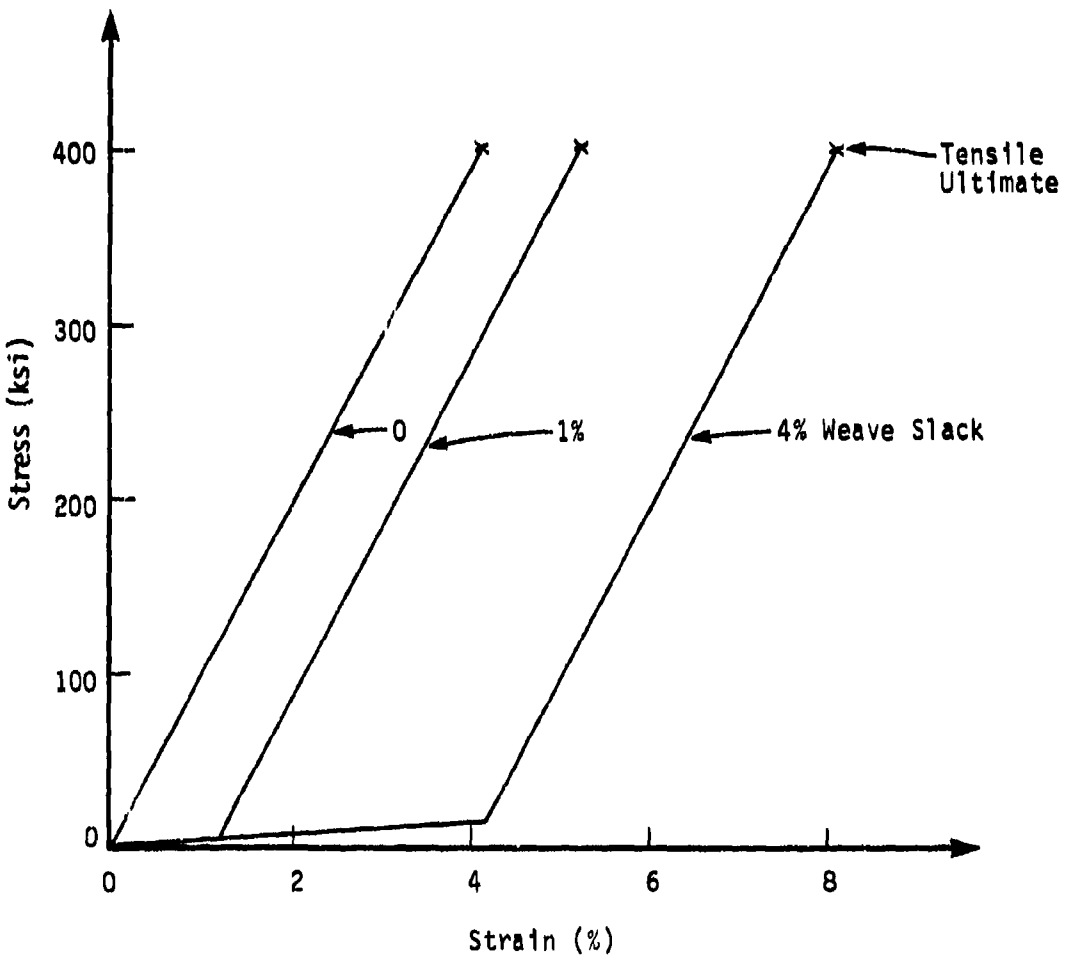

Figure 5.27. Stress-strain Curves for Baseline, 1% and 4% Initial Weave Slack Fabric.

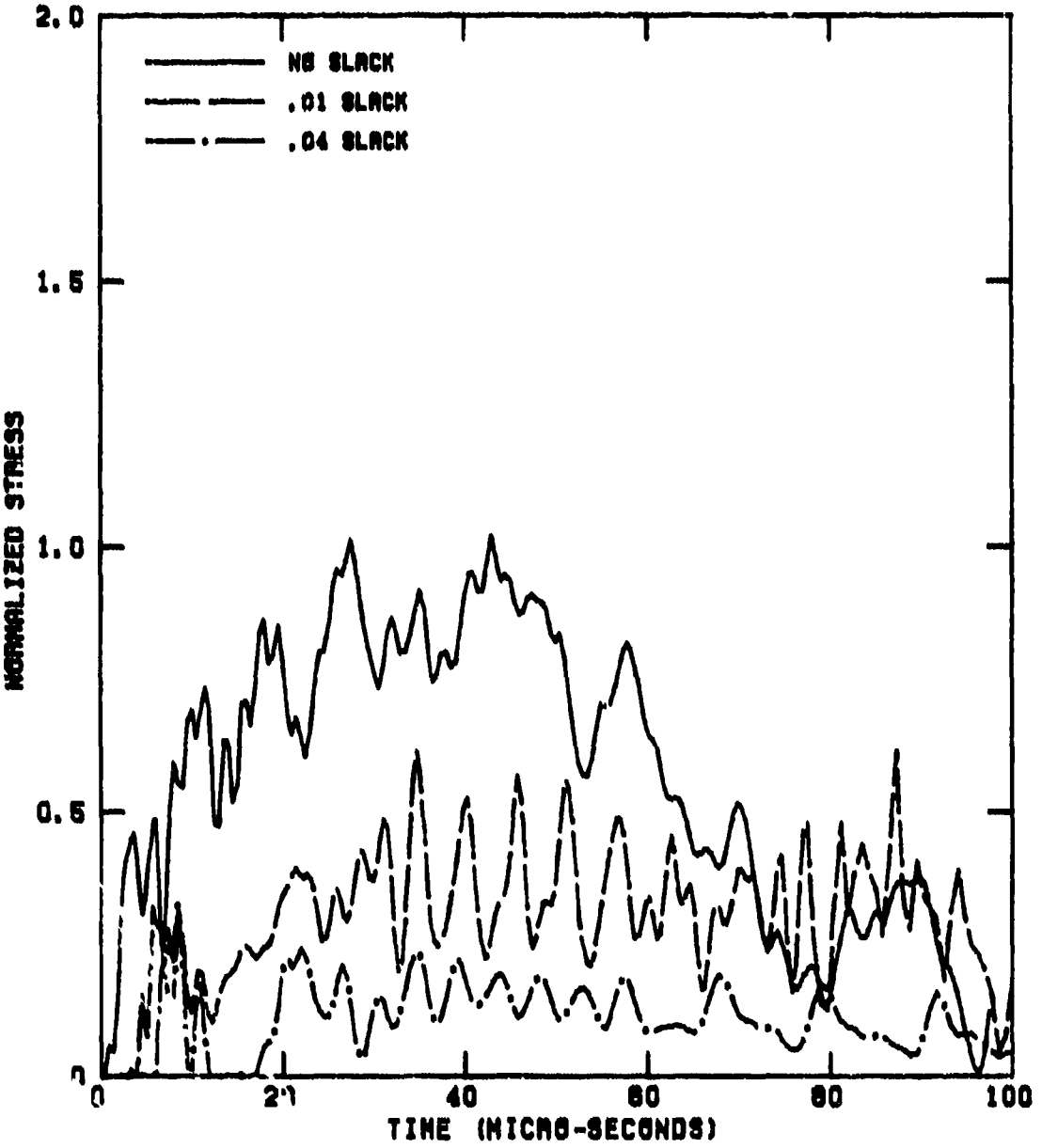

Figure 5.28. Effect of Initial Weave Slack on Fabric Stress. (Stress Normalized to 18-ply, 600 fps Solution.)

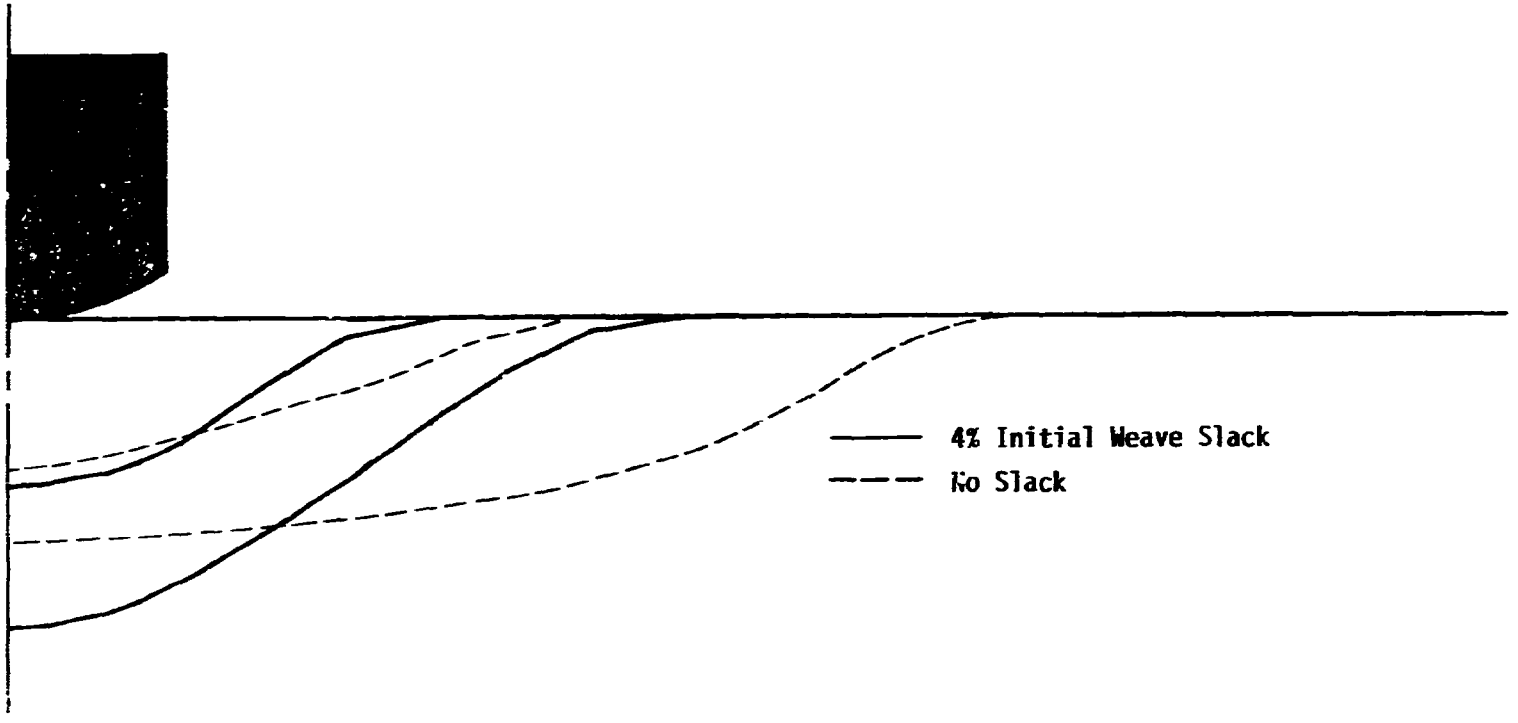

Figure 5.29. Comparison of 18-ply Fabric Response with and without Initial Weave Slack. (600 fps Impact.)

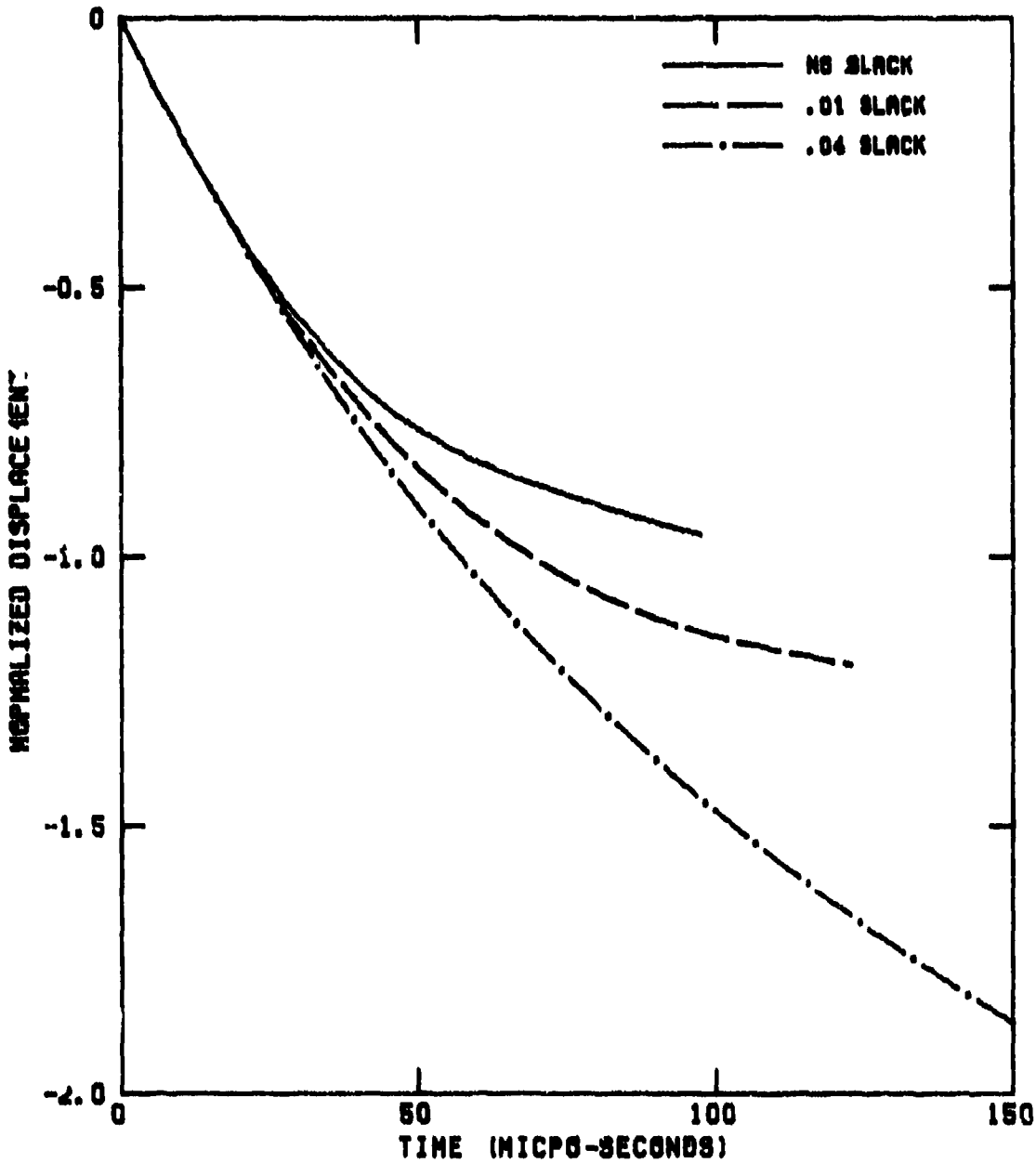

Figure 5.30. Effect of Weave Slack on 18-ply Fabric Deflections. (Deflections Normalized to 18-ply, 600 fps Solution.)

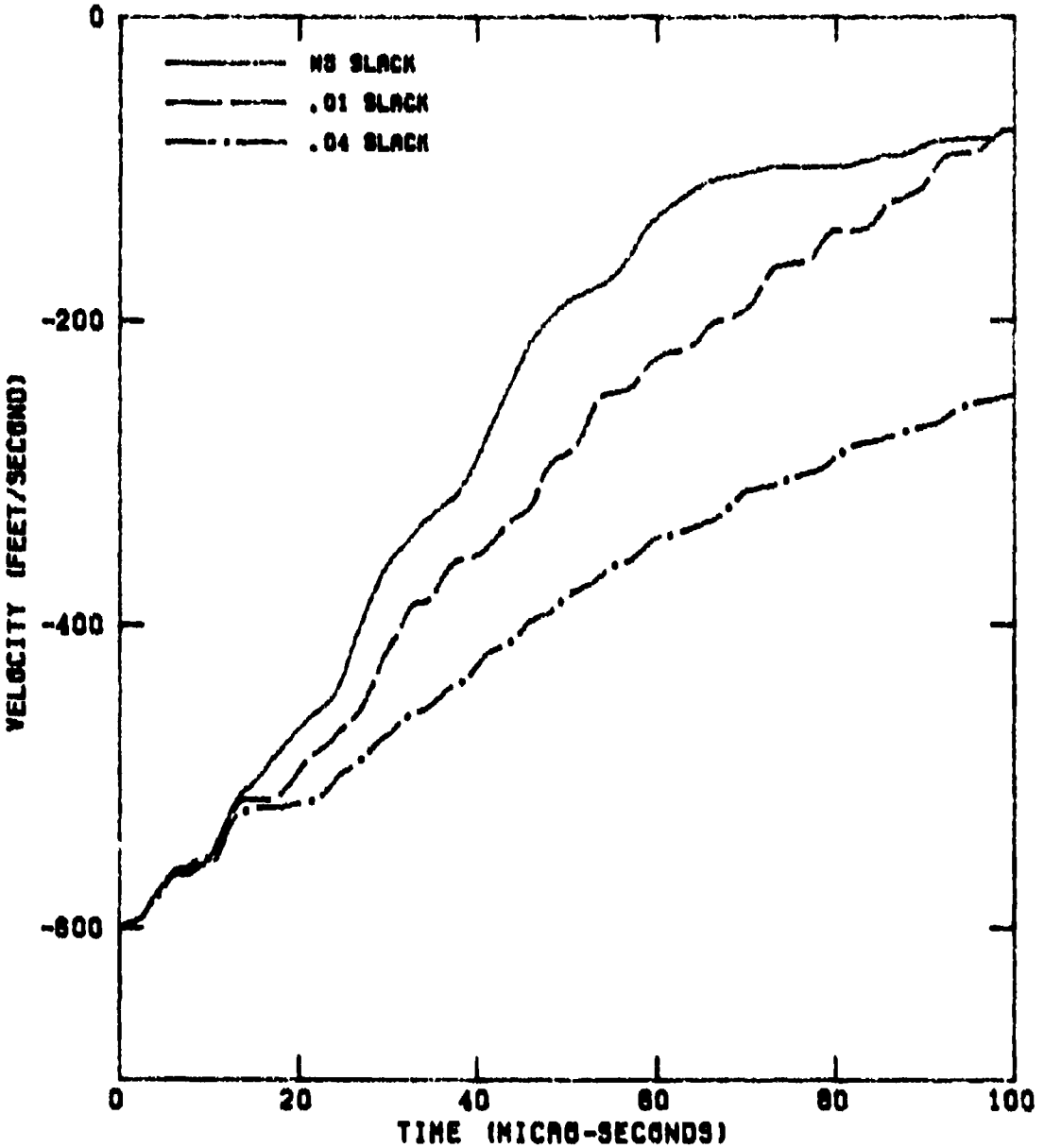

Figure 5.31. Comparison of Velocity-time Histories; 18-ply Targets with and without Initial Weave Slack, 600 fps Impact.

projectile or fragment thereby reducing the lethality of sharp edges to the underlying fabric.

A question of special interest is how much improvement in back layer performance can be gained through the additional weight of a buffering layer. If the increase in weight could be more than offset by a reduction in the number of fabric plys required, the buffering concept would be beneficial. To numerically investigate this relationship, a CALSAP finite element model of a metallic honeycomb buffer was developed. The model, consisting of a 9-ply back layer and honeycomb buffer, was designed to be equivalent in weight to the baseline 18-ply back layer.

Although both aluminum and beryllium are prime candidate honeycomb materials due to low densities relative to yield strengths and elastic moduli, aluminum was employed for numerical simulation. Honeycomb dimensions of .6-in. thickness, .125-in. cell size and .003-in. wall thickness were chosen to assure that a projectile encounter several cells at an areal density of .6 psf.

The honeycomb truss element properties were reflective of experimentally obtained data [12]. A typical experimentally obtained load deflection curve for honeycomb is shown in Figure 5.32. This figure depicts cell axial behavior; honeycomb is extremely flexible in the transverse directions. Due to this uniaxial stiffness, honeycomb cells were modeled with truss finite elements.

Gap elements were placed to model contact at the projectile/honeycomb and honeycomb/fabric interfaces. A 9-ply fabric was modeled exactly as in previous numerical simulations.

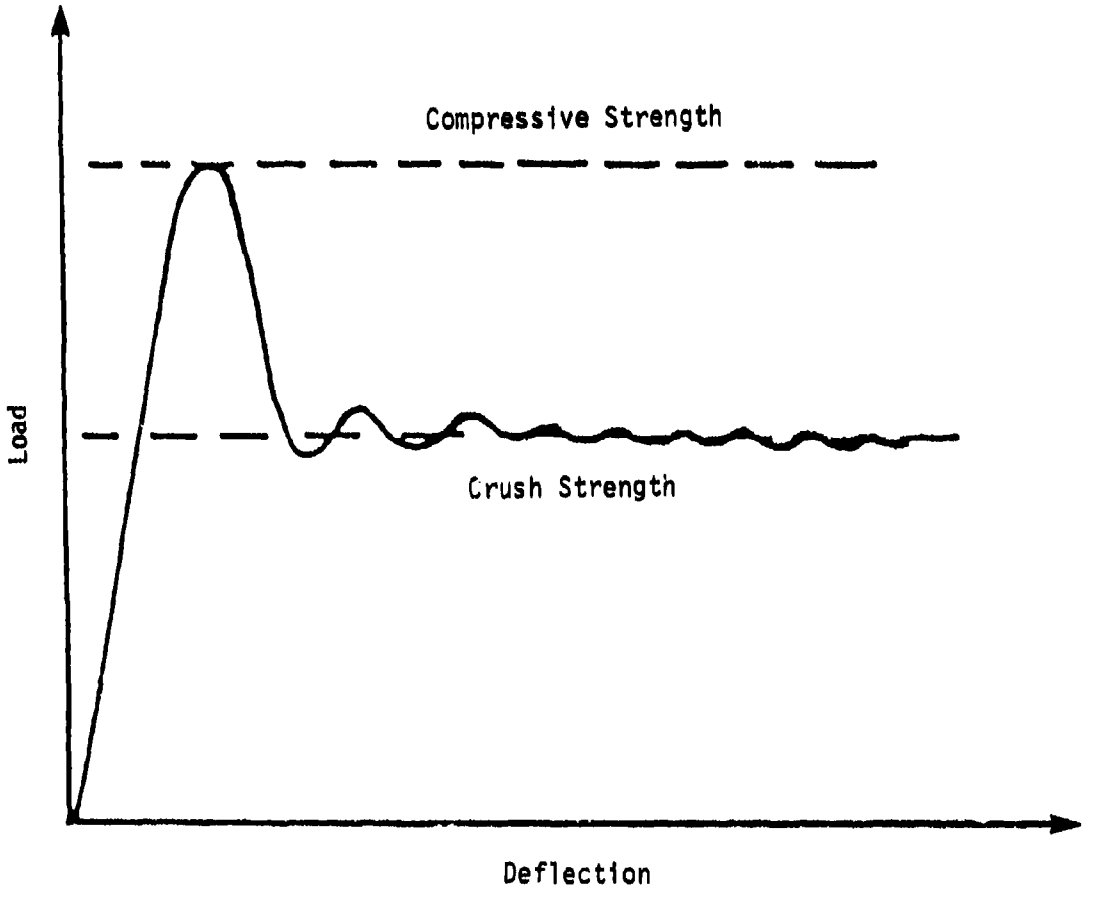

Figure 5.32. Typical Load-deflection Relationship for Aluminum Honeycomb. (Note Constant Load During Crushing.)

The complete finite element model, Figure 5.33, represents a 1.2 psf back layer system.

The model developed, while able to identify a potentially promising concept, should be considered as non-conservative in estimating the effect of honeycomb. The load-deflection relationship for honeycomb when loaded over a small area, such as impact of a small arms projectile, may be considerably more flexible than obtained in experiment testing. Also, non-normal impacts would encounter less resistance in passing through honeycomb due to the strongly uniaxial properties.

Figures 5.34 - 5.37 depict the honeycomb fabric impact response to 600 fps and 900 fps impacts. As seen in these figures, honeycomb initiates fabric motion before fragment contact with the fabric. The 600 fps fragment, in fact, never makes fabric contact. The center displacement comparisons are shown in Figures 5.38 and 5.39 and illustrate the softening of transverse response afforded by the honeycomb. As seen in Figures 5.40 and 5.41, this softening leads to reduced peak stresses.

The two analyses conducted indicate some promise for the buffering concept. The incorporation of a honeycomb buffer in conjunction with weave slack could lead to further improvements in the excellent weave slack performance.

5.6 SUMMARY

Table 5.1 summarizes the results of the ten numerical analyses discussed in this section. Rear layer concepts are compared by weight, final center deflections (or deflections at

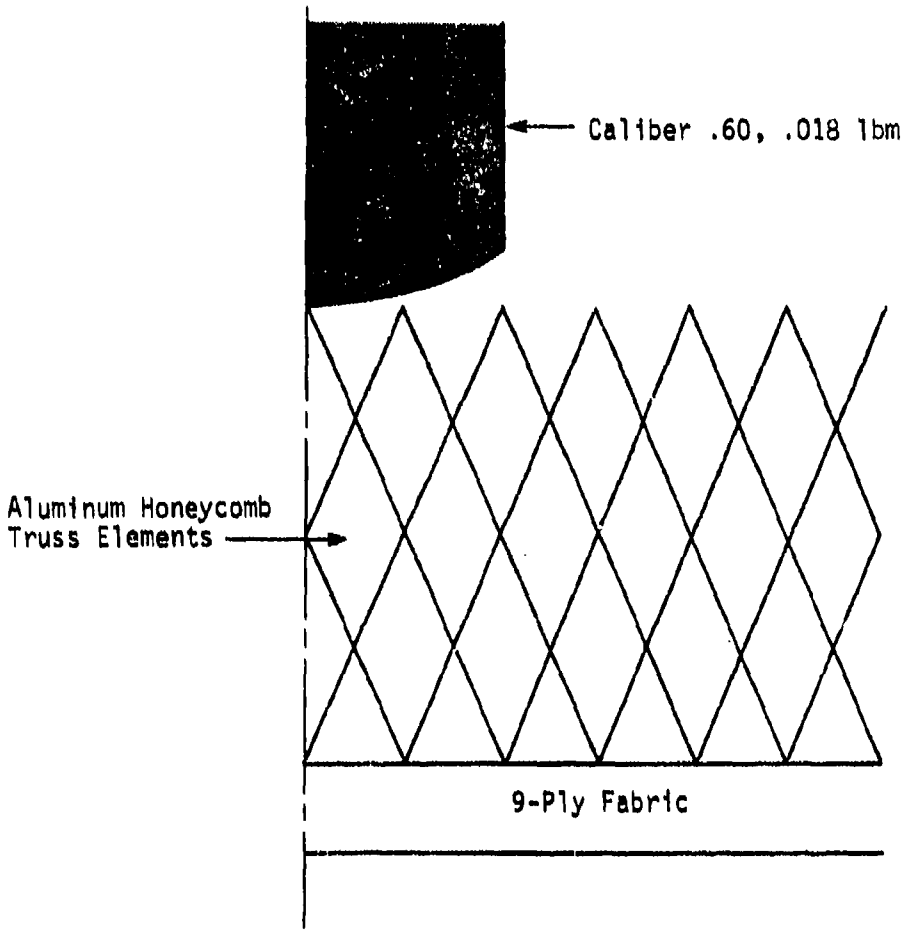

Figure 5.33. Finite Element Model for Analysis of Honeycomb Buffer Concept.

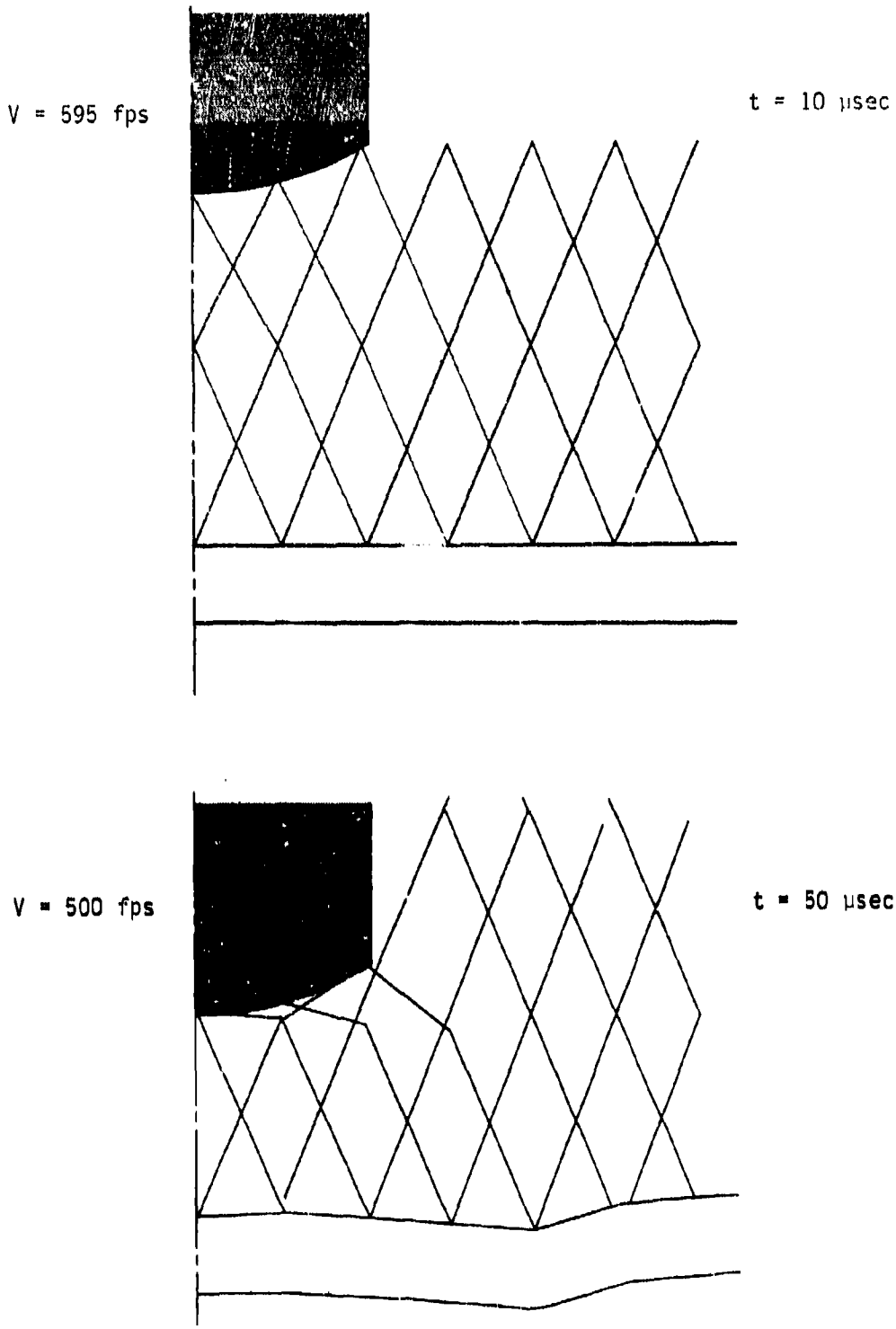

Figure 5.34. Early-time Response of Honeycomb/fabric to 600 fps Impact.

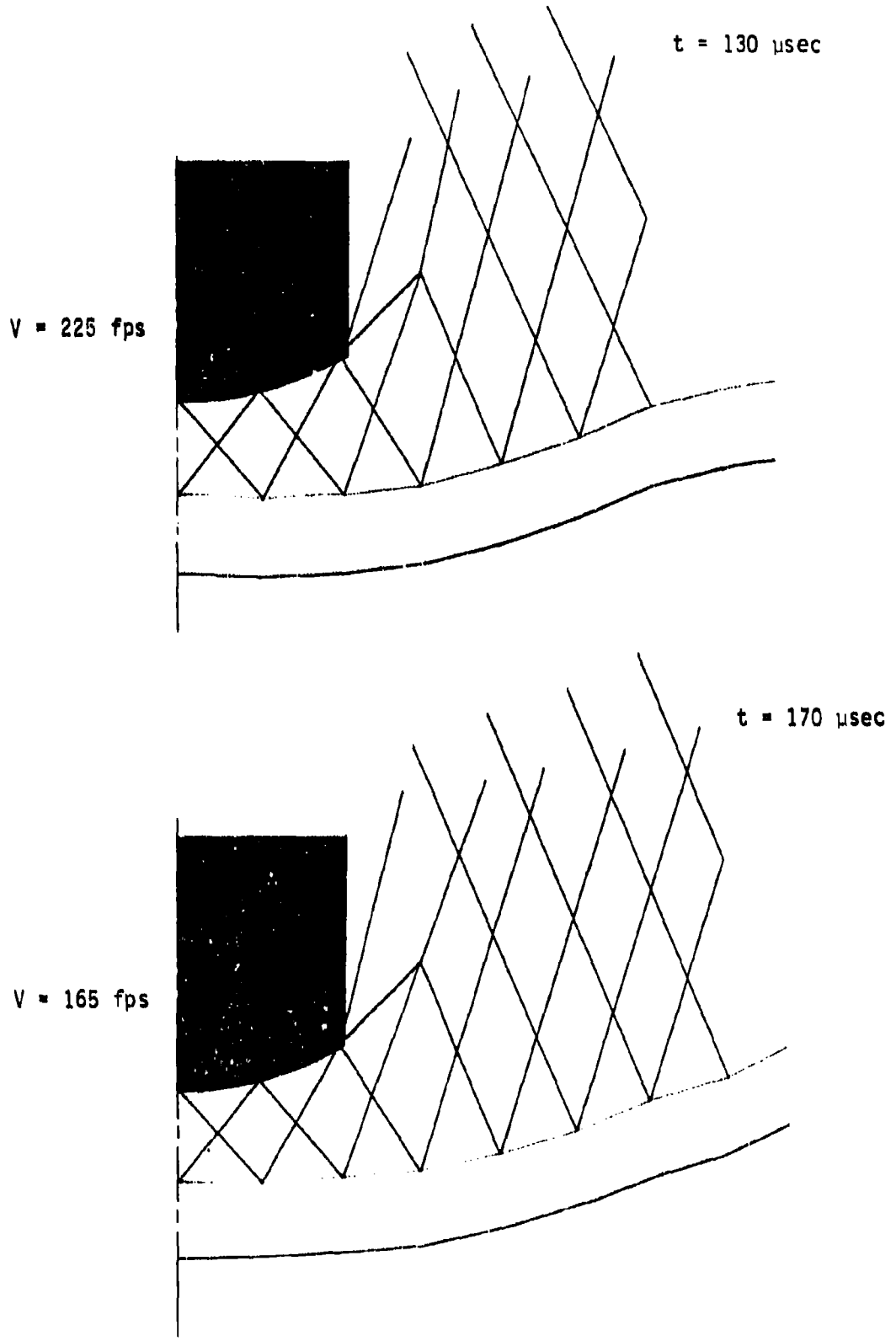

Figure 5.35. Late-time Response of Honeycomb/fabric to 600 fps Impact.

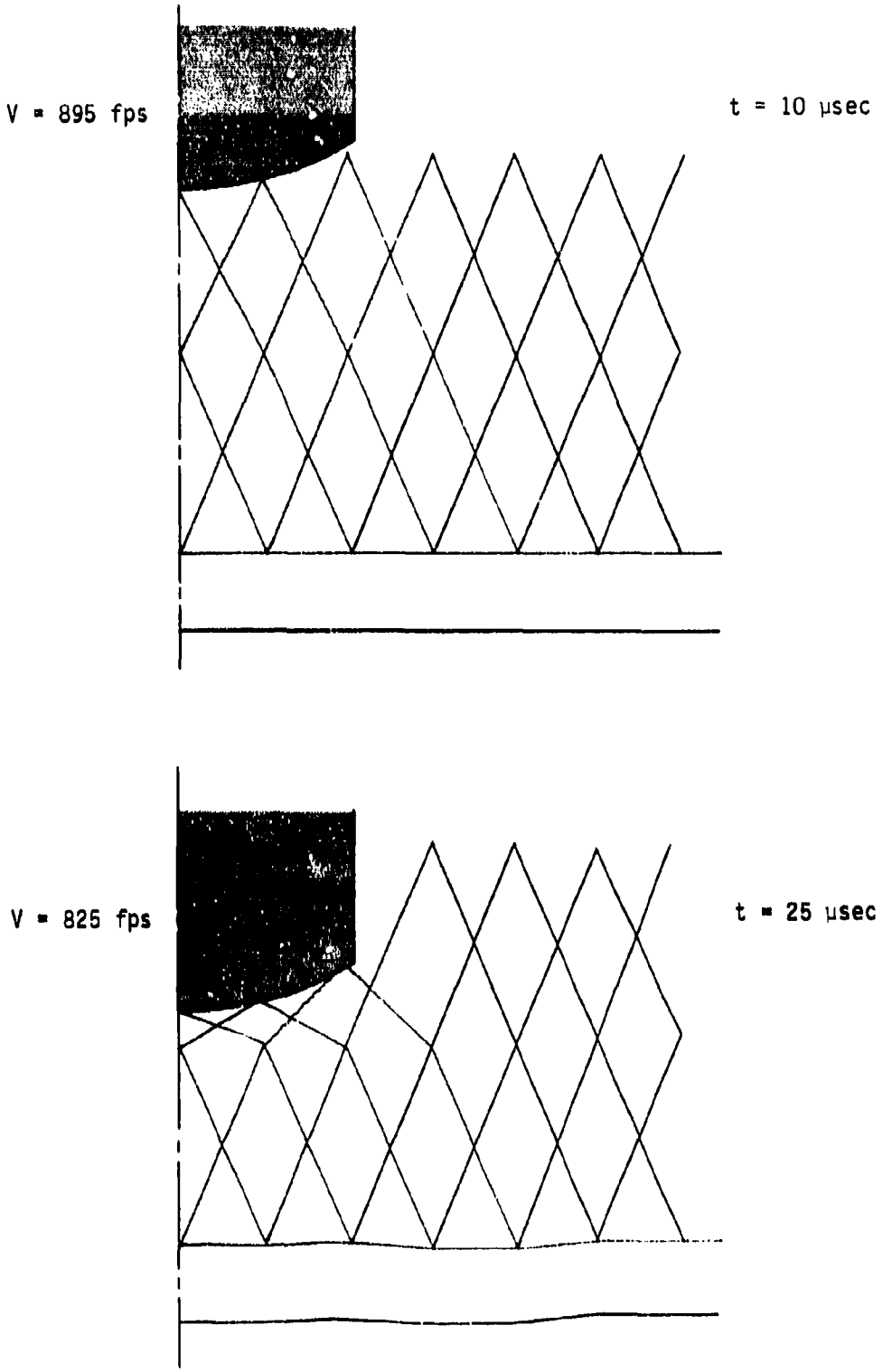

Figure 5.36. Early-time Response of Honeycomb/fabric to 900 fps Impact.

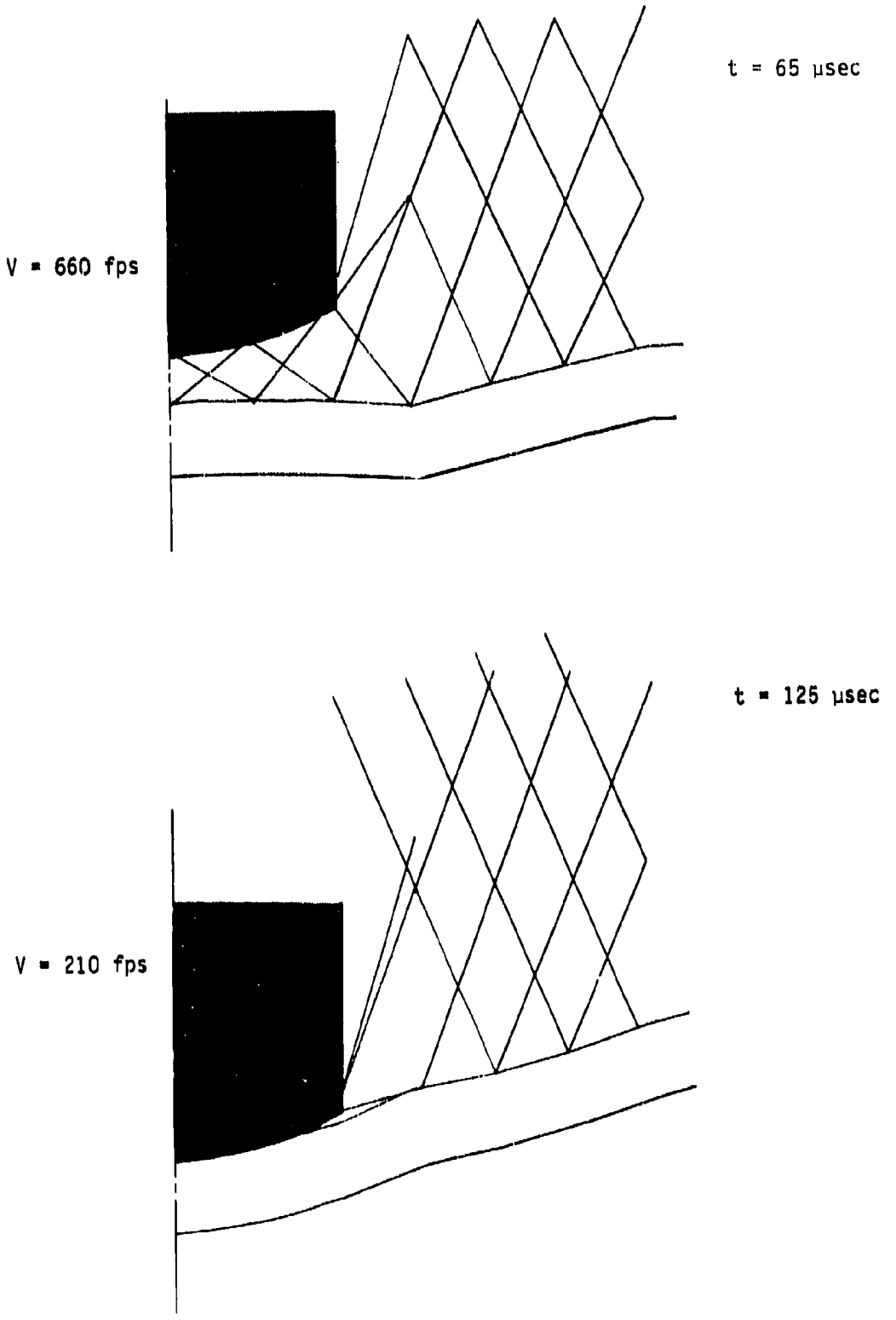

Figure 5.37. Late-time Response of Honeycomb/fabric to 900 fps Impact.

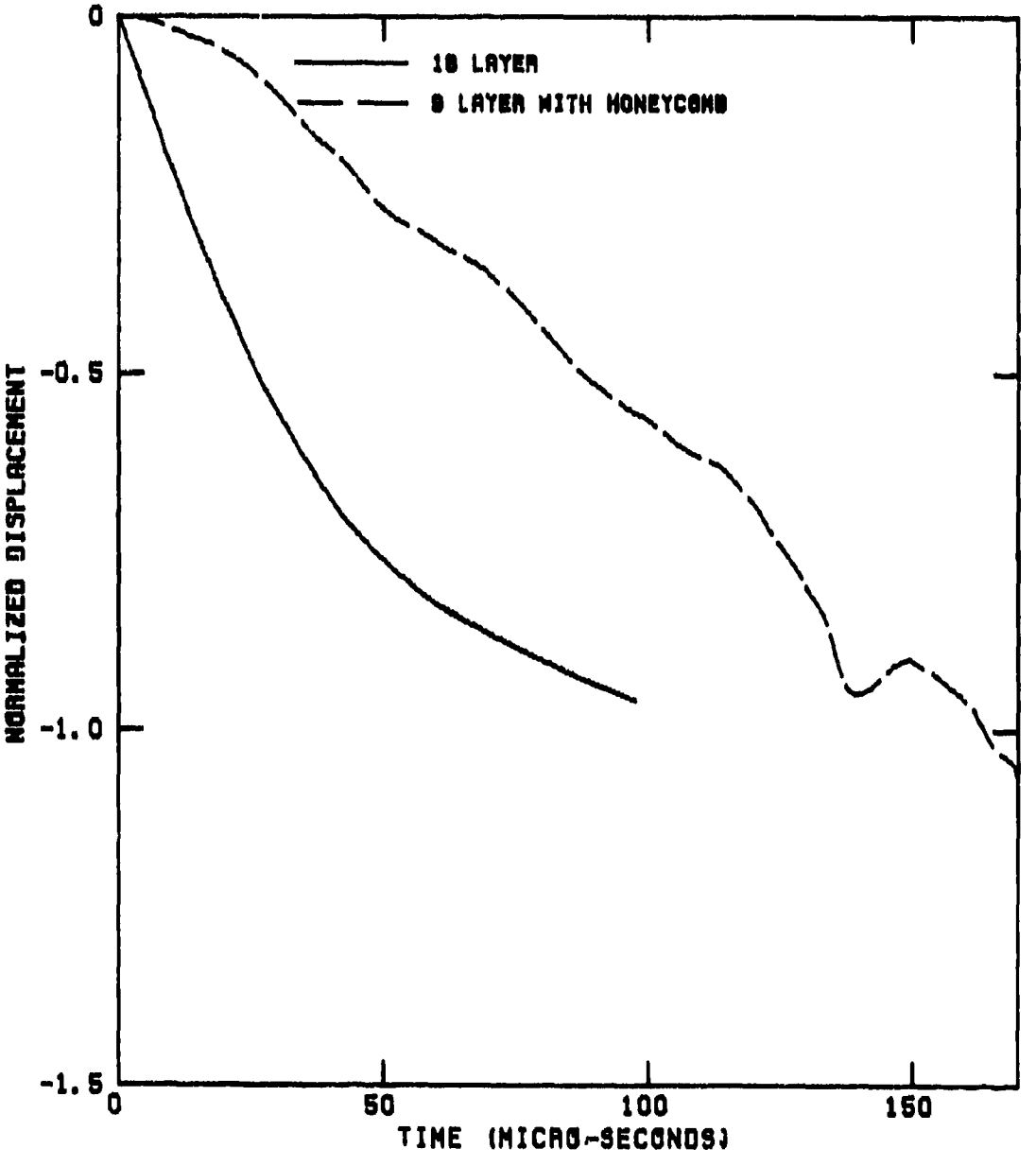

Figure 5.38. Comparison of Center Fabric Deflections by 600 fps Impact; 18-ply vs 9-ply with Honeycomb. (Deflections Normalized to 18-ply, 600 fps Solution.)

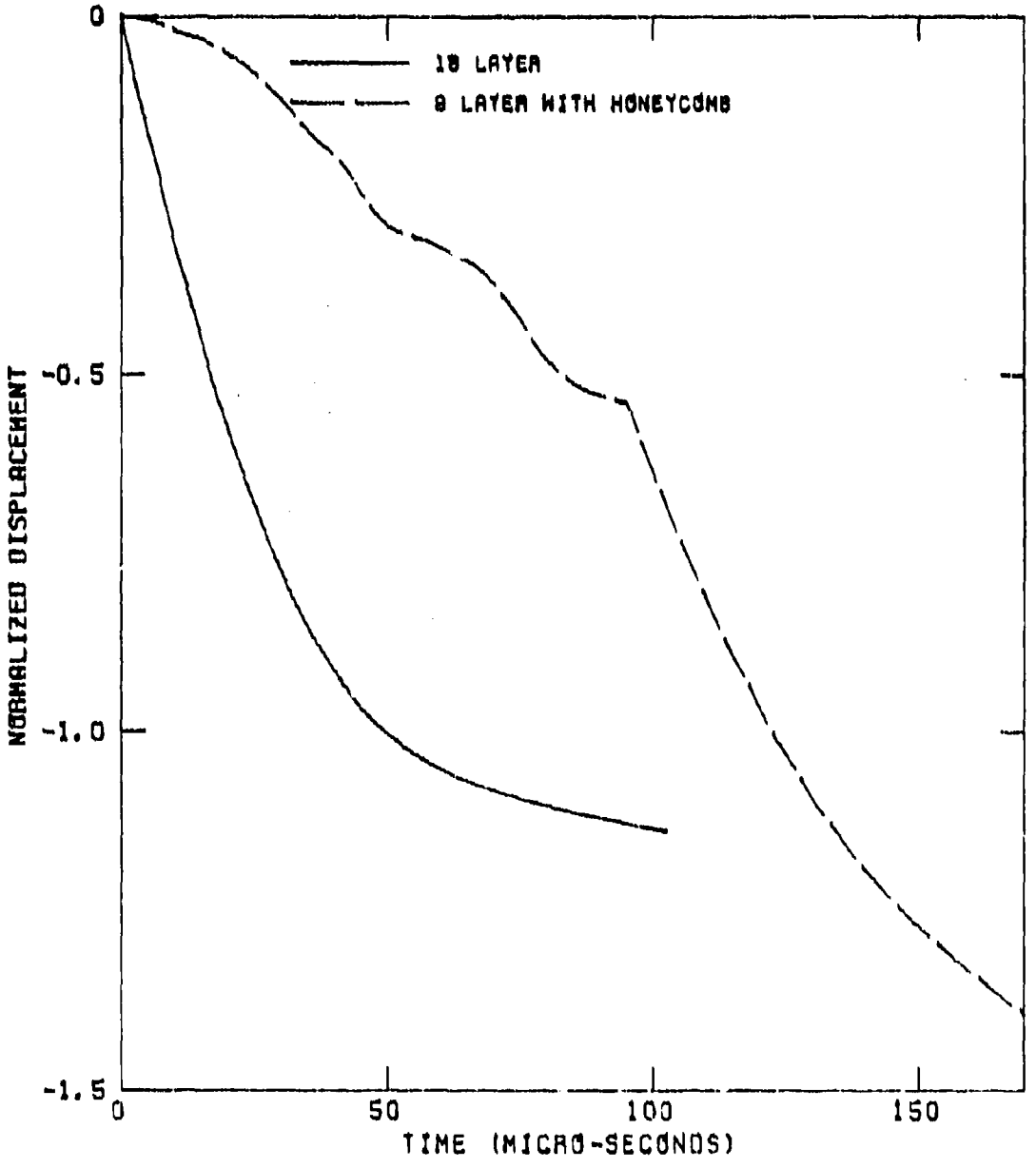

Figure 5.39. Comparison of Center Fabric Deflections by 900 fps Impact; 18-ply vs 9-ply with Honeycomb. (Deflection Normalized to 18-ply, 600 fps Solution.)

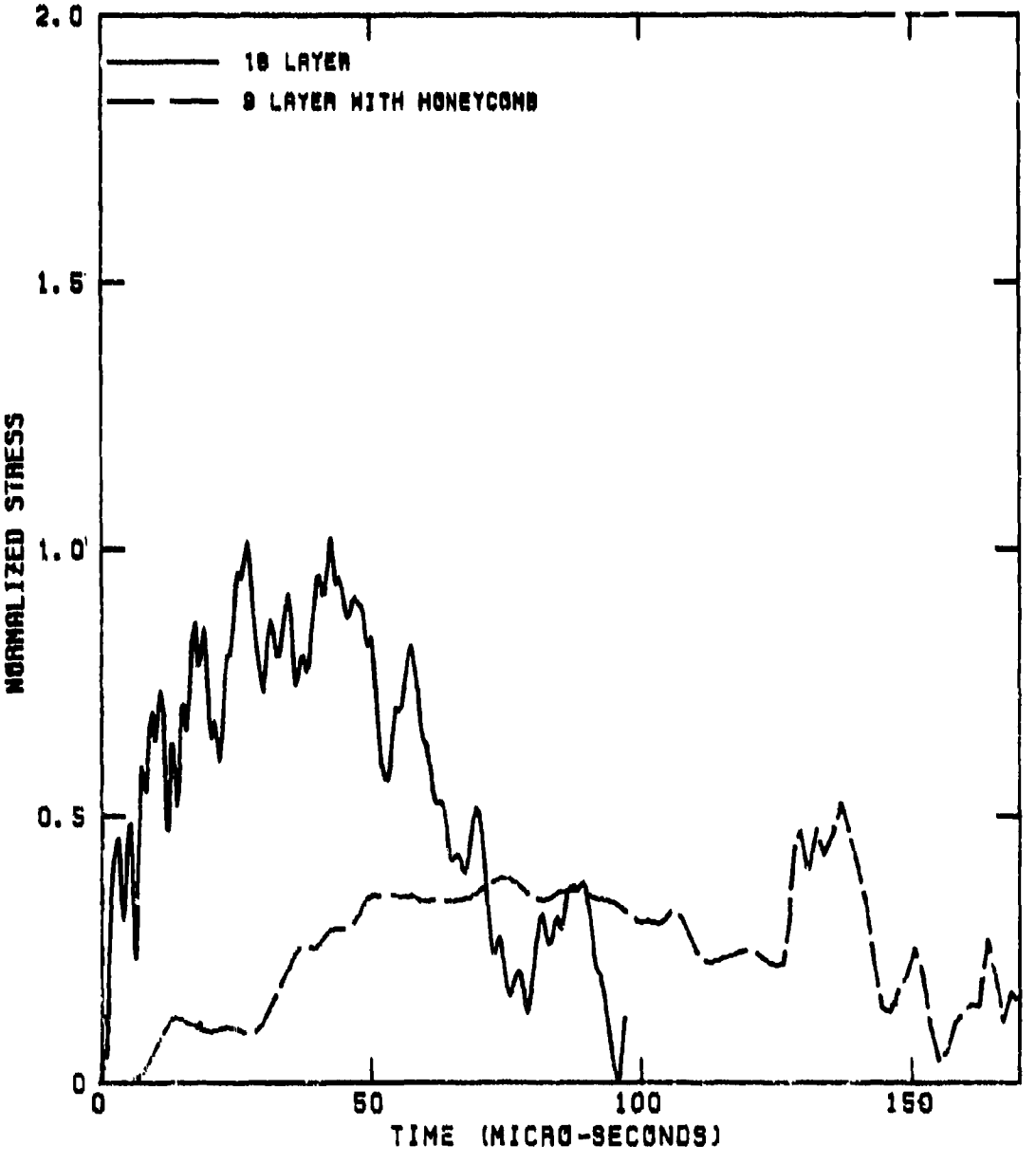

Figure 5.40. Comparison of Stress-time Histories; 18-ply and 9-ply with Honeycomb Targets, 600 fps Impact. (Stress Normalized to 18-ply, 600 fps Solution.)

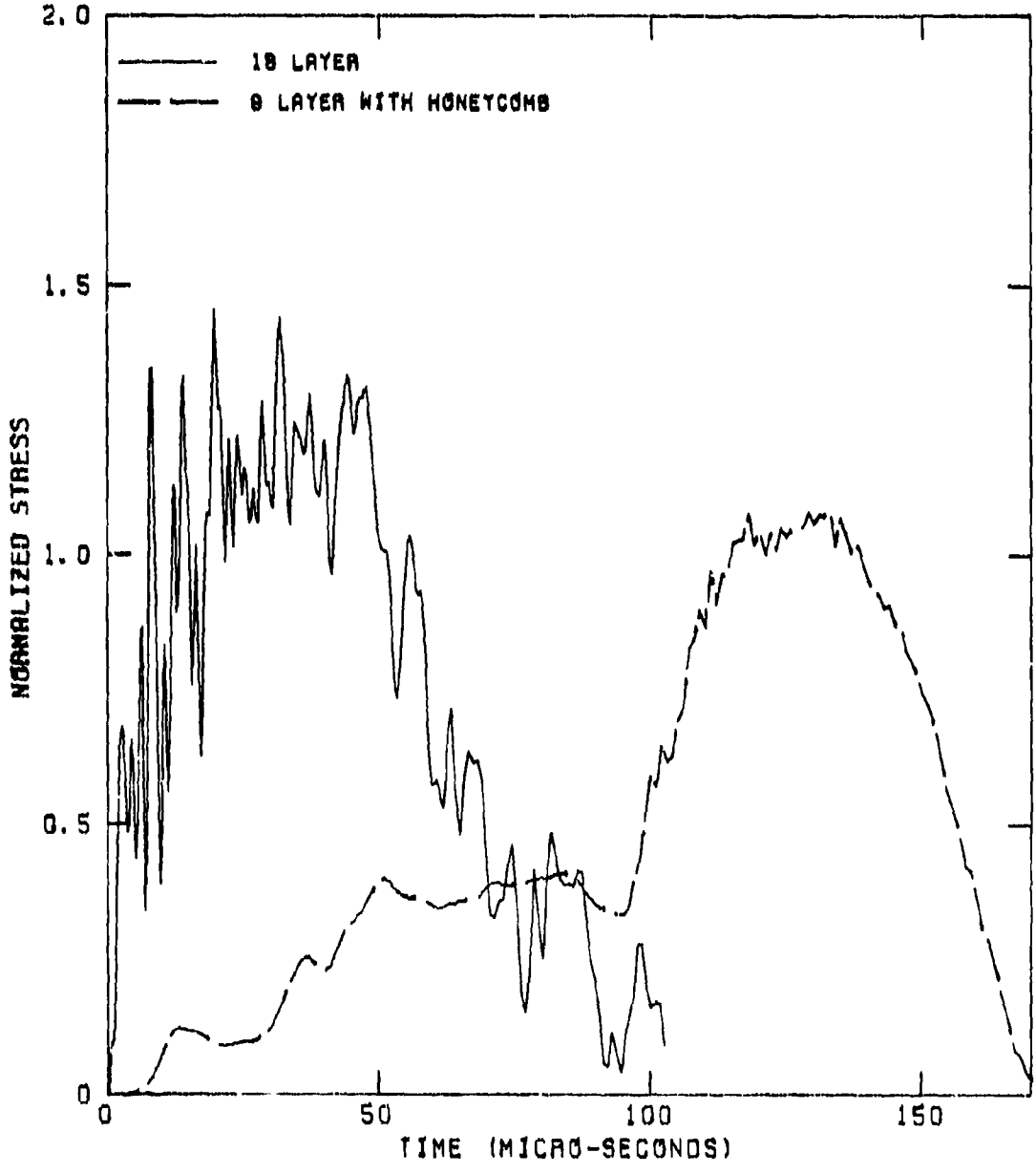

Figure 5.41. Comparison of Stress-time Histories; 18-ply and 9-ply with Honeycomb Targets, 900 fps Impact. (Stress Normalized to 18-ply, 600 fps Solution.)

Table 5.1. Summary of Rear Plate Concept Screening.

Velocity*	Target	Areal Density	Normalized Peak Stress†	Normalized Peak Displacement†
300 fps	9-ply Impregnated	.9 psf	a	.9 b
600 fps	18-ply	1.2 psf	1.00	1.00
	18-ply Impregnated	1.8 psf	a	.9 b
	18-ply 1% Slack	1.2 psf	.65	1.20
	18-ply 4% Slack	1.2 psf	.25	2.15
	9-ply w/Honeycomb	1.2 psf	.50	1.20
	36-ply	2.4 psf	.85	.65
900 fps	18-ply	1.2 psf	1.45	1.15
	9-ply w/Honycomb	1.2 psf	1.10	1.60
	36-ply	2.4 psf	1.25	.75

* Caliber .60, .018 lbm

† Stresses and displacements are normalized to 18-ply, 600 fps solution peaks.

a. Target failure, stresses limited to fiber tensile ultimate

b. Target failure displacement

failure) and peak stresses attained. Final deflections given are extrapolated from the solutions by eliminating the free boundary effect (Figure 5.9). Deflections and stresses are normalized to the peaks attained in the 600 fps, 18-ply fabric case (460 ksi and .33 in.).

As seen in the table, the most significant improvement in back layer capability resulted from the incorporation of fabric weave slack. Increased deflections were the penalty for this improvement. Honeycomb analyses, which predicted gains in ballistic capability of lesser magnitude than weave slack, also predicted honeycomb concepts to suffer less from increased deflections. The application of both concepts to back layer design could lead to further improvements in ballistic capability.

SECTION VI

CONCLUSIONS AND RECOMMENDATIONS

The requirements of a very lightweight (5 psf) armor system capable of providing multi-hit ballistic protection against hard-steel core caliber .30 armor piercing projectiles exceed the capabilities of any single state-of-the-art material. In order to effectively utilize the positive attributes of available materials, a multi-phase armor system with a hard front phase to break up the projectile and a tough rear phase to arrest residual momentum is necessary. The front phase should incorporate high compressive strength lightweight ceramics, notably Boron Carbide. The preferred primary back phase material is Kevlar, a very high tensile strength fabric.

Based on numerical calculations and supporting test data a ceramic front plate with areal density of 5 psf or less will be breached by relatively high velocity fragments which possess approximately 70% of the initial impact momentum. A narrow cylindrical plug of shattered ceramic is ejected in front of the blunted projectile. The plug forms when conoidal damage from the impact side of the ceramic plate merges with damage progressing from the back face of the ceramic and overall breaching then occurs. Thus the conical crack pattern often associated with projectile impact onto ceramics is basically an early time occurrence and is significant only until the plug is formed.

The primary means to reduce the velocity of the projectile is to increase the amount of ceramic mass which will be accelerated. To accomplish this, it is very important to design a system in which as much target mass as possible is engaged with

the projectile for as long as possible. Since the failure mechanisms in the ceramic are generally associated with tensile cracking, the logical manner for delaying armor breakup without increasing weight is to enhance the effective strength of the ceramic.

The use of biaxial prestressing was considered both numerically and experimentally as a method to enhance the strength of a ceramic front phase. The impact environment was found to be sufficiently harsh to overcome the available prestress. Early failure mechanisms were delayed but major failures eventually developed in the unprestressed orientation and led to ceramic plugging. Thus, additional stress enhancement in the third direction is necessary.

An alternative concept which may hold promise is a front phase consisting of discrete elements. Discrete elements may be capable of maintaining structural integrity for a greater period of time than a continuous plate of the same areal density and/or produce tumbling of the projectile. An additional benefit is to limit the extent of damage.

Numerical calculations supported by experimental data showed that if spherical inclusions of sufficient mass were employed, significant projectile break-up and/or rotations could be induced. However this would require high areal densities to be effective. Disc type platelets were then investigated as a possible front face element which would effectively engage as much mass as possible with the projectile during impact while at the same time providing a low areal density.

The numerical analysis of a disc-shaped ceramic platelet subjected to a centered impact showed a more uniform velocity field developing in the platelet, notably behind the conical crack region. These results suggest that if the ceramic material could be made more resistive to tension failure the platelet might hold together long enough to transfer significant amounts of projectile momentum.

Analyses were conducted to determine the level of ceramic strength enhancement sufficient to maintain material resistance. It was found that ceramic tensile strength would have to be increased by factors of 2 or 3 depending on available ductility. These levels of improvement would in all probability require major improvements in lightweight ceramic materials although heavy ceramic materials now give tensile strengths in this range.

The use of a buffer layer between the front phase and the Kevlar backing was also investigated, as there appears to be some potential in using such a buffer to cushion impact of the ejecta from the front phase to the back phase and coat the sharp front face/projectile fragments with this buffer material. Further improvements could result from the incorporation of Kevlar fabric weave slack which allow greater flexibility.

By virtue of the very low amount of front face mass which can be made to interact effectively with the projectile the attainment of a successful 5 psf armor is a formidable task. It appears that significant improvements relative to current lightweight armors are limited by the low tensile strength and ductility of state-of-the-art front face materials. Therefore it is recommended that promising avenues for improving these characteristics be actively pursued.

REFERENCES

1. M. L. Wilkins, "Third Progress Report of Light Armor Program", UCRL-50460, Lawrence Livermore National Laboratory, 1968.

2. M. L. Wilkins, C. F. Cline and C. A. Honodel, "Fourth Progress Report of Light Armor Program", UCRL-50694, Lawrence Livermore National Laboratory, 1969.

3. M. L. Wilkins, R. L. Landingham and C. A. Honodel, "Fifth Progress Report of Light Armor Program", UCRL-50980, Lawrence Livermore National Laboratory, 1971.

4. M. L. Wilkins, "Mechanics of Penetration and Perforation", International Journal of Engineering Science, Vol. 16, pp. 793-807, 1978.

5. R. C. Laible, "Ballistic Materials and Penetration Mechanics", Methods and Phenomena: Their Applications in Science and Technology, Vol. 5, Elsevier Scientific Publishing Co., New York, 1980.

6. M. Rosenblatt, L. Y. Cheng, D. Eitman and J. Courtney, "Multiple Impact Modeling of Composites", AFWAL-TR-80-4112, California Research & Technology, Inc., August 1980.

7. Y. M. Ito, M. Rosenblatt, R. H. England and R. B. Dirling, Jr., "Investigations of Effects of TaC Loading Parameters on Erosion Resistance of Carbon-Carbon Composites", AFWAL-TR-81-4108, California Research & Technology, Inc., October 1981.

8. L. H. Miner, "The Ballistic Resistance of Fabrics of Kevlar Aramid Fiber - Their Care and Use", A-37, E. I. du Pont de Nemours & Co., Inc., April 1980.

9. M. W. Wardle, "High Performance Coated Fabrics of Kevlar Aramid Fiber", A-22, E. I. du Pont de Nemours & Co., Inc., December 1979.

10. Y.M. Ito, R.B. Nelson and D.E. Burks, "Numerical Method for Rock Rubble Fortification Analysis", DNA 5869F, California Research & Technology, Inc., July 1981.

11. "CALSAP, A Finite Element Program for Nonlinear Static and Dynamic Response of Solid and Structural Systems, Users Manual", CALSAP Users Network, California Research & Technology, Inc., March 1982.

12. "Mechanical Properties of Hexcel Honeycomb Materials", TSB 120, Hexcel Corp., 1981.

DISTRIBUTION LIST

DEPARTMENT OF DEFENSE

Armed Forces Radiobiology Rsch Institute
ATTN: DD
ATTN: SD
ATTN: Director

Armed Forces Staff College
ATTN: Library

Assistant Secretary of Defense
International Security Affairs
ATTN: Policy Plans & NSC Affairs
ATTN: ISA/PP
ATTN: F. Miller

Assistant to the Secretary of Defense
Atomic Energy
ATTN: Mil Appl, W. Kahn
ATTN: R. Wagner
ATTN: J. Wade

Command & Control Technical Center
ATTN: C-312, R. Mason

Commander-in-Chief, Atlantic
ATTN: J3
ATTN: J22

Commander-in-Chief, Pacific
ATTN: C3SRD
ATTN: J-54

Defense Advanced Rsch Proj Agency
ATTN: TTO

Defense Communications Agency
ATTN: Code J300, M. Scher

Defense Intelligence Agency
ATTN: DE, Estimates
ATTN: DB-4C, P. Johnson
ATTN: DT-J, Vorona
ATTN: DB-1, Rsch, Sov Wpn Div, C. Ferrell
ATTN: DIO-GPF, W. Magathan
ATTN: DN
ATTN: DB-4C
ATTN: DT, Sci-Tech Intell
ATTN: RTS-2C, Tech Svcs & Spt
ATTN: DB
ATTN: DB-4C, J. Burfening
ATTN: Library

Defense Technical Information Center
12 cy ATTN: DD

Deputy Under Sec of Def, S&TNF
ATTN: T. Jones

Field Command
Defense Nuclear Agency, Det 1
Lawrence Livermore Lab
ATTN: FC-1

DEPARTMENT OF DEFENSE (Continued)

Defense Nuclear Agency
ATTN: NATD
ATTN: RAAE
ATTN: SPTD
ATTN: RAEV
ATTN: SPSS
ATTN: RAEE
ATTN: STNA
ATTN: STRA
ATTN: STSP
ATTN: STBE
ATTN: NAFD
ATTN: NASD
4 cy ATTN: NATA
4 cy ATTN: TITL

Field Command
Defense Nuclear Agency, Det 2
Los Alamos National Lab/DST
ATTN: MS-635, FC-2

DNA PACOM Liaison Office
ATTN: J. Bartlett

Field Command
Defense Nuclear Agency
ATTN: FCTT, S. Humpries
ATTN: FCTT, W. Summa
ATTN: FCTXE
ATTN: FCTT, G. Ganong
ATTN: FCPR
ATTN: FCPRK, R. Wells

Interservice Nuclear Weapons School
ATTN: Document Control

Joint Chiefs of Staff
ATTN: J-3, Strategic Operations Division
ATTN: SAGA/SSD
ATTN: J-5, Strategy Division, W. McClain
ATTN: J-5, Nuc/Chem Pol Br, J. Steckler
ATTN: J-5, Nuc Div/Strategy Div
ATTN: SAGA/SFD

Joint Strat Tgt Planning Staff
ATTN: JP
ATTN: JLKC

National Defense University
ATTN: NWCLB-CR

Office of the Sec of Defense
Net Assessments
ATTN: Document Control

Principal Dep Under Sec of Defense
Research & Engineering
ATTN: J. Wade, Jr

DEPARTMENT OF DEFENSE (Continued)

Program Analysis & Evaluation
ATTN: S. Johnson
ATTN: Strategic Programs

US European Command
ATTN: ECJ-3
ATTN: ECJ-5

US National Military Representative
SHAPE
Attention US Doc Ofc for
ATTN: Intel
ATTN: Nuc Plans
ATTN: Ops, Nuc Concepts

US Readiness Command
ATTN: J-3

Under Sec of Defense for Policy
ATTN: Dir Negotiations Policy, S. Buckley
ATTN: Dir Strategic Policy, C. Estes
ATTN: Dir Plng & Requirements, M. Sheridan
ATTN: F. Ikle

Under Secy of Def for Rsch & Engrg
ATTN: Strat & Arms Control, L. Menichiello
ATTN: K. Hinman
ATTN: Strat & Space Sys (OS), C. Knowles
ATTN: R. Delauer

United States Central Command
ATTN: CCJE-03, DAIGNEAULT

DEPARTMENT OF THE ARMY

Asst Ch of Staff for Intelligence
ATTN: DAMI-FIT

Dep Ch of Staff for Ops & Plans
ATTN: DAMO-RQA, Firepower Div
ATTN: DAMO-NCN
ATTN: DAMO-RQS
ATTN: DAMO-SSM, Pol-Mil Div
ATTN: Technical Advisor
5 cy ATTN: DAMO-NC, Nuc Chem Dir

Harry Diamond Laboratories
ATTN: DELHD-DE
ATTN: DELHD-NP
ATTN: DELHD-TD, Tech Dir
ATTN: DELHD-NW-P
ATTN: 00100 Commander/Tech Dir/Div Dir

US Army Armament Rsch Dev & Cmd
ATTN: DRDAR-LCN-E

US Army Ballistic Research Labs
ATTN: R. Reisler
ATTN: DRDAR-BLV
ATTN: DRDAR-BLA-S

US Army Chemical School
ATTN: ATZN-CM-CC

US Army Comd & General Staff College
ATTN: DTAC
3 cy ATTN: Combined Arms Research Library
3 cy ATTN: ATZZL-CAD-LN

DEPARTMENT OF THE ARMY (Continued)

US Army Concepts Analysis Agency
ATTN: CSSA-ADL

US Army Engineer School
ATTN: Library

US Army Engr Waterways Exper Station
ATTN: J. Houston

US Army Europe and Seventh Army
ATTN: AEAGC-O-W
ATTN: AEAGD-MM, DCSLOG, Mun & Msl Div
3 cy ATTN: DCSI-AEAGB-PDN

US Army Forces Command
ATTN: AF-OPTS

US Army Foreign Science & Tech Ctr
ATTN: DRXST-SD-1

US Army Infantry Ctr & Sch
ATTN: ATSH-CD-CSO

US Army Intel Threat Analysis Det
ATTN: IAX-ADT

US Army Intelligence Center & School
ATTN: ATSI-CD-CS

US Army Logistics Center
ATTN: ATCL-OSS, S. Cockrell

US Army Materiel Dev & Readiness Cmd
ATTN: DRCDE-D

US Army Materiel Sys Analysis Actvy
ATTN: X5, W3JCAA

US Army Mobility Equip R&D Cmd
ATTN: DRDME-WC, Technical Lib, Vault

US Army Nuclear & Chemical Agency
ATTN: MONA-OPS
ATTN: MONA-OPS, B. Thomas
ATTN: Library
ATTN: MONA-OPS, J. Ratway

US Army TRADOC Sys Analysis Actvy
ATTN: ATAA-TAC

US Army Training and Doctrine Comd
ATTN: ATCD-FA

US Army War College
ATTN: War Gaming Facility
ATTN: Library
ATTN: AWCAC, F. Braden, Dept of Tactics

USA Military Academy
ATTN: Document Library

USA Missile Command
ATTN: DRSMI-RH
ATTN: DRSMI-XF

USAFACFS
ATTN: ATZR-MG

DEPARTMENT OF THE ARMY (Continued)

V Corps
ATTN: Commander
ATTN: G-3
ATTN: G-2

VII Corps
ATTN: Commander
ATTN: G-2
ATTN: G-3

DEPARTMENT OF THE NAVY

Anti-Submarine Warfare Sys Proj Ofc
ATTN: PM-4

Charleston Naval Shipyard
ATTN: Commanding Officer

David Taylor Naval Ship R&D Ctr
ATTN: Code L42-3, Library
ATTN: Code 174
ATTN: Code 1750, J. Sykes
ATTN: Code 1750, W. Conley

Joint Cruise Missiles Project Ofc
ATTN: JCMG-707

Marine Corps
ATTN: DCS, P&O, Requirements Div
ATTN: Code OOTO-31
ATTN: DCS, P&O, Strategic Plans Div

Marine Corps Dev & Education Command
ATTN: Commander

Naval Air Development Center
ATTN: Code 702, B. McHugh

Naval Air Force
US Atlantic Fleet
ATTN: Commander

Naval Air Systems Command
ATTN: Code 350D, H. Benefiel

Naval Civil Engineering Laboratory
ATTN: Code L-51, S. Johnson

Naval Intelligence Command
ATTN: NIC-01

Naval Intelligence Support Ctr
ATTN: NISC-30
ATTN: NISC-40

Headquarters
Naval Material Command
ATTN: MAT-00
ATTN: MAT-046

Naval Ocean Systems Center
ATTN: R. Hammond
ATTN: J. Hooper

Naval Postgraduate School
ATTN: Code 56PR
ATTN: Code 1424 Library

DEPARTMENT OF THE NAVY (Continued)

Naval Research Laboratory
ATTN: Code 2627

Naval Sea Systems Command
ATTN: SEA-06H2
ATTN: SEA-406
2 cy ATTN: SEA-6431, H. Seguine

Naval Submarine School
ATTN: Commanding Officer

Naval Surface Force
US Atlantic Fleet
ATTN: Commander

Naval Surface Force
US Pacific Fleet
ATTN: Commander

Naval Surface Weapons Center
ATTN: Code F31
ATTN: Code R14
ATTN: Code U41
ATTN: Code F30
ATTN: Code R44, H. Glaz

Naval Surface Weapons Center
ATTN: Code DG-802, E. Freiling

Naval War College
ATTN: Code E-11, Tech Service

Naval Weapons Center
ATTN: Code 32007, L. Thompson

Naval Weapons Evaluation Facility
ATTN: G. Binns
ATTN: Technical Director
ATTN: H. Struve

Navy Field Operational Intelligence Office
ATTN: Commanding Officer

Newport Laboratory
ATTN: K. Walsh

Nuclear Weapons Tng Group, Atlantic
ATTN: Nuclear Warfare Department

Nuclear Weapons Tng Group, Pacific
ATTN: Nuclear Warfare Department

Office of Naval Research
ATTN: Code 431
ATTN: Code 200

Office of the Chief of Naval Operations
ATTN: OP-00K

Sixth Fleet
ATTN: Commander

Submarine Force
US Atlantic Fleet
ATTN: Commander

DEPARTMENT OF THE NAVY (Continued)

Submarine Force
US Pacific Fleet
ATTN: Commander

Surface Warfare Development Group
ATTN: Commander

Surface Warfare Officers School Cmd
ATTN: Combat Systems Dept

US Naval Air Forces
Pacific Fleet
ATTN: Commander

US Naval Forces, Europe
ATTN: N54

US Navy Second Fleet
ATTN: Commander
4 cy ATTN: ACOS TAC D&E Div

US Navy Seventh Fleet
ATTN: Commander

US Navy Third Fleet
ATTN: Commander

US Pacific Fleet
ATTN: Code N2
ATTN: CINC

Ofc of the Deputy Chief of Naval Ops
ATTN: NOP 963
ATTN: NOP 022
ATTN: NOP 985F
ATTN: NOP 02
ATTN: NOP 654, Strat Eval & Anal Br
ATTN: NOP 32, Surf Warf Div
ATTN: NOP 987
ATTN: NOP 954, Strike & Amphib Warf Div
ATTN: NOP 098, Ofc Res-Dev-Test & Eval
ATTN: NOP 50, Avn Plns & Rqmts Dev
ATTN: NOP 06
ATTN: NOP 35, Surf Cbt Sys Div
ATTN: NOP 981, U/Sea/St War/Nuc En Dev
ATTN: NOP 953, Tac Readiness Div
ATTN: NOP 955, AAW Div
ATTN: NOP 03
ATTN: NOP 021
ATTN: NOP 05
ATTN: NOP 950, Force Level Plns Div
ATTN: NOP 951, ASW Div
ATTN: NOP 09
3 cy ATTN: NOP 96, N Prog Ofc-Sys Anal Div

DEPARTMENT OF THE AIR FORCE

Air Force
ATTN: INE, Estimates

Air Force Operational Test & Eval Ctr
ATTN: OAY, Capt Lutz
ATTN: OA

Air Force Propulsion Lab
ATTN: LKDH, Stop 24, E. Haberman

DEPARTMENT OF THE AIR FORCE (Continued)

Air Force Weapons Laboratory
ATTN: SUL
ATTN: NTYC, J. Burgio

Air University Library
ATTN: AUL-LSE

Assistant Chief of Staff
Studies & Analysis
ATTN: AF/SAGF
2 cy ATTN: AF/SAMI, Tech Info Div

Ballistic Missile Office
ATTN: ENMP
ATTN: ENMP, D. Van Gari
2 cy ATTN: ENSN

Deputy Chief of Staff
Research, Development & Acq
ATTN: AFRDQA
ATTN: AFRDQI
4 cy ATTN: AFRD-M, Spec Asst for MX

Deputy Chief of Staff
Plans and Operations
ATTN: AFXOOR, Opns, Opnl Spt
ATTN: AFXOXFM, Plns, Frc Dev Mun Plns
ATTN: Dir of Plans, AFXOX

Foreign Technology Division
ATTN: SD
ATTN: TQ

Pacific Air Forces
ATTN: XO
ATTN: IN

Strategic Air Command
ATTN: XPFS

Tactical Air Command
ATTN: TAC/DR
ATTN: TAC/IND
ATTN: TAC/SMO-G
ATTN: TAC/XPS

US Air Force Academy Library
DFSEL
ATTN: Library

US Air Force Scientific Advisory Bd
ATTN: AF/NB

US Air Forces in Europe
ATTN: USAFE/DO&I
ATTN: USAFE/DOA, Opns Anal
ATTN: USAFE/DOJ, Cbt Opns
ATTN: USAFE/IN
ATTN: USAFE/XPX, Plns

OTHER GOVERNMENT AGENCIES

Central Intelligence Agency
ATTN: OSWR/NED
ATTN: OSR/SE/F

OTHER GOVERNMENT AGENCIES (Continued)

Federal Emergency Management Agency
ATTN: Asst Assoc Dir for Rsch, J. Kerr
ATTN: Ofc of Rsch/NP, D. Bensen

National Security Council
ATTN: R. Linhard
ATTN: H. Nau
ATTN: G. Kemp
ATTN: W. Clark
ATTN: A. Myer
ATTN: R. McFarland
ATTN: M. Guhin

NORAD
ATTN: J5YS, F. Smith

Office of Technology Assessment
ATTN: M. Harris

US Arms Control & Disarmament Agcy
ATTN: A. Lieberman

US Department of State
ATTN: PM

The White House
ATTN: Counsellor to the President, E. Meese

NATO

NATO School, SHAPE
ATTN: US Doc Ofc For, Ltc Williamson

DEPARTMENT OF ENERGY CONTRACTORS

University of California
Lawrence Livermore National Lab
ATTN: L-35, J. Immele
ATTN: L-8, F. Barrish
ATTN: L-21, M. Gustavson
ATTN: L-389, R. Andrews
ATTN: R. Werne
ATTN: R. Corallo

Los Alamos National Laboratory
ATTN: R. Sandoval
ATTN: MS634, T. Dowler
ATTN: R. Stolpe

Sandia National Laboratories
ATTN: Tech Lib 3141
ATTN: 0332, J. Keizur
ATTN: 0333, R. Stratton
ATTN: 0334, J. Struve

DEPARTMENT OF DEFENSE CONTRACTORS

Abbott Associates, Inc
ATTN: R. McLaurin

Academy for Interscience Methodology
ATTN: N. Painter

BDM Corp
ATTN: D. Peercy

DEPARTMENT OF DEFENSE CONTRACTORS (Continued)

BDM Corp
ATTN: J. Braddock
ATTN: C. Wasaff
ATTN: R. Buchanan
ATTN: J. Bode
ATTN: J. Morgan
ATTN: P. White
ATTN: J. Herzog
ATTN: H. Portnoy
ATTN: R. Welander
ATTN: L. Schlipper

California Research & Technology, Inc
2 cy ATTN: Y. Ito
2 cy ATTN: R. Nelson
2 cy ATTN: A. Frederickson, III

CACI, Inc - Federal
ATTN: A. Berry

66th MI Group
ATTN: K. Moran

Data Memory Systems, Inc
ATTN: T. Dupuy

Harold Rosenbaum Associates, Inc
ATTN: H. Rosenbaum

Hudson Institute, Inc
ATTN: NAVWAG

Inst for Foreign Anal, Inc
ATTN: J. Record

Inst for Foreign Pol Anal, Inc
ATTN: R. Schweitzgraph

Institute for Defense Analyses
ATTN: V. Utgoff
ATTN: Classified Library
ATTN: D. Moody

International Energy Associates, Inc
ATTN: L. Scheinman

JAYCOR
ATTN: E. Almquist

Kaman Sciences Corporation
ATTN: R. Miller

Kaman Tempo
ATTN: C. Anderson
ATTN: DASIAC

Kaman Tempo
ATTN: DASIAC

Leon Sloss Associates, Inc
ATTN: L. Sloss

McLean Research Center, Inc
ATTN: W. Schilling

DEPARTMENT OF DEFENSE CONTRACTORS (Continued)

University of Miami
ATTN: Contract Office, S. Wang

Natl Institute for Public Policy
ATTN: C. Gray

ORI, Inc
ATTN: B. Buc
ATTN: R. Wiles

Orion Engineering, Inc
ATTN: W. Parks

Pacific-Sierra Research Corp
ATTN: S. Finn
ATTN: G. Lang
ATTN: H. Brode, Chairman SAGE

Pacific-Sierra Research Corp
ATTN: D. Gormley
ATTN: G. Moe

Palomar Corp
ATTN: B. Glaser
ATTN: B. Garrett
ATTN: C. Feldbaum

Physical Research, Inc
ATTN: K. Schwartz

R&D Associates
ATTN: F. Field
ATTN: G. Jones
ATTN: G. Ivy
ATTN: J. Marcum
ATTN: J. Lewis
ATTN: A. Wohlstetter
ATTN: P. Haas
ATTN: R. Montgomery

R&D Associates
ATTN: J. Thompson
ATTN: H. Polk
ATTN: A. Deverill

Rand Corp
ATTN: B. Bennett

DEPARTMENT OF DEFENSE CONTRACTORS (Continued)

Rand Corp
ATTN: Library
ATTN: J. Digby
ATTN: T. Parker
ATTN: P. Davis

Science Applications, Inc
ATTN: J. Martin
ATTN: M. Drake

Science Applications, Inc
ATTN: B. Dial

Science Applications, Inc
ATTN: P. Setty
ATTN: W. Zimmerman
ATTN: J. Goldstein
ATTN: W. Layson
ATTN: J. McGahan

SRI International
ATTN: B. Low
ATTN: G. Abrahamson
ATTN: J. Naar
ATTN: W. Jaye

SY Corp
ATTN: S. Weiss

System Planning Corp
ATTN: G. Parks
ATTN: S. Shrier
ATTN: J. Jones

Systems Research & Applications Corp
ATTN: S. Greenstein

Tetra Tech, Inc
ATTN: J. Preston
ATTN: F. Bothwell

Titan Systems, Inc
ATTN: C. Albo